Precambrian Research 309 (2018) 56–87

Contents lists available at ScienceDirect

Precambrian Research

journal homepage: www.elsevier.com/locate/precamres

Neoproterozoic amalgamation between Yangtze and Cathaysia blocks: The magmatism in various tectonic settings and continent-arc-continent collision

Yan Xia [a], Xisheng Xu [a,*], Yaoling Niu [b], Lei Liu [c]

[a] State Key Laboratory for Mineral Deposits Research, School of Earth Sciences and Engineering, Nanjing University, Nanjing 210023, China
[b] Department of Earth Sciences, Durham University, Durham DH1 3LE, UK
[c] Guangxi Key Laboratory of Hidden Metallic Ore Deposits Exploration, College of Earth Sciences, Guilin University of Technology, Guilin 541004, China

ARTICLE INFO

Article history:
Received 6 April 2016
Revised 21 February 2017
Accepted 24 February 2017
Available online 6 March 2017

Keywords:
Neoproterozoic igneous rocks
Arc-trench-basin system
Amalgamation of South China
Jiangnan Orogeny
Zircon U-Pb-Hf isotopes
Nd isotopes

ABSTRACT

According to the temporal-spatial distribution of Neoproterozoic igneous rocks and relative rocks in South China, including ophiolites, arc volcanic and intrusive rocks and subsequent bimodal magmatism, we identified the presence of a Neoproterozoic intra-oceanic arc, continent-arc-continent collision and three tectono-magmatic zones between the Yangtze Block and Cathaysia Block. We have also unraveled the amalgamation and tectono-magmatic histories between the Yangtze and Cathaysia blocks: At ~1000–860 Ma, northwestward ocean-ocean subduction and southeastward ocean-continent subduction resulted in the intra-oceanic arc magmatism and active continental margin magmatism in the Cathaysia Block respectively. At ~860–825 Ma, the steepening subduction caused development of back-arc basin in the intra-oceanic arc zone and the slab rollback induced the arc and back-arc magmatism in the Cathaysia Block. Meanwhile, a shallow dip northwestward ocean-continent subduction formed active continental margin magmatism in the Yangtze Block. At ~825–805 Ma, the continent-arc-continent collision and final amalgamation between the Yangtze and Cathaysia blocks yielded the Jiangnan Orogen. At ~805–750 Ma, the Jiangnan Orogen collapsed, and the Nanhua rift basin formed. Our study also rules out any Grenvillian Orogenic event and mantle plume activity in South China and indicates a marginal position of South China in the Rodinia supercontinent.

Contents

* Corresponding author.
E-mail addresses: xiayan@nju.edu.cn (Y. Xia), xsxu@nju.edu.cn (X. Xu), yaoling.niu@foxmail.com (Y. Niu), liulei@glut.edu.cn (L. Liu).

http://dx.doi.org/10.1016/j.precamres.2017.02.020
0301-9268/

1. Introduction

South China, or the greater South China Block, is an important geological region in Eastern Asia, and comprising the Yangtze Block to the northwest and the Cathaysia Block to the southeast (Fig. 1a). These two blocks have been considered to have amalgamated in the early Neoproterozoic. Meanwhile, various igneous rocks in distinct tectonic setting (such as ~1000–860 Ma ophiolites and arc volcanic and intrusive rocks, ~850–805 Ma peraluminous S-type granites, and ~820–750 Ma bimodal volcanic rocks and mafic dyke swarms; Fig. 1b; Table 1) have been formed. The accepted geodynamic scheme can be summarized as follows: the closing of an ocean that existed in the Neoproterozoic through northward seafloor subduction beneath an active continental margin of the Yangtze Block and the subsequent continent-continent collision between the Yangtze and Cathaysia blocks, giving rise to the Jiangnan Orogeny (e.g., Charvet, 2013; Chen et al., 2014; Li et al., 2009, 2013; Wang et al., 2012a, 2013c; Yao et al., 2014b, 2014c; Zhang et al., 2012b, 2013a). However, the timing of this assembly has not yet been precisely constrained. Some studies propose the amalgamation at ~1000–900 Ma (e.g., Greentree et al., 2006; Li et al., 1995, 2002, 2007b, 2008c, 2009; Ye et al., 2007), correlating the Neoproterozoic Jiangnan Orogeny in South China as part of the global Grenvillian-aged orogenic events (Li et al., 2002, 2008b). However, based on Precambrian stratigraphic sequences and magmatic records, others suggest that the Jiangnan Orogeny lasted until 830 Ma, or even to 800 Ma, and is unrelated to the main Grenvillian Orogeny (e.g., Shu, 2012; Wang et al., 2006a, 2007b, 2010b, 2012b, 2012c; Yao et al., 2013; Zhao and Cawood, 1999, 2012; Zhao et al., 2011; Zhou et al., 2002). The existence of ~860–820 Ma magmatic arcs in both west and east segments of the Jiangnan Orogen has also been proposed in some recent work (Chen et al., 2014; Wang et al., 2012a, 2014a; Yao et al., 2013, 2014a; Zhao, 2015).

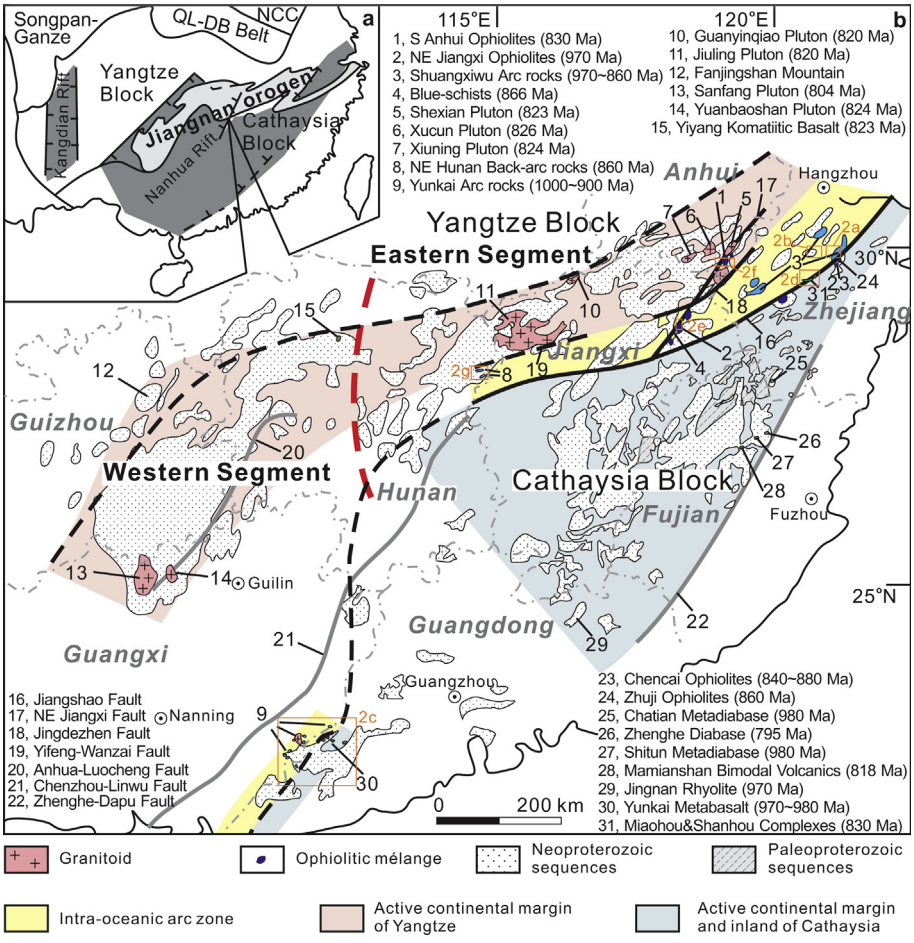

Fig. 1. Schematic map showing the main distribution area of Neoproterozoic rocks and major deep faults in South China (modified after Cawood et al., 2013; Xia et al., 2012; Yao et al., 2014a; Wang and Li, 2003; Wang et al., 2013b, 2014a, 2014b). Data sources are the same as in Table 1, some typical Neoproterozoic igneous rocks in South China (i.e. No. 1, 2, 3, 5, 8, 9, 30 and 31) are also shown in Fig. 2.

Table 1
List of reliable ages, $\varepsilon_{Hf}(t)$ and $\varepsilon_{Nd}(t)$ values of Neoproterozoic igneous rocks in South China.

Location	Batholith or Pluton/ Group or Formation	Rock type	Age (Ma)	Method	Zircon $\varepsilon_{Hf}(t)$	Whole-rock $\varepsilon_{Nd}(t)$	Reference
Intra-oceanic arc zone							
Stage I (ca. 1000 ~ 860 Ma): Oceanic arc and Cathaysia continental arc development							
N Zhejiang	Pingshui Formation	Seafloor basalt and andesite	978 ± 44 Ma	Sm-Nd isochron			Zhang et al. (1990)
			904 ± 8 ~ 906 ± 10 Ma	LA-ICP-MS zircon	8.6 ~ 15.4	6.4 ~ 7.9	Chen et al. (2009b)
					11.3 ~ 15.3*	5.2 ~ 7.3	Li et al. (2009)
	Beiwu Formation	Andesite, Dacite and Rhyolite	926 ± 15 Ma	SHRIMP U-Pb zircon	12.3 ~ 15.3*	5.8 ~ 8.7	
	Zhangcun Formation	Felsic ignimbrite	891 ± 12 Ma	SHRIMP U-Pb zircon	11.8 ~ 13.1*	5.6 ~ 7.4	
	Taohong	Tonalite			8.2 ~ 12.8*	6.9 ~ 8.6	
		Tonalite–granodiorite	913 ± 15 Ma	SHRIMP U-Pb zircon			Ye et al. (2007)
	Xiqiu	Tonalite–granodiorite	905 ± 14 Ma	SHRIMP U-Pb zircon			
		Granodiorite			9.5 ~ 11.5*	6.4 ~ 7.8	Li et al. (2009)
	Pingshui	Basaltic porphyry	916 ± 6 Ma	LA-ICP-MS zircon		6.8 ~ 8.0	Chen et al. (2009a)
		Diorite	932 ± 7 Ma	LA-ICP-MS zircon	8.6 ~ 13.2	7.0 ~ 7.7	
		Plagiogranite	902 ± 5 Ma	LA-ICP-MS zircon	11.0 ~ 16.2	7.5 ~ 8.4	
	Shuangxiwu Group	Seafloor andesite				3.4 ~ 4.6	Chen and Jahn (1998)
	Jiangshan	Quartz diorite	924 ± 23 Ma	Single-grain zircon TIMS		2.4 ~ 4.4	Quote from a secondary source of Wang et al. (2012b)
NE Jiangxi	Ophiolitic mélange	Pyroxenite, Gabbro	930 ± 34 Ma	Sm-Nd isochron		5.1 ~ 5.5	Xu and Qiao (1989)
		Xiwan Albite granites	968 ± 23 Ma	SHRIMP U-Pb zircon			Li et al. (1994)
						4.9 ~ 6.7	Li and Li (2003)
		Xiwan Leucogranites	880 ± 19 Ma	SHRIMP U-Pb zircon		−3.9 ~ 0.8	Li et al. (2008a)
		Peridotite, Pyroxenite, Dolerite, Gabbro, Diorite, Anorthosite	956 ± 48 Ma	Sm-Nd isochron		4.5 ~ 11.1	Li et al. (1997)
		Enclave bearing plagiogranite	970 ± 21 Ma	SHRIMP U-Pb zircon		6.6 ~ 7.4	Gao et al. (2009)
		Enclave-free plagiogranite				−1.3 ~ −1.2	
		Enclave				6.2	
	Dexing	Blueschist	866 ± 14 Ma	K-Ar glaucophane			Shu et al. (2006)
N Jiangxi	Shuangqiaoshan Group	Quartz-keratophyre	878 ± 5 Ma	LA-ICP-MS zircon	3.3 ~ 14.7		Wang et al. (2008a)
		Tuff	879 ± 6 Ma	LA-ICP-MS zircon	7.3 ~ 18.8		
Boundary between E Guangxi and W Guangdong (Yunkai domain)	Mala village, Xinyi	Plagioclase amphibolite				4.8 ~ 4.9	Wang et al. (2013b)
	Jintong, Xinyi	Plagioclase amphibolite				3.1 ~ 4.9	
	Zhaimen, Xinyi	Plagioclase amphibolite				3.1 ~ 4.2	
	Liuwan, Rongxian	Plagioclase amphibolite, Metagabbro				2.3 ~ 4.4	
		Amphibolite, Metabasalt				5.3 ~ 5.4	Zhang et al. (2012a)
	Licun, Rongxian	Amphibolite				4.4	
	Shiwo, Beiliu	Amphibolite	997 ± 21 Ma	LA-ICP-MS zircon		3.8 ~ 4.3	
	Fenjie, Luoding	Metabasalt				4.1	
	Tiantangshan	Granitic gneiss	906 ± 24 Ma	SHRIMP U-Pb zircon			Qin et al. (2006)
	Luoyu formation	Metadacite	922 ± 6 ~ 940 ± 5 Ma	Single-grain zircon TIMS			Zhang et al. (1998)
Stage II (ca. 860 ~ 825 Ma): Bidirectional subduction and continental arc development							
N Zhejiang	Shenwu	Dolerite	849 ± 7 Ma	SHRIMP U-Pb zircon		0.4 ~ 2.3	Li et al. (2008b)
	Daolinshan	Dolerite	863 ± 7 Ma	LA-ICP-MS zircon	4.5 ~ 7.5		Yao et al. (2014c)
W Jiangxi	Fangxi	Dolerite	847 ± 18 Ma	LA-ICP-MS zircon		1.3 ~ 9.6	Zhang et al. (2013b)
NE Hunan	Shuikou	Basalt	860 ± 20 Ma	SHRIMP U-Pb zircon			
	Nanqiao	Basalt	838 ± 12 Ma	SIMS U-Pb zircon			
			1271 ± 2 Ma	Single-grain zircon TIMS		6.9 ~ 9.0	Zhou et al. (2003)
	Wenjiashi	Diabase	860 ± 15 Ma	LA-ICP-MS zircon			Yao et al. (2014c)

Table 1 (*continued*)

Location	Batholith or Pluton/ Group or Formation	Rock type	Age (Ma)	Method	Zircon $\varepsilon_{Hf}(t)$	Whole-rock $\varepsilon_{Nd}(t)$	Reference
Stage IV (ca. 805 ~ 750 Ma): Continental rift development							
N Zhejiang	Hongchicun Formation	Intermediate to felsic volcanic rocks	797 ± 11 Ma	SHRIMP U-Pb zircon			Li et al. (2003b)
	Daolinshan	Diabase				−1.8 ~ 7.0	Li et al. (2008b)
		Granite	790 ± 6 Ma	LA-ICP-MS zircon	7.0 ~ 14.4		Yao et al. (2014c)
			775 ± 13 ~ 780 ± 5 Ma	SHRIMP and LA-ICP-MS U-Pb zircon	6.7 ~ 17.4	3.6 ~ 6.2	Wang et al. (2010a,b)
			794 ± 9 Ma	SHRIMP U-Pb zircon		4.7 ~ 7.0	Li et al. (2008b)
	Shangshu Formation	Basalt				5.7 ~ 7.4	
		Rhyolite	792 ± 5 Ma	SHRIMP U-Pb zircon		4.5 ~ 5.9	
NE Jiangxi	Minjiawu	Basalt, Basaltic andesite, Andesite, Dacite	802 ± 8 Ma	LA-ICP-MS zircon		3.7 ~ 4.8	Wang et al. (2012a)
N Jiangxi	Shuangqiaoshan Group	Gabbro	801 ± 4 Ma	LA-ICP-MS zircon	2.5 ~ 9.6		Wang et al. (2008a)
Active continental margin and inland of Cathaysia							
Stage I (ca. 1000 ~ 860 Ma): Oceanic arc and Cathaysia continental arc development							
E Zhejiang	Chencai	Hornblende gneiss	879 ± 10 Ma	LA-ICP-MS zircon	3.4 ~ 14.4		Yao et al. (2014b)
SW Zhejiang	Chatian, Songyang	Amphibolite	969 ± 13 Ma	SHRIMP U-Pb zircon	6.3 ~ 15.3	4.1 ~ 4.2	Wang et al. (2013b)
			984 ± 6 Ma	LA-ICP-MS zircon			
	Yuyan-Shanlintuo, Songyang	Plagioclase amphibolite				2.8 ~ 3.8	
	Huangtian, Qinyuan	Metagabbro				4.2	
	Zhuhuang, Qinyuan	Amphibolite				2.4 ~ 3.8	
	Zhuyuan	Plagioclase amphibolite				2.9	
	Huangtian, Qinyuan	Metagabbro				3.8	
NW Fujian	Shitun	Metadiabase	978 ± 11 Ma	SIMS U-Pb zircon	4.5 ~ 10.2	5.6	
			970 ± 10 Ma	LA-ICP-MS zircon			
SW Fujian	Masha	Granitic gneiss	909 ± 10 ~ 916 ± 6 Ma	SIMS and LA-ICP-MS U-Pb zircon	−5.8 ~ 1.3	−9.5 ~ −3.9	Wang et al. (2014b)
SE Jiangxi	Xunwu Group	Granitic gneiss	963 ± 11 ~ 982 ± 27 Ma	LA-ICP-MS zircon	−9.6 ~ 0.8	−9.2 ~ −4.8	
Guangdong	Jingnan	Rhyolite	972 ± 8 Ma	SHRIMP U-Pb zircon			Shu et al. (2008a)
					−7.9 ~ 10.0		Shu et al. (2011)
Boundary between E Guangxi and W Guangdong (Yunkai domain)	Chashan, Xinyi	Plagioclase amphibolite, Metagabbro	824 ± 77 Ma	Sm-Nd isochron		1.4 ~ 1.8	Peng et al. (2006)
	Guizi, Xinyi	Metabasalt				2.4 ~ 5.0	
	Tantu, Xinyi	Metabasalt	980 ± 8 Ma	LA-ICP-MS zircon	4.8		Wang et al. (2013b)
			978 ± 19 Ma	SHRIMP U-Pb zircon		4.7	Zhang et al. (2012a)
	Fenjie, Luoding	Metabasalt				3.9	
	Huaixiang, Xinyi	Metagranite	954 ± 14 Ma	LA-ICP-MS zircon		−9.0 ~ −8.5	Wang et al. (2014b)
	Shuanglong, Luoding	Granitoid gneiss	926 ± 28 Ma	LA-ICP-MS zircon	−7.3 ~ −5.5	−3.8	
Stage II (ca. 860 ~ 825 Ma): Bidirectional subduction and continental arc development							
E Zhejiang	Zhuji	Plagioclase amphibolite	845 ± 10 Ma	$^{40}Ar/^{39}Ar$ hornblende			Shui et al. (1986)
		Ophiolitic gabbro	858 ± 11 Ma	SHRIMP U-Pb zircon			Shu et al. (2006)
		Shijiao tebinite	832 ± 7 Ma	$^{40}Ar/^{39}Ar$ hornblende			Kong et al. (1995)
		Shijiao amphibole pyroxenite	844 ± 3 Ma	LA-ICP-MS zircon			Wang et al. (2012b)
	Chencai	Basalt	857 ± 7 Ma	SHRIMP U-Pb zircon	2.1 ~ 7.1		Shu et al. (2011)
		Gabbro	841 ± 12 Ma	SHRIMP U-Pb zircon	8.1 ~ 12.5		
	Zhangcun	Metarhyolite	838 ± 5 Ma	SHRIMP U-Pb zircon			Li et al. (2010b)
	Lipu	Gabbro-diorite	841 ± 6 Ma	SHRIMP U-Pb zircon			
W Zhejiang	Miaohou	Gabbro	828 ± 11 Ma	LA-ICP-MS zircon	4.8 ~ 9.6	3.9	Xia et al. (2015)
		Diorite	832 ± 8 ~ 834 ± 14 Ma	LA-ICP-MS zircon	−6.1 ~ 12.3	1.1 ~ 3.6	
		Granite	830 ± 9 ~ 833 ± 12 Ma	LA-ICP-MS zircon	−1.7 ~ 8.1	0.3 ~ 3.2	
	Shanhou	Diorite	830 ± 12 Ma	LA-ICP-MS zircon	4.1 ~ 10.9	5.5	
		Granite	832 ± 9 Ma	LA-ICP-MS zircon	−3.8 ~ 11.3	−2.7 ~ 2.6	
NW Fujian	Mamianshan	Gabbro	836 ± 7 Ma	SHRIMP U-Pb zircon	8.7 ~ 11.2		Shu et al. (2011)
	Jianou	Gabbro	847 ± 8 Ma	SHRIMP U-Pb zircon	9.6 ~ 11.5		

(*continued on next page*)

Table 1 (*continued*)

Location	Batholith or Pluton/ Group or Formation	Rock type	Age (Ma)	Method	Zircon $\varepsilon_{Hf}(t)$	Whole-rock $\varepsilon_{Nd}(t)$	Reference
Stage III (ca. 825 ~ 805 Ma): Collision between Yangtze and Cathaysia Blocks and Jiangnan Orogen development							
E Zhejiang	Zhuji	Huangshan quartz diorite	818 ± 6 Ma	LA-ICP-MS zircon			Wang et al. (2012b)
NW Fujian	Mamianshan Group	Felsic volcanic rocks	818 ± 9 Ma	SHRIMP U-Pb zircon		0.2 ~ 0.9	Li et al. (2005)
		Mafic volcanic rocks				−4.4 ~ 3.3	
Stage IV (ca. 805 ~ 750 Ma): Continental rift development							
NW Fujian	Wanquan Group	Metavolcanics	788 ± 27 ~ 800 ± 14 Ma	SHRIMP U-Pb zircon			Li et al. (2010b)
	Zhenghe	Diabase	795 ± 7 Ma	SHRIMP U-Pb zircon			Shu et al. (2008b)
					0.8 ~ 6.2		Shu et al. (2011)
Active continental margin of Yangtze							
Stage II (ca. 860 ~ 825 Ma): Bidirectional subduction and continental arc developing/ Stage III (ca. 825 ~ 805 Ma): Collision between Yangtze and Cathaysia Blocks and Jiangnan Orogen development							
S Anhui	Fuchuan Ophiolitic mélange	Wehrlite	827 ± 9 Ma	SHRIMP U-Pb zircon			Ding et al. (2008)
						4.3	Zhang et al. (2012b)
		Pyroxenite				3.5	
		Gabbro	824 ± 3 Ma	SHRIMP and LA-ICP-MS U-Pb zircon	10.3 ~ 13.4	3.3 ~ 5.7	
			819 ± 3 ~ 827 ± 3 Ma	LA-ICP-MS zircon	5.8 ~ 17.3	3.6	Zhang et al. (2013a)
			848 ± 12 Ma	SHRIMP U-Pb zircon			Ding et al. (2008)
						3.6	Zhang et al. (2011b)
		Seafloor basalt				−1.2 ~ 0.4	Zhang et al. (2012b)
						2.6	Zhang et al. (2013a)
		Seafloor andesite				−1.1	
						−0.2 ~ 4.3	Zhang et al. (2011b)
	Xikou	Tuff	828 ± 4 Ma	LA-ICP-MS zircon	1.9 ~ 10.3		Wang et al. (2014a)
	Jingtan Formation	Dacite	820 ± 16 Ma	SHRIMP U-Pb zircon	2.3 ~ 8.6	−2.8	Zheng et al. (2008)
	Xucun	Granodiorite	826 ± 5 Ma	LA-ICP-MS zircon	−22.5 ~ 6.6		Wang et al. (2014a)
			850 ± 10 Ma	LA-ICP-MS zircon			Xue et al. (2010)
			823 ± 7 ~ 827 ± 7 Ma	LA-ICP-MS zircon	−0.8 ~ 9.9	−1.1 ~ −0.0	Wu et al. (2006)
		Granite	823 ± 8 Ma	SHRIMP U-Pb zircon		−1.7 ~ −0.8	Li et al. (2003a)
		Granodiorite	823 ± 8 Ma	SHRIMP and LA-ICP-MS U-Pb zircon	−25.6 ~ 11.2	−1.1	Wang et al. (2013a)
	Xiuning	Granodiorite				−0.8 ~ −0.2	Li et al. (2003a)
			832 ± 8 Ma	LA-ICP-MS zircon			Xue et al. (2010)
			824 ± 7 ~ 825 ± 7 Ma	LA-ICP-MS zircon	1.6 ~ 5.1	−1.0 ~ −0.6	Wu et al. (2006)
	Shexian	Granodiorite				−1.1	Li et al. (2003a)
			838 ± 11 Ma	LA-ICP-MS zircon			Xue et al. (2010)
			823 ± 9 ~ 824 ± 6 Ma	LA-ICP-MS zircon	−28.4 ~ 7.1	−2.1 ~ −0.4	Wu et al. (2006)
Boundary between S Anhui and SW Zhejiang	Shi'ershan	Lingshan Granite	823 ± 18 Ma	LA-ICP-MS zircon			Xue et al. (2010)
		Lianhuashan Granite	814 ± 26 Ma	LA-ICP-MS zircon			
Boundary between N Jiangxi and S Anhui	Shuangqiaoshan Group	Andesite	822 ± 6 Ma	LA-ICP-MS zircon		2.7	Zhou et al. (2012)
		Tuff	830 ± 5 Ma	LA-ICP-MS zircon		−0.3 ~ 0.7	
		Rhyolite	821 ± 5 Ma	LA-ICP-MS zircon			
N Jiangxi	Xingzi Group	Amphibolite	811 ± 12 Ma	SHRIMP U-Pb zircon		3.4 ~ 4.0	Li et al. (2013)
	Shaojiwa Formation	Basalt				0.0 ~ 0.7	
		Rhyolite	828 ± 6 Ma	SHRIMP U-Pb zircon		−0.8 ~ 0.8	
	Hanyangfeng Formation	Rhyolite	838 ± 4 Ma	SHRIMP U-Pb zircon			Shi et al. (2014)
	Guanyinqiao	Granitic gneiss	820 ± 5 Ma	LA-ICP-MS zircon	3.1 ~ 13.2		Wang et al. (2014a)
	Zhenzhushan	Dacite	849 ± 6 Ma	SIMS U-Pb zircon		−1.9 ~ −0.3	Li et al. (2010a)
		Basalt				2.1 ~ 4.8	
	Zhangyuan	Metabasalt				−1.0 ~ 3.9	Zhang et al. (2011b)
	Jiuling	Granodiorite	823 ± 8 Ma	SHRIMP U-Pb zircon		−3.1 ~ −0.6	Li et al. (2003a)
			814 ± 8 ~ 820 ± 4 Ma	LA-ICP-MS zircon	0.2 ~ 4.9	−1.8	Wang et al. (2014a)
					−20.6 ~ 8.9	−3.2	Wang et al. (2013a)
		Monzogranite	813 ± 4 Ma	LA-ICP-MS zircon	−2.4 ~ 7.1		Zhang et al. (2011a)

Table 1 (*continued*)

Location	Batholith or Pluton/ Group or Formation	Rock type	Age (Ma)	Method	Zircon $\varepsilon_{Hf}(t)$	Whole-rock $\varepsilon_{Nd}(t)$	Reference
		Cordierite bearing monzogranite	823 ± 2 Ma	LA-ICP-MS zircon	−1.4 ~ 8.5		
		Granite	819 ± 9 Ma	SHRIMP and LA-ICP-MS U-Pb zircon	0.8 ~ 6.5	−1.3	Wang et al. (2013a)
		Diorite enclave	831 ± 9 Ma	SHRIMP U-Pb zircon	−1.6 ~ 12.8	2.2	
NE Hunan	Xiyuankeng	Biotite monzogranite	804 ± 3 Ma	LA-ICP-MS zircon	−2.8 ~ 2.7		Zhang et al. (2011a)
	Yiyang	Komatiitic basalt	823 ± 6 Ma	SHRIMP U-Pb zircon			Wang et al. (2007a)
		Komatiitic basalt				1.6 ~ 1.8	Wang et al. (2004)
		Andesite				−2.6 ~ −1.9	
	Cangshuipu	High-mg volcanic rocks	824 ± 7 Ma	SIMS U-Pb zircon		−4.7 ~ −1.7	Zhang et al. (2012c)
			822 ± 28 Ma	SHRIMP U-Pb zircon			
	Changsanbei	Two-mica granite				−1.8	Wang et al. (2004)
		Plagiogranite				−2.5	
		Granodiorite	837 ± 6 Ma	LA-ICP-MS zircon	1.6 ~ 5.5	−2.5	Wang et al. (2014a)
	Daweishan	Granodiorite	805 ± 4 Ma	LA-ICP-MS zircon	1.4 ~ 5.2	−2.7	
						−2.7	Wang et al. (2004)
	Zhangbangyuan	Granodiorite	816 ± 5 Ma	SHRIMP U-Pb zircon		−3.6	Ma et al. (2009)
	Luoli	Granodiorite				−1.2	
	Weidong	Granodiorite				−1.5	
N Guangxi	Bendong	Biotite granodiorite				−5.5 ~ −3.9	Li et al. (2003a)
		Granodiorite	820 ± 18 Ma	SHRIMP U-Pb zircon			Li (1999)
			823 ± 4 Ma	LA-ICP-MS zircon			Wang et al. (2006a)
					−5.9 ~ −2.4		Wang et al. (2006b)
						−5.0 ~ −3.8	Ge et al. (2001b)
			823 ± 4 Ma	LA-ICP-MS zircon	−6.9 ~ −1.9	−5.0	Wang et al. (2013a)
						−5.2 ~ −4.2	Chen et al. (2014)
					−2.6 ~ −1.0		Zheng et al. (2007)
	Yuanbaoshan	Granite			−3.2 ~ −1.3		
			824 ± 4 Ma	ID-TIMS U-Pb zircon			Li (1999)
			824 ± 4 Ma	SHRIMP and LA-ICP-MS U-Pb zircon	−10.9 ~ −0.4	−5.6	Wang et al. (2013a)
			838 ± 5 Ma	LA-ICP-MS zircon	−4.0 ~ 0.3	−5.3	Wang et al. (2014a)
		Two-mica granite	823 ± 5 ~ 831 ± 5 Ma	LA-ICP-MS zircon	−14.9 ~ −0.4		Yao et al. (2014a)
		Muscovite granite	833 ± 6 Ma	LA-ICP-MS zircon	−9.4 ~ −1.2		
		Olivine pyroxenite				3.0 ~ 5.2	Ge et al. (2001c)
		Diabase				−3.4	
		Gabbro	855 ± 5 Ma	LA-ICP-MS zircon	5.2 ~ 12.3		Yao et al. (2014a)
	Sanfang	Leucogranite				−9.0 ~ −4.5	Li et al. (2003a)
		Leucogranite			−5.7 ~ −0.6		Zheng et al. (2007)
		Granite			−4.5 ~ −1.5		
			804 ± 5 Ma	LA-ICP-MS zircon			Wang et al. (2006a)
					−7.5 ~ −1.6		Wang et al. (2006b)
						−8.2 ~ −5.4	Ge et al. (2001b)
			826 ± 13 Ma	SHRIMP U-Pb zircon			Li (1999)
			804 ± 5 Ma	LA-ICP-MS zircon	−9.5 ~ −2.6	−5.9	Wang et al. (2013a)
	Dongma	High-Mg diorite			−6.2 ~ −2.0	−5.0 ~ −4.9	Chen et al. (2014)
		Granodiorite			−1.1 ~ −0.1	−5.9 ~ −3.2	
			824 ± 13 Ma	LA-ICP-MS zircon			Wang et al. (2006a)
			824 ± 13 Ma	LA-ICP-MS zircon	−2.8 ~ 0.8	−5.4	Wang et al. (2013a)
			837 ± 7 Ma	LA-ICP-MS zircon	−3.6 ~ 5.1	−5.9	Wang et al. (2014a)
						−5.1	Ge et al. (2001b)
	Zhaigun	Granodiorite	836 ± 3 Ma	LA-ICP-MS zircon		−4.9	Wang et al. (2006a)
						−2.9 ~ −2.7	Ge et al. (2001b)
	Longyou	Granodiorite				−4.4	
						−5.4	Wang et al. (2006a)

(*continued on next page*)

Table 1 (*continued*)

Location	Batholith or Pluton/ Group or Formation	Rock type	Age (Ma)	Method	Zircon $\varepsilon_{Hf}(t)$	Whole-rock $\varepsilon_{Nd}(t)$	Reference
			832 ± 5 Ma	LA-ICP-MS zircon	−5.5 ~ −0.6	−5.3	Wang et al. (2013a)
			832 ± 5 Ma	LA-ICP-MS zircon	−5.4 ~ 4.5	−5.4	Wang et al. (2014a)
	Mengdong	Granodiorite	833 ± 5 Ma	LA-ICP-MS zircon	−3.0 ~ −0.5	−3.3	
						−5.5 ~ −5.4	Ge et al. (2001b)
						−3.3	Wang et al. (2006a)
	Pingxing	Granite	835 ± 5 Ma	LA-ICP-MS zircon	−5.1 ~ 1.0	−4.2	Wang et al. (2014a)
						−4.2	Wang et al. (2006a)
	Hejiawan	Diabase	812 ± 5 Ma	LA-ICP-MS zircon			
	Dazhai	Granodiorite	834 ± 8 Ma	LA-ICP-MS zircon	−5.2 ~ −1.3		Wang et al. (2014a)
	Baotan	Pyroxene peridotite				−1.9	Ge et al. (2001c)
		Olivine pyroxenite				−1.2	
		Pyroxenite				−0.5	
		Gabbro-diabase				−2.9	
						−2.0	Zhou et al. (2004)
		Diabase				−7.0 ~ −4.2	Ge et al. (2001c)
		Diorite				−6.7	
						−5.1	Zhou et al. (2004)
	Longsheng	Gabbro				−0.8 ~ 2.4	
	Yangmeiao	Diabase	828 ± 7 Ma	SHRIMP U-Pb zircon			Li et al. (1999)
NE Guizhou	Fanjingshan Group	Basalt	814 ± 15 Ma	SHRIMP U-Pb zircon		−1.9	Zhou et al. (2009)
		Diabase	814 ± 6 ~ 831 ± 6 Ma	LA-ICP-MS zircon	−6.1 ~ 6.0	−1.5 ~ −0.4	
		Pillow lava				−3.6 ~ −1.9	
		Seafloor basalt				−4.2	
	Taoshulin	Muscovite-bearing leucogranite	839 ± 2 Ma	LA-ICP-MS zircon	−11.5 ~ 5.7		Wang et al. (2011a)
SE Guizhou	Xiutang	Granite	836 ± 5 Ma	LA-ICP-MS zircon			Fan et al. (2010)
Stage IV (ca. 805 ~ 750 Ma): Continental rift development							
S Anhui	Xucun	Diabase	804 ± 7 Ma	LA-ICP-MS zircon	3.7 ~ 14.5	−6.6 ~ −1.4	Wang et al. (2012a)
		Granitic porphyry	805 ± 4 Ma	LA-ICP-MS zircon	−4.1 ~ 6.7	−8.4 ~ −7.4	
	Puling Formation	Rhyolite, Tuff, Basalt	751 ± 8 ~ 765 ± 7 Ma	LA-ICP-MS zircon		−9.2 ~ 6.2	Wang et al. (2012a)
	Jingtan Formation	Tuff, Dacite	776 ± 10 Ma	LA-ICP-MS zircon	0.7 ~ 6.8	−1.9 ~ −1.7	Zheng et al. (2008)
Boundary between S Anhui and SW Zhejiang	Shangshu Formation	Diabase, Gabbro, Basalt, Andesite, Dacite, Rhyolite	794 ± 7 ~ 797 ± 5 Ma	LA-ICP-MS zircon		−1.9 ~ 6.2	Wang et al. (2012a)
	Shi'ershan	Leucogranite	779 ± 11 Ma	SHRIMP U-Pb zircon			Li et al. (2003b)
		Shi'ershan Granitic porphyry	785 ± 11 Ma	LA-ICP-MS zircon			Xue et al. (2010)
		Lianhuashan Granite	771 ± 17 Ma	SHRIMP U-Pb zircon	4.4 ~ 8.4	−1.1 ~ 0.0	Zheng et al. (2008)
			777 ± 7 Ma	LA-ICP-MS U-Pb zircon			
		Qixitian Granite	775 ± 5 Ma	LA-ICP-MS U-Pb zircon	0.9 ~ 8.5	0.4 ~ 0.7	
		Granite	779 ± 11 Ma	LA-ICP-MS U-Pb zircon	2.9 ~ 6.6	−1.0	Wang et al. (2013a)
NE Hunan	Yiyang	Dacite	797 ± 4 Ma	LA-ICP-MS zircon	−4.3 ~ 1.0		Wang et al. (2014a)
W Hunan	Qianyang	Gabbro				0.2	Wang et al. (2008b)
		Gabbro-diabase				0.2 ~ 0.4	
		Diabase	747 ± 18 Ma	SHRIMP U-Pb zircon		0.8	
						0.2 ~ 0.8	Wang et al. (2004)
		Basalt				2.7	
	Guzhang	Diabase				−0.5 ~ 1.1	
						−0.4 ~ 0.0	Wang et al. (2008b)
	Tongdao	Pyroxenite	772 ± 11 Ma	SHRIMP U-Pb zircon		−2.9	
N Guangxi	Tianpeng	Granite	794 ± 8 Ma	LA-ICP-MS zircon		−2.9	Wang et al. (2006a)
					−13.6 ~ −1.0		Wang et al. (2006b)
	Longsheng	Gabbro	761 ± 8 Ma	Single-grain zircon TIMS		−1.3 ~ −0.1	Ge et al. (2001a)
		Diabase				0.2 ~ 5.0	

* The whole-rock Hf isotopic compositions of Pingshui Formation, Beiwu Formation, Zhangcun Formation, Taohong tonalite and Xiqiu granodiorite.

On the basis of our studies on the stratigraphic sequences and magmatic records of the Yangtze and Cathaysia blocks, the boundary between these two blocks is marked by the Pingxiang-Jiangshan-Shaoxing Fault in the northeast with ophiolite exposed in places (e.g. Charvet et al., 1996; Guo et al., 1985; Shu et al., 1994, 2006; Shu, 2012; Shu and Charvet, 1996), but the boundary in the southwest is unclear because of poor outcrops and complex tectonic overprints. The southwestern margin of the Jiangnan Orogen (or Anhua-Luocheng Fault) or the Chenzhou-Linwu Fault has been suggested to be the possible location of the boundary in the southwest (Fig. 1b, e.g., Cawood et al., 2013; Charvet, 2013; Chen and Jahn, 1998; Wang et al., 2008c; Zhang and Zheng, 2013; Zhao and Cawood, 2012; Zheng et al., 2013). Still others insist on the Qinhang belt (also called the "Shihang belt") as the boundary between the Yangtze and Cathaysia blocks based on their regional research on the Mesozoic mineralization (e.g., Mao et al., 2011, 2013; Pan et al., 2009; Shui, 1987; Yang et al., 2009). According to Mesozoic mafic rocks with distinct Sr-Nd-Pb isotopes on either side of the Chenzhou-Linwu Fault, Wang et al. (2008c) suggested Chenzhou-Linwu Fault as the early Mesozoic boundary of the lithospheric mantle between the Yangtze and Cathaysia blocks. However, recent studies concluded that most of the early Paleozoic granites south of the Anhua-Luocheng Fault belong to crust-derived peraluminous S-type genesis and sharing the same Nd-Hf isotopes, implying the Anhua-Luocheng Fault as the crustal boundary between the Yangtze and Cathaysia blocks (e.g., Charvet, 2013; Wang et al., 2012e; Xia et al., 2014; Zhao et al., 2013).

Prior to the Neoproterozoic, the Yangtze Block and Cathaysia Block experienced independent histories (e.g., Gao et al., 1999; Qiu et al., 2000; Zheng et al., 2004, 2006; Xia et al., 2012; Yu et al., 2009, 2012). Since the Neoproterozoic, the Yangtze Block and Cathaysia Block as a unified South China entity underwent multiple tectono-magmatic activities such as in the early Paleozoic, early Mesozoic and late Mesozoic (e.g., Charvet, 2013; Xia et al., 2014; Xu et al., 2007; Zhou et al., 2006). The Mesozoic magmatism also produced a variety of large scale mineralization of economic significance (Sun et al., 2012). Thus, to sort out the Neoproterozoic tectonic evolution of both the Yangtze and Cathaysia blocks in terms of seafloor subduction and continental amalgamation is of fundamental importance towards a better understanding of the continental crustal evolution, crust-mantle interaction and mineralization in South China, which may also contribute to an objective assessment on whether supercontinent Rodinia may have any influenced on South China geology. Furthermore,

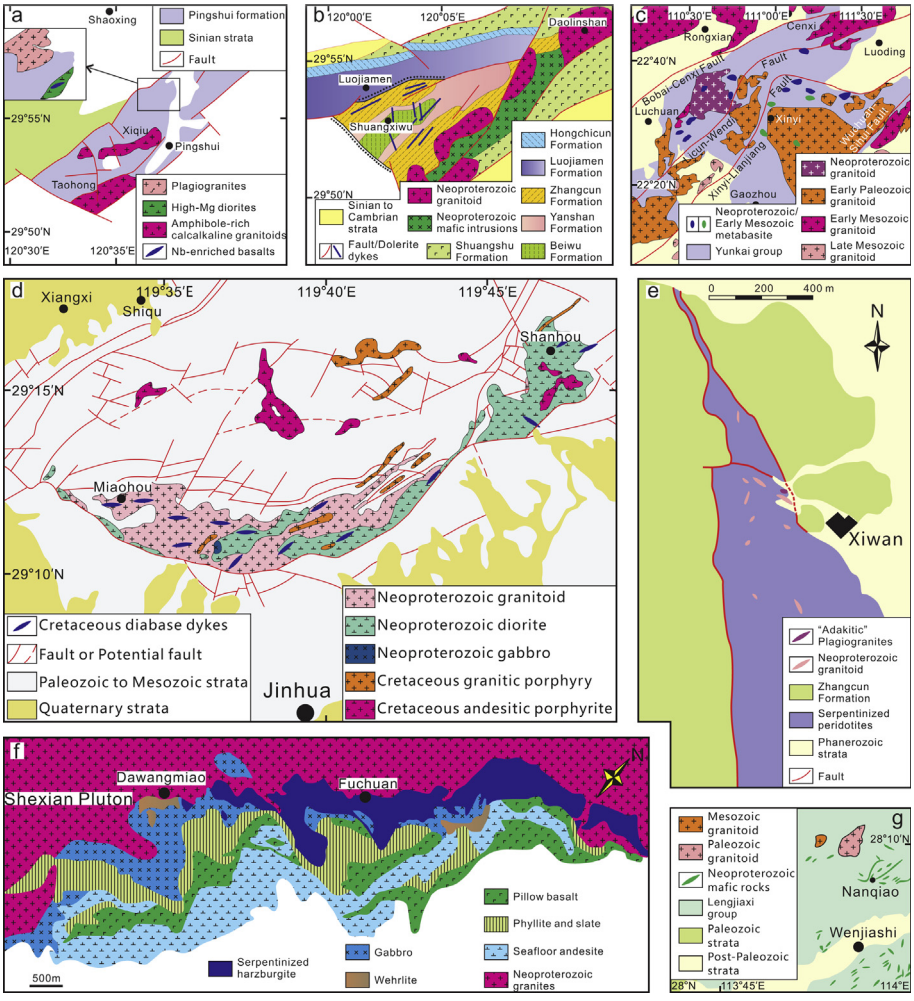

Fig. 2. Geological map of representative Neoproterozoic igneous rocks in South China: (a) Taohong and Xiqiu I-type tonalite-granodiorite together with Pingshui high-Mg diorites, Nb-enriched basalts and plagiogranites (modified after Chen et al., 2009a; Li et al., 2009). (b) Neoproterozoic sequences and intrusions in Shuangxiwu area showing the Baiwu, Yanshan and Zhangcun Formations of the Shuangxiwu Group together with shangshu, Hongchicun and Luojiamen Formations and Daolinshan granites (modified after Li et al., 2009; Yao et al., 2014c). (c) Neoproterozoic metabasites and Tiantangshan granites of the Yunkai domain (modified after Qin et al., 2007; Wang et al., 2014b). (d) Miaohou and Shanhou complexes (Xia et al., 2015). (e) NE Jiangxi ophiolite melange showing the Xiwan ultramafic rocks with granitic and plagiogranites lenses (modified after Li and Li, 2003; Li et al., 2008a). (f) Fuchuan ophiolite and Shexian granites (modified after Zhang et al., 2012b, 2013a). (g) Neoproterozoic mafic rocks of Nanqiao and Wenjiashi (modified after Yao et al., 2014c).

previous studies are mostly parochial with limited coverage in space and time, and thus there has been no generally preferred model of Neoproterozoic tectono-magmatic evolution in South China (e.g., Charvet, 2013; Chen et al., 2014; Greentree et al., 2006; Li et al., 1995, 2002, 2007b, 2008c, 2009; Shu et al., 2006; Shu, 2012; Wang et al., 2012a, 2013a, 2013b, 2014a, 2014b; Yao et al., 2014a, 2014c; Ye et al., 2007). Therefore, an integrated study on regional scale with a comprehensive coverage in space and time is needed to decode the unsolved mysteries, e.g., (1) the timing and processes of the amalgamation between the Yangtze and Cathaysia blocks; (2) the formation and evolution of Neoproterozoic subduction- and collision-related magmatism; (3) the southwestern extension of the boundary between the Yangtze and Cathaysia blocks; and (4) the possible relationship between the South China Block and supercontinent Rodinia.

2. Three tectono-magamatic belts in South China

South China separated from the North China Craton by the Qinling-Dabie belt to the north, from Tibet to the west by the Songpan-Ganzi belt and Panxi-Hannan belt, and from the Indochina Block by the Ailaoshan-Song Ma suture zone in the southwest. The Yangtze Block consists of minor Archean-Paleoproterozoic crystalline basement (e.g., TTG rocks, felsic gneisses and amphibolites) in northern Hubei Province and widespread Neoproterozoic igneous and sedimentary rocks (e.g., Gao et al.,1999, 2011; Qiu et al., 2000; Zheng et al., 2004, 2006; Jiao et al., 2009). However, in the Cathaysia Block, the Neoarchean basement is rarely found and the Paleoproterozoic migmatite, granitoid gneisses and amphibolite only outcrop in NW Zhejiang and NE Fujian Provinces (e.g., Fujian BGMR, 1985; Zhejiang BGMR, 1989; Xia et al., 2012; Yu et al., 2009, 2012; Zheng et al., 2011).

The collision between Yangtze and Cathaysia blocks gave rise to the Jiangnan Orogeny (also called the "Sibao" or "Jinning" Orogeny) (Fig. 1a). The Jiangnan Orogen (Fig. 1a), with a width of ~120 km and ENE-WSW extend of ~1500 km (Guo et al., 1980), located along the suture zone between the Yangtze and Cathaysia blocks. The orogen is composed of preexisting arc terranes (1000–860 Ma) and Neoproterozoic (860–750 Ma) igneous and

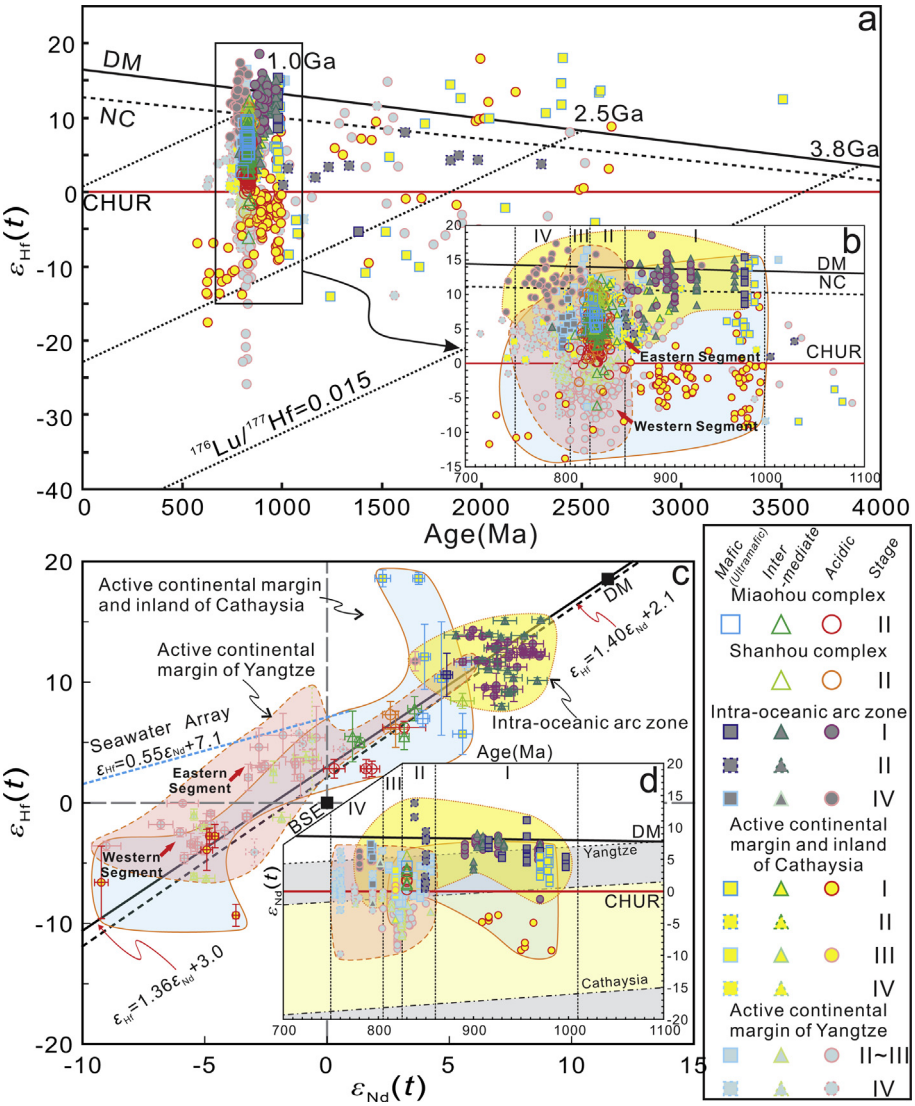

Fig. 3. (a), (b) Hf-isotope compositions of representative Neoproterozoic igneous rocks in South China. (c) $\varepsilon_{Nd}(t)$ vs. $\varepsilon_{Hf}(t)$ diagram for the Neoproterozoic igneous rocks in South China. The trend of the terrestrial array and seawater array after Vervoort and Blichert-Toft (1999) and Albarède et al. (1998). Bulk Silicate Earth (BSE) and Depleted Mantle (DM) from Blichert-Toft and Albarède (1997). (d) Whole-rock Nd-isotope compositions of Neoproterozoic igneous rocks in South China (the area of Yangtze and Cathaysia basement is after Chen and Jahn, 1998). Data sources are the same as in Table 1.

metasedimentary rocks (Fig. 1b; Table 1) (e.g., Gao et al., 2009; Li and Li, 2003; Li et al., 2003a, 2003b, 2009; Wang et al., 2013a, 2013b, 2014a, 2014b; Zhang and Zheng, 2013; Zhao and Cawood, 2012; Zheng et al., 2013). The metasedimentary rocks include two sets of lower greenschist facies sequences separated by a prominent angular unconformity (Wang et al., 2012a, 2014a). The underlying basement sequences are tightly folded and are dominated by sandstone, siltstone, slate, and phyllite and show flysch-like sedimentary characteristics, including the Sibao Group in north Guangxi, the Fanjingshan Group in northeast Guizhou, the Lengjiaxi Group in central Hunan, the Shuangqiaoshan/Jiuling Group in northwest Jiangxi, and the Xikou/Shangxi Group in south Anhui and northeast Jiangxi. All these rocks are locally unconformably overlain by slightly metamorphosed cover sequences which show open folds with rifting-environment depositional features (e.g., the Danzhou, Xiajiang, Banxi, Luokedong and Likou groups, respectively) and unmetamorphosed Sinian cover (Wang and Li, 2003; Wang et al., 2007a, 2014a; Zhang and Zheng, 2013; Zhao and Cawood, 2012; Zheng et al., 2013).

However, the volcanic rocks of Pingshui Formation and Shuangxiwu Group (~970–890 Ma) show very high $\varepsilon_{Hf}(t)$ and $\varepsilon_{Nd}(t)$ and geochemical characteristics of island arc magmatic rocks (Fig. 2a; Table 1; Chen et al., 2009b; Chen and Jahn, 1998; Li et al., 2009), implying an intra-oceanic arc regime. The ~860–840 Ma mafic rocks in N Zhejiang, NE Hunan and W Jiangxi are mainly tholeiitic in compositions and show both geochemical signatures of volcanic arc (e.g., mafic rocks from the Daolinshan and Liuyang-Wenjiashi area; Fig. 2g; Li et al., 2008b; Yao et al., 2014c) and N-MORB (e.g., mafic rocks from Fangxi and Nanqiao-Liuyang area; Fig. 2b, g; Yao et al., 2014c; Zhang et al., 2013b). Especially in the Nanqiao-Wenjiashi area (NE Hunan), both volcanic arc- and N-MORB-like mafic rocks exposed (Fig. 2g; Yao et al., 2014c), resembling those of modern back-arc basin basalts from intra-oceanic arc terranes. Thus, we propose a new scheme to disassemble the Jiangnan Orogen of the southeastern margin of the Yangtze Block into two belts along the Jingdezhen-Yifeng-Wanzai Fault: the intra-oceanic arc zone to the southeast closer to the Cathaysia Block and the active continental margin of the Yangtze Block to the northwest inner land (Fig. 1b).

In the Cathaysia Block, the Neoproterozoic sequences are defined as the Mamianshan Group in Fujian, Longquan Group in Zhejiang and Taoxi Group in NE Guangdong (Fig. 1b; e.g., Fujian BGMR, 1985; Zhejiang BGMR, 1989). However, in the previously defined Cathaysia basement (including the previously defined Badu, Chencai, Mayuan, Hezi/Xunwu and Yunkai Groups along the Wuyi, Nanling and Yunkai domains), abundant schist, granitoid gneiss, migmatite and pyroclastic rocks were recently dated to be of Neoproterozoic and even early Paleozoic age (e.g., Gao et al., 2014; Wan et al., 2007, 2010; Li et al., 2010b; Zeng et al., 2008; Charvet et al., 2010; Yu et al., 2009, 2010, 2012; Wang et al., 2013b, 2014b and references therein). In addition, relatively minor amphibolite, metagabbro, metadiabase, bimodal volcanic rocks and even ophiolitic mélange expose sporadically or occur as lens, pods and fragments, which might be relics of Neoproterozoic subduction assemblages in the Cathaysia block (e.g., Shu, 2012; Shu et al., 2006, 2008a, 2008b, 2011; Wang et al., 2011a, 2013b, 2014b; Yao et al., 2014b; Zhang et al., 2012a; This work). The recent studies of Miaohou and Shanhou complexes (Fig. 2d; Table 1; Xia et al., 2015) together with Zhuji and Chencai mafic rocks (Table 1; Shu et al., 2011; Wang et al., 2012b) near the Jiangshao Fault also imply a tectonic setting of active continental margin in the Cathaysia Block.

Thus, we here divide the amalgamation domain between the Yangtze and Cathaysia blocks into three zones from northwest to southeast: the Yangtze active continental margin, the intra-oceanic arc zone, and the Cathaysia active continental margin

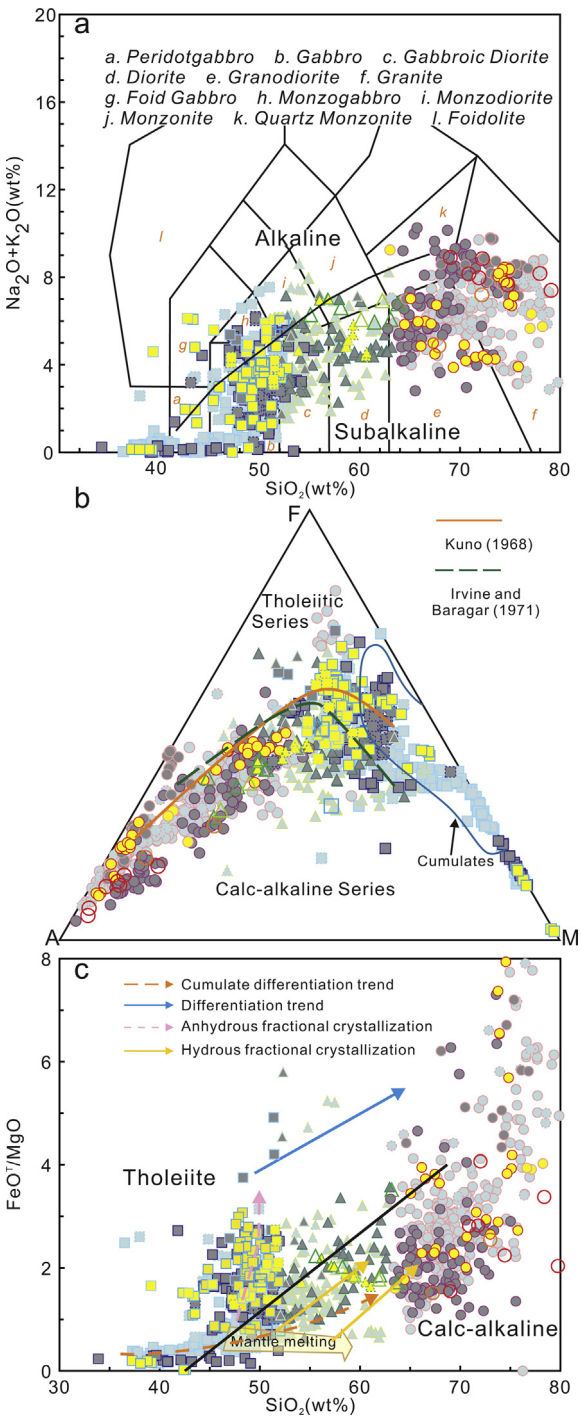

Fig. 4. (a) The total alkali vs. silica (TAS) diagram (after Middlemost, 1994) used for the classification of the Neoproterozoic igneous rocks in South China. (b) The AFM diagram of Neoproterozoic igneous rocks in South China; the boundary lines are after Kuno (1968) and Irvine and Baragar (1971) and the field for cumulates is after Beard (1986). (c) FeO^T/MgO vs. SiO_2 variation diagram for the data shown in (a) and (b). The calc-alkaline and tholeiite dividing line of Miyashiro (1974) is plotted for reference. Mantle melting, anhydrous fractional crystallization and hydrous fractional crystallization trends are after Grove et al. (2012). Symbols are the same as in Fig. 3. Data sources are: Chen et al., 2009a, 2009b, 2014; Ding et al., 2008; Fan et al., 2010; Gao et al., 2009; Ge et al., 2000a, 2000b, 2001a, 2001b, 2001c; Li and Li, 2003; Li et al., 1997, 2003a, 2005, 2007a, 2008a, 2008b, 2009, 2010a, 2013; Ma et al., 2009; Peng et al., 2006; Qi et al., 1986; Qin et al., 2005, 2007; Shu et al., 2008a, 2011; Xia et al., 2015; Xing et al., 1988; Xu and Qiao, 1989; Xue et al., 2010; Yao et al., 2014a, 2014b, 2014c; Ye et al., 2007; Wang and Shu, 2007; Wang et al., 2004, 2006a, 2007a, 2008a, 2008b, 2012a, 2013b, 2014b; Wu et al., 2001, 2006; Zhang et al., 2011b, 2012a, 2012b, 2012c, 2013a, 2013b; Zheng et al., 2008; Zhou, 1989; Zhou et al., 2003, 2004, 2009, 2012, 1993.

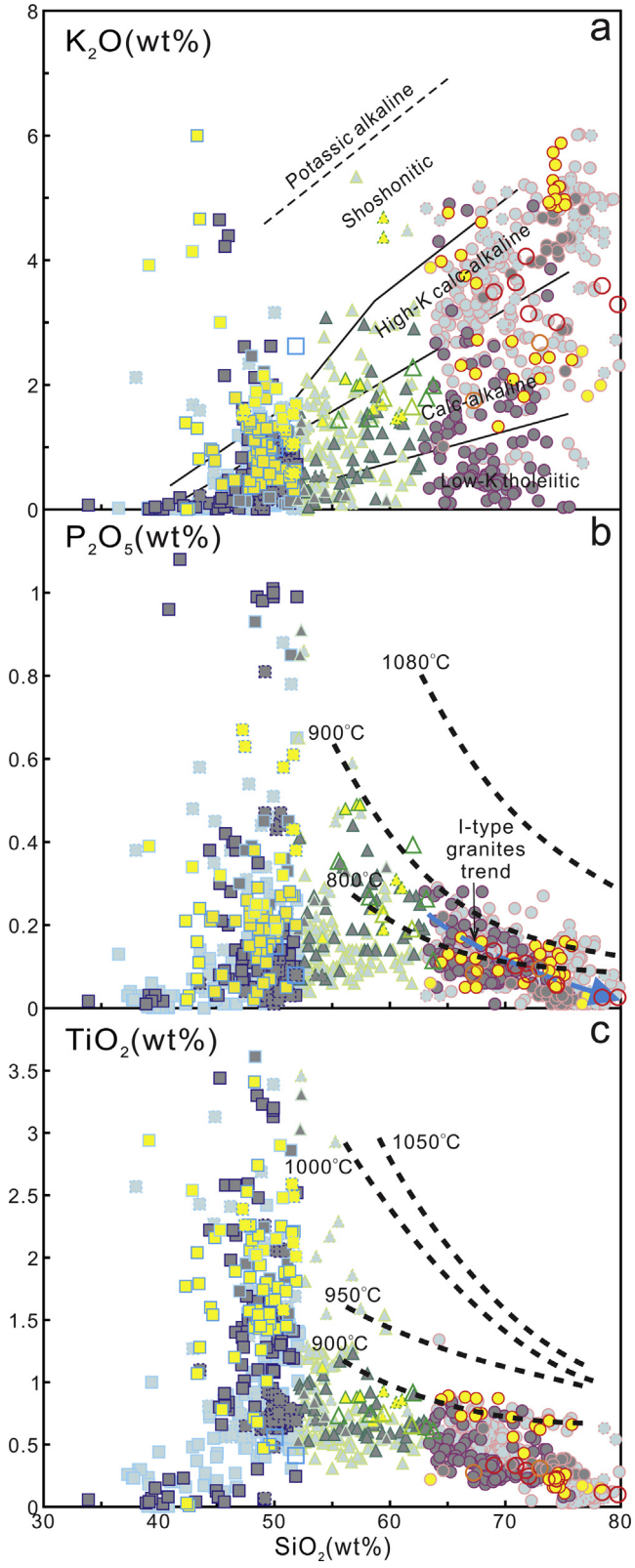

Fig. 5. Harker diagram of major-element compositions of the Neoproterozoic igneous rocks in South China: (a) K_2O vs. SiO_2 diagram (after Peccerillo and Taylor, 1976), where the dotted line represents the division between potassic alkaline and shoshonitic suites (after Calanchi et al., 2002); (b) P_2O_5 vs. SiO_2 diagram (after Harrison and Watson, 1984), where the I-type granite trend follows Chappell (1999); (c) TiO_2 vs. SiO_2 diagram (after Green and Pearson, 1986). Symbols and data sources are the same as in Fig. 4.

and inland (Fig. 1b). Based on synthesis of the previous studies, we also propose to divide the Neoproterozoic amalgamation and magmatism between the Yangtze Block and Cathaysia Block into four stages: stage I (~1000–860 Ma), development of oceanic arc and Cathaysia continental arc; stage II (~860–825 Ma), development of bidirectional subduction and continental arc on the Yangtze Block; stage III (~825–805 Ma), Yangtze-island arc-Cathaysia continent-arc-continent collision and the Jiangnan Orogenesis; stage IV (ca. 805–750 Ma), development of continental rift between the Yangtze Block and Cathaysia Block (also see Table 1).

3. Intra-oceanic arc zone

3.1. Stage I (ca. 1000–860 Ma) oceanic arc development

Wang et al. (2014a) divided the Jiangnan Orogen into the eastern and western segments largely along a nearly N-S boundary stretching across northern and central Hunan Province (Fig. 1b). Ophiolite suites have been found in two localities within the basement sequences in the eastern Jiangnan Orogen (i.e., the South Anhui and Northeast Jiangxi ophiolites; Figs. 1b, 2e, f and Table 1). The ophiolites have been previously dated at 1.05–0.96 Ga by the Sm-Nd isochron method (e.g., Chen et al., 1991; Li et al., 1997; Zhang et al., 1990; Zhou and Zhu, 1993; also see Table 1). However, new SHRIMP and LA-ICP-MS U-Pb zircon ages of gabbros in the South Anhui have shown that the ophiolites (Fig. 2f) may have formed at ca. 830 Ma (Ding et al., 2008; Zhang et al., 2012b, 2013a). The NE Jiangxi ophiolite are a suite of ophiolitic mélange that occurs scattered along the NE Jiangxi Fault System, extending for ~100 km (Fig. 1b). It is well exposed in a few localities including Zhangshudun, Xiwan (Fig. 2e), Maoqiao, Rao'er and Zhangcun, where a large number of ophiolitic blocks were structurally enclosed in a volcanic-sedimentary sequence of Shuangqiaoshan Group (Li and Li, 2003). Two types of basalts were observed within the NE Jiangxi ophiolites (Li et al., 1997). Island arc-type basalt is predominant and displays varying enrichment in LILEs (Sr, K and Rb), Th and LREEs and depletion in HFSEs (Zr, Hf, Nb, Ta and Ti). Minor N-MORB-type basalt was also observed in the ophiolites, and shows LREE-depletion with no negative Nb-Ta anomaly. Combined with their consistently high initial Nd isotopic ratios and the geochemical characteristics (Table 1), the NE Jiangxi ophiolites are best interpreted as reflecting a "supra-subduction zone" (SSZ) setting (Pearce et al., 1984; Li et al., 1997). The plagiogranite of NE Jiangxi ophiolitic rocks (Fig. 2e) yielded a SHRIMP zircon U-Pb age of 968 ± 23 Ma (Li et al., 1994) and 970 ± 21 Ma (Gao et al., 2009). The age range among subduction-related ophiolitic subunits can be longer than 20–30 m.y, but the age range of the SSZ-type ophiolite is commonly less than 10 m.y. (Dilek and Furnes, 2011). Therefore, although both considered as the SSZ-type ophiolite suite (Ding et al., 2008; Li and Li, 2003; Zhang et al., 2012b, 2013a), the South Anhui and Northeast Jiangxi ophiolites might be two different ophiolite suites formed at different time during the Neoproterozoic amalgamation in South China.

The Shuangxiwu Group (Fig. 2a–b), composed mainly of basaltic, andesitic and rhyolitic volcanic rock and flysch formation (Zhejiang BGMR, 1989) were previously suggested to be formed in an active continental margin setting (Li et al., 2008b, 2009). Li et al. (2009) suggested that the basaltic, andesitic and rhyolitic volcanic rocks from the lower, middle and upper Shuangxiwu Group (i.e., Pingshui, Beiwu and Zhangcun Formation) have formed at ~970 Ma, 926 Ma and 891 Ma, respectively. In fact, well-preserved in the Shuangxiwu area of NE Zhejiang and the Zhangshudun area of NE Jiangxi (Fig. 2a, b, e) are the SSZ-type

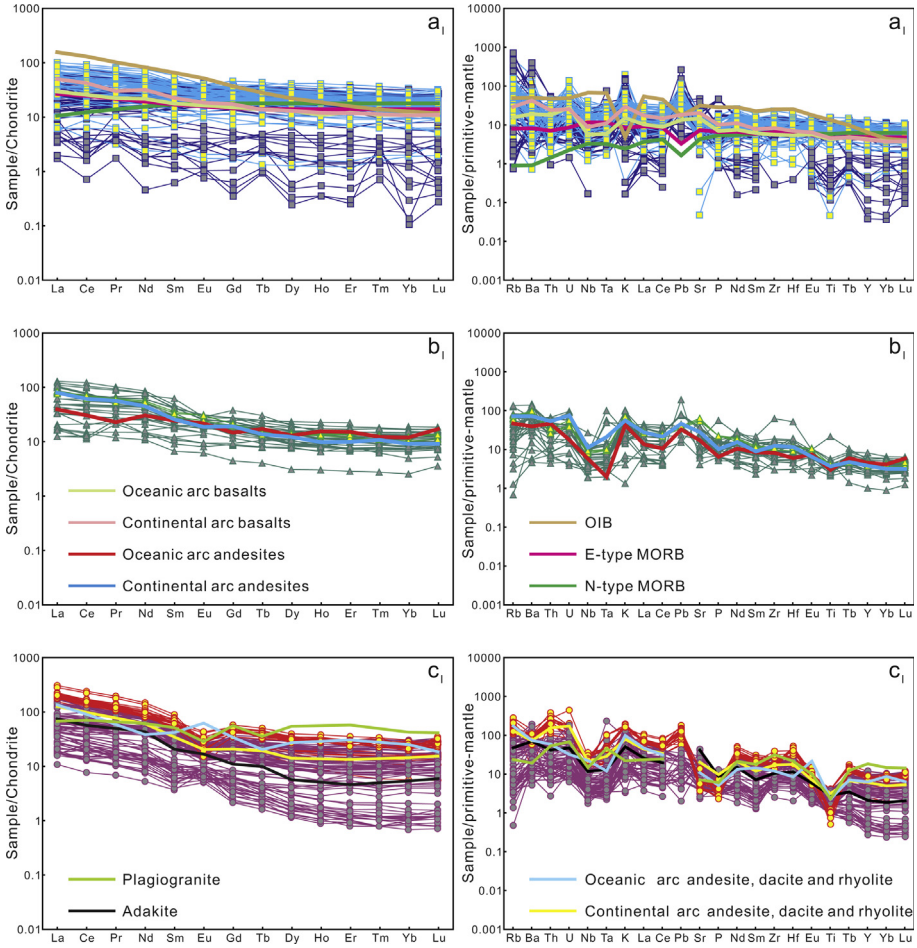

Fig. 6. Chondrite-normalized REE patterns and Primitive mantle-normalized multiple trace element diagrams (spidergrams) of the Neoproterozoic igneous rocks in South China. (a_I), ($a_{II–III}$) and (a_{IV}) ultramafic and mafic rocks of stage I, stage II–III and stage IV magmatism, respectively; (b_I), ($b_{II–III}$) and (b_{IV}) intermediate rocks of stage I, stage II–III and stage IV magmatism, respectively; (c_I), ($c_{II–III}$) and (c_{IV}) felsic rocks of stage I, stage II–III and stage IV magmatism, respectively. The chondrite and primitive mantle values are from Sun and McDonough (1989). The present-day average E-type MORB, N-type MORB and OIB are from Sun and McDonough (1989); Oceanic arc basalts, Continental arc basalts, Oceanic arc andesites and Continental arc andesites are from Condie (1989) and Kelemen et al. (2003). Adakite, Plagiogranite, Oceanic arc ADR (andesite, dacite and rhyolite) and Continental arc ADR are from Drummond et al. (1996). Symbols and data sources are the same as in Fig. 4.

ophiolite suite (including Xiwan "adakitic" plagiogranite lenses exposed as separate blocks scattered within the serpentinized matrix), arc-like volcanic rocks (e.g., seafloor basalt, andesite, dacite and rhyolite from Shuangxiwu Group), subduction-related granitoids (e.g., Taohong and Xiqiu tonalite–granodiorite which intruded into the Pingshui Formation), plagiogranites (e.g., Pingshui plagiogranite), adakitic rocks (eg., Pingshui high-Mg andesites) and Nb-enriched basalts, which were dated at 970–860 Ma (e.g., Chen et al., 1991, 2009a, 2009b; Gao et al., 2009; Li et al., 1994, 2009; Li and Li, 2003; Wang et al., 2013c; Ye et al., 2007; also see Fig. 1b and Table 1). The associated plagiogranite, andesite, amphibolite-bearing tonalite and I-type granodiorite have zircon U-Pb ages of 970–890 Ma and show an arc-like geochemical affinity with positive $\varepsilon_{Hf}(t)$ and $\varepsilon_{Nd}(t)$ (e.g., Chen et al., 2009a, 2009b; Gao et al., 2009; Li et al., 1994, 2009; Li and Li, 2003; Ye et al., 2007; also see Figs. 1b, 3a–d and Table 1). Considering that there are no existence of pre-Neoproterozoic basement rocks in this area, we propose that study proves that these arc-like magmatic rocks were likely to have formed in an intra-oceanic arc regime. Micas from a very small outcrop of the Tianli schists in the eastern Jiangnan Orogen were dated at ~1000 Ma by *in situ* laser-ablation Ar-Ar method (Li et al., 2007b), and the glaucophane-bearing schist gave the metamorphic age of 866 ± 10 Ma (K-Ar method; Shu et al., 1994; Charvet et al., 1996). The Xiwan leucogranites in the NE Jiangxi ophiolitic suite, interpreted as anatexis product of arc-derived sedimentary materials, were dated at 880 ± 19 Ma (e.g., Li et al., 2008a). It is obvious that the magmatism along the Zhangshudun-Shuangxiwu areas in the eastern segment of the Jiangnan Orogen (closer to the Jiangshan-Shaoxing Fault) is significantly older than that along the western segment of the Jiangnan Orogen and Fuchuan area in South Anhui (Fig. 2f) (e.g., Chen et al., 2009a, 2009b; Ding et al., 2008; Gao et al., 2009; Li et al., 2008a, 2009; Wang et al., 2013a, 2014a; Ye et al., 2007; Zhang et al., 2013a; also see Table 1).

In the Yunkai Group, there occur abundant ultramafic-mafic rocks as interlayers, lenses and pods. These rocks have commonly experienced strong deformation and greenschist- to amphibolite-facies metamorphism (Zhang et al., 2012a; Fig. 2c). Li (1993) gave a Sm-Nd isochron age of 971 ± 69 Ma for plagioclase amphibolite in the Yunkai Group. Nan (1994) reported the zircon U-Pb ages of ~1035–900 Ma and ~940–910 Ma for the amphibolite and dacite-porphyry in the Yunkai Group, respectively. Qin et al. (2006) and Zhang et al. (1998) also considered that the plagioclase amphibolite and dacite-porphyry in the Yunkai Group most likely formed at ~1000–910 Ma (Lao and Hu, 1997). Recently, a small amount of ~1000–980 Ma amphibolite, metagabbro and metadiabase lens or pods are found in the Yunkai Domain and were considered to be the relics of the earliest Neoproterozoic arc and back-arc

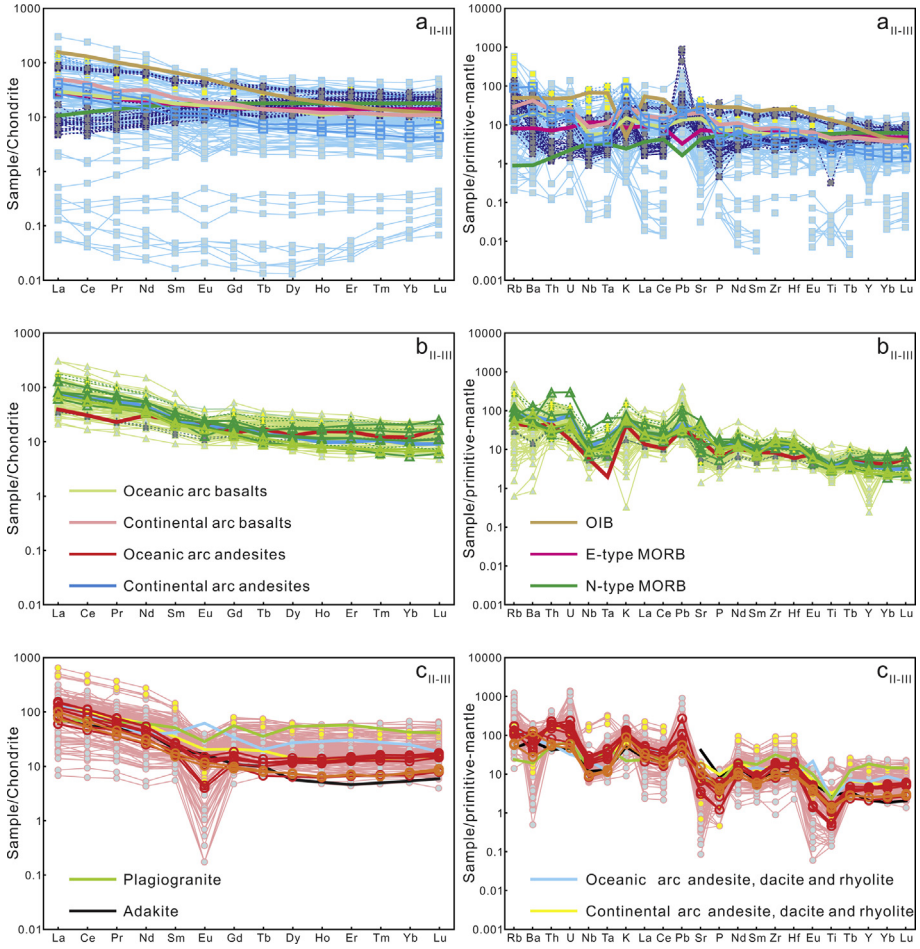

Fig. 6 (*continued*)

system in the Cathaysia block (e.g., Peng et al., 2006; Qin et al., 2006; Wang et al., 2013b; Zhang et al., 2012a; also see Figs. 1b, 2c and Table 1). Nevertheless, our study shows that those meta-mafic rocks exhibit different geochemical characteristics on either side of the possible boundary along Xinyi and Luoding (or Lianjiang-Xinyi Fault) (Fig. 2c). The meta-mafic rocks located on the northwest side of the Xinyi-Luoding Fault are mainly tholeiitic and show intra-oceanic arc-like affinity whereas those on the southeast of the Fault are mainly calc-alkaline and show continental arc-like affinity (Figs. 4b–c, 6, 7a–d; Wang et al., 2013b; Zhang et al., 2012a). Beside the mafic rocks, there are also felsic rocks on the northwest of the Xinyi-Luoding fault which intruded the Yunkai Group such as dacite-porphyry with the zircon evaporate age of ~940–920 Ma (Zhang et al., 1998) and Tiantangshan granitic gneiss with SHRIMP U-Pb zircon age of 906 ± 24 Ma (Qin et al., 2006). The 1000–900 Ma arc-related magmatic rocks northwest of the Xinyi-Luoding Fault resemble those in the Zhangshudun-Shuangxiwu area, implying that the line along Xinyi and Luoding (or Lianjiang-Xinyi Fault, Fig. 2c) might be the southwestern boundary between the Yangtze Block and Cathaysia Block in the Neoproterozoic. Accordingly, we can distinguish the Yangtze Block and Cathaysia Block along Jiangshan-Shaoxing-Pingxiang-Shuangpai-Xinyi structure zone (Yao et al., 2014c and this work).

The stage I ultramafic rocks (e.g., peridotite, pyroxenite and some gabbro; Table 1) from the NE Jiangxi ophiolite suite exhibit typical cumulate textures with high MgO and low Fe_2O_3, K_2O and Na_2O (Fig. 4a–c; Li et al., 1997; Xu and Qiao, 1989; Zhou, 1989; Zou et al., 1993). Their chondrite-normalized REE patterns (REE patterns) and primitive mantle-normalized incompatible element spidergrams (spidergram patterns) resemble those of typical cumulate rocks highly depleted in these incompatible elements (Fig. 6a_I). Here we declare that geochemistry of cumulate rocks may not be suitable for discriminating petrogenesis and tectonic setting when using some diagrams.

The mafic rocks include altered arc tholeiite, Nb-enriched basalt, dolerite and gabbro with some being metamorphosed (Table 1). The majority of these rocks are sub-alkaline, straddling the boundary of tholeiite and calc-alkaline series (Fig. 4a–c). In the K_2O vs. SiO_2 diagram (Fig. 5a), they dominantly fall into the low-K tholeiite and calc-alkaline fields although a few plot in the high-K calc-alkaline and shoshonitic fields. Most of these rocks have oceanic arc basalt- or continental arc basalt-like REE and spidergram patterns characterized by enrichments of Rb, Ba, Th, U and LREEs but depletion of high field strength elements (HFSEs) with pronounced negative Nb-Ta and weak negative P, Ti anomalies relative to the neighboring elements (Fig. 6a_I), whereas some rocks show N-MORB or E-MORB like REE and spidergram patterns (Fig. 6a_I). The apparent positive Pb anomaly may be due to crustal assimilation or subducted oceanic sediment contribution (Fig. 6a_I). Although minor mafic rocks fall into the alkaline within-plate basalt field in the Hf/3-Th-Ta diagram, the majority of these rocks plot into the fields of island arc tholeiites, back-arc basalts and N-type or E-type MORB in both Hf/3-Th-Ta and Y/15-La/10-Nb/8 diagrams (Fig. 7a–b). Although some intraplate basalts show depletion in Nb, Ta and Ti probably due to crustal contamination (Ellam and Cox, 1991; Hawkesworth et al., 1995), their high Ti/Zr

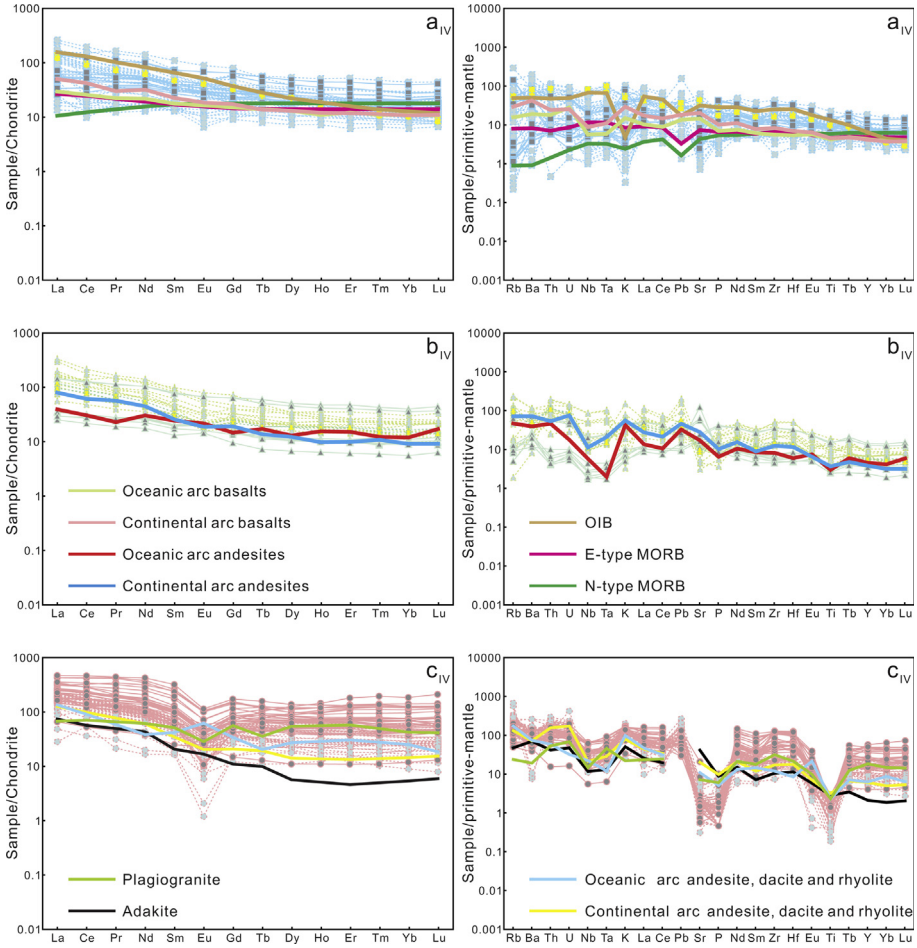

Fig. 6 (*continued*)

and low Zr/Y, Th/Yb and Ta/Yb also indicate the oceanic arc basalts and MORB affinities (Fig. 7c–d). It is worth to note that the Nb-enriched arc basalts (Defant et al., 1992; Kepezhinskas et al., 1996) are found in both Pingshui and Yunkai areas with high Nb/La and TiO_2 (Figs. 5c, 10b).

The andesite, high-Mg diorite and tonalite constitute the assembly of intermediate rocks in stage I. Although these rocks staddle the boundary between volcanic arc and within-plate fields in the Rb/30-Hf-Ta*3 diagram, they all plot in the volcanic arc field in the Y + Nb vs. Rb diagram (Fig. 8c–d). Most of these intermediate rocks show steep REE patterns with enrichment of LREEs and remarkably negative Nb-Ta, P, Sr and Ti anomalies in spidergram patterns, corresponding to oceanic arc or continental arc andesites (Fig. 6b_I). However, their low Th, La/Yb and Th/Yb character is similar to that of oceanic arc andesites (Fig. 8a–b). In the Pingshui area, the high-Mg andesites display high Sr/Y and low Y, which are characteristic of adakites (Fig. 10a), and their high Na_2O/K_2O (7.93–10.6), $Mg^{\#}$ (>60) and MgO (5.84–6.91 wt.%) (Chen et al., 2009a) are consistent with the definition of normal adakites (O-type adakites) and differ from other adakite-like rocks (e.g., "C-type" adakites or "K"-adakites; Moyen, 2009). Their incompatible element patterns are also similar to those of adakites with relatively weak Ta depletion (Castillo, 2012; Fig. 6b_I).

The felsic rocks of stage I mainly consist of amphibole-bearing granodiorite, amphibole-bearing plagiogranite, leucogranite, dacite and rhyolite. it is noteworthy that the Xiwan leucogranites, the peraluminous (A/CNK = 1.0–1.24) S-type granites show low total REEs and flat REE patterns with a significant positive Eu anomaly and relative enrichments in Th, Sr, P, Zr, Hf and Ti, probably due to small degrees of partial melting of metasedimentary rocks (Li et al., 2008a). Considering the distinct genesis between the leucogranites and other felsic rocks of stage I magmatism, we will not consider the leucogranites when discussing the stage I magmatism. Except for the Xiwan leucogranites, the majority of these feisic rocks are analogous to island arc granitoid or oceanic plagiogranite. These feisic rocks are metaluminous to weakly peraluminous, mostly Na_2O rich, and plot in the field of I-type granites (Fig. 9a, e). Compositionally intermediate, these felsic rocks also straddle the boundary between volcanic arc and within-plate fields in the Rb/30-Hf-Ta*3 diagram and plot in the volcanic arc field of the Th/Yb vs. Nb/Yb diagram (Fig. 8c–d). The majority of these rocks exhibit right-leaning REE patterns with depletion of HREEs and enrichment in LILEs with strong negative Nb-Ta, P and Ti anomalies in spidergrams, consistent with being of oceanic arc or continental arc affinity (Fig. 6c_I). It is noteworthy that the Xiwan plagiogranite show positive or no Eu anomalies, high Sr/Y and low Y, resembling adakites (Fig. 10a). Li and Li (2003) and Gao et al. (2009) thus suggest these plagiogranites as adakitic granites. Nevertheless, plagioclase holds such high Sr/Y and low Y itself, hence the plagioclase rich plagiogranites commonly display adakite signatures. Thus, it remains unclear if we should call the Xiwan plagiogranite as adakites or adakitic granites and ascribed them to products of low degree partial melting of subducted, hydrous oceanic crust at pressures high enough to stabilize garnet and amphibole (Li and Li, 2003). Although Li and Li (2003) and Chen et al. (2009a) interpreted that Xiwan and Pingshui plagiogranites, which

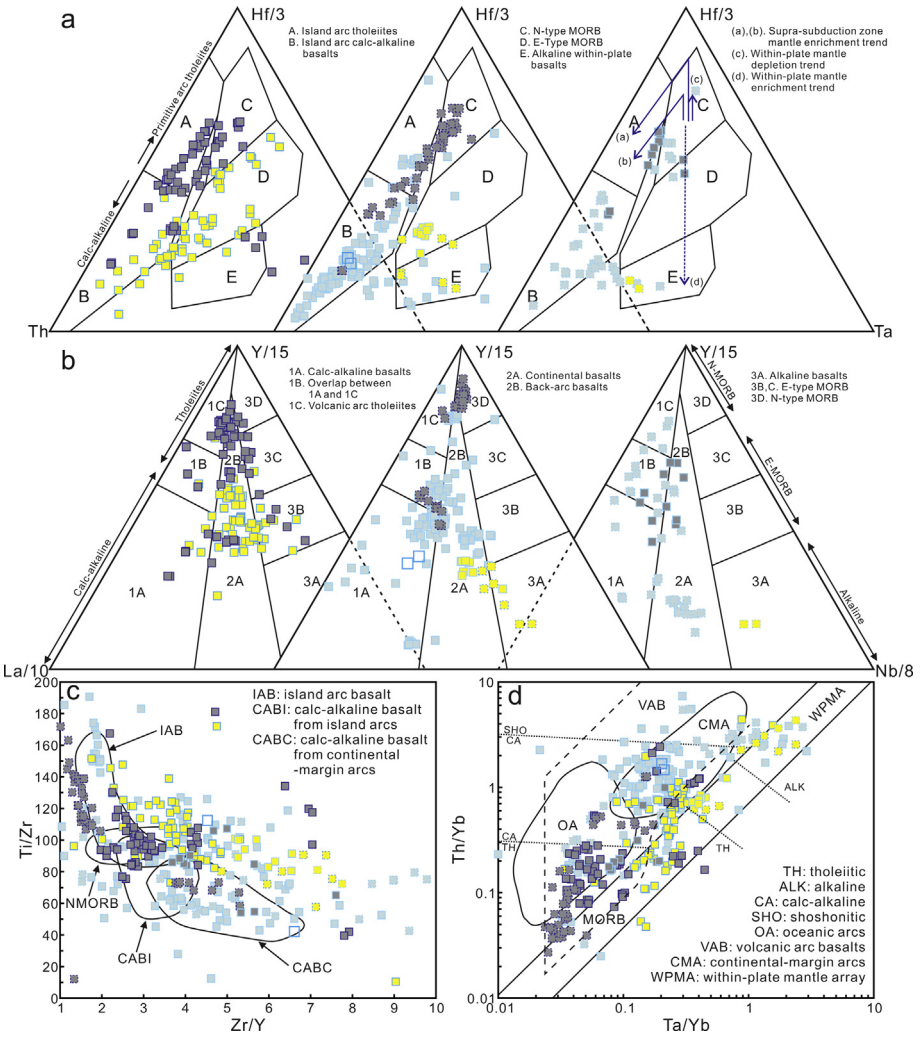

Fig. 7. (a) Hf/3-Th-Ta diagram (after Wood, 1980); (b) Y/15-La/10-Nb/8 diagram (after Cabanis and Lecolle, 1989); (c) Ti/Zr vs. Zr/Y diagram (after Condie, 1989); (d) Th/Yb vs. Ta/Yb diagram (after Condie, 1989 and Alabaster et al., 1982). Symbols and data sources are the same as in Fig. 4.

might not be regarded as adakitic granites, were generated by partial melting of subducted slab. Gao et al. (2009) argued that the plagiogranite more likely resulted from fractional crystallization of hornblende and accessory minerals such as apatite and ilmenite from basaltic parent magmas derived from melting of the mantle wedge beneath an island arc.

All the geochemical features of stage I magmatic rocks, in combination with their extremely depleted Nd and Hf isotopic compositions (Fig. 3a–d; Table 1), are most consistent with their formation from parental magmas derived from partial melting of metasomatized mantle wedge similar to the petrogenesis of the present-day Izu-Bonin and Tonga-Kermadec arc magmatism (Tamura and Tasumi, 2002; Leat et al., 2007). In Fig. 4c, they also yield along the differentiation trend or fractional crystallization trend of mantle-derived melt. All the stage I magmatic rocks from intra-oceanic arc zone, especially those felsic rocks with high Na_2O/K_2O and Low K_2O content (Fig. 5a), implying a low-K tholeiitic source. In this regard, the geochemical and Nd-Hf isotopic compositions of the stage I magmatic rocks indicate an ocean-ocean subduction and island arc setting without the involvement of K-rich continental crustal materials. Otherwise, the association of adakitic rocks (eg., Pingshui high-Mg andesites) and Nb-enriched arc basalts points to the possibility of slab melting where the subducting ocean crust is warm and yound (≤25 Ma) (Castillo, 2012; Defant and Drummond, 1990; Defant and Kepezhinskas, 2001; Kepezhinskas et al., 1996). Thus, the subduction-related melt in stage I were derived from mantle wedge metasomatized by both melting and dehydration of subducting slab, which is also supported by its high Hf, Cr and Ni contents and high Th/Yb, Nb/Yb and Nb/Th (Fig. 11a–d). In addition, according to our $\varepsilon_{Nd}(t)$ and SiO_2 modelling (Fig. 12), the stage I magmatism could also be explained by fractionation crystallization of primary arc magmas or the mixing of mantle-derived and slab-derived melt.

3.2. Stage II (ca. 860–825 Ma) back-arc basin development

The stage II magmatism produced mainly mafic rocks with minor rocks of intermediate composition (Table 1). The ~860–840 Ma N-type MORB and within-plate mafic rocks include gabbro or diabase dykes parallelly intruding the Shuangxiwu Group strongly deformed and metamorphosed to greenschist facies and basalts or dolerites interlayered and stratoid in the greenschist-facies sedimentary sequences of the Lengjiaxi and Shuangqiaoshan Groups (Li et al., 2008b; Yao et al., 2014c; Zhang et al., 2013b). These mafic rocks with variably high Hf, Cr and Ni and Nb/Th (Fig. 11a, c, d) straddle the tholeiitic-calc-alkaline compositional boundary (Figs. 4b–c, 5a) and can be divided into two groups. The first group is characterized by LREE depletion, mostly with a weak Eu anomaly and without a negative Nb, Ta, Zr, Hf anomaly, resembling the present-day N-type MORB. The second group

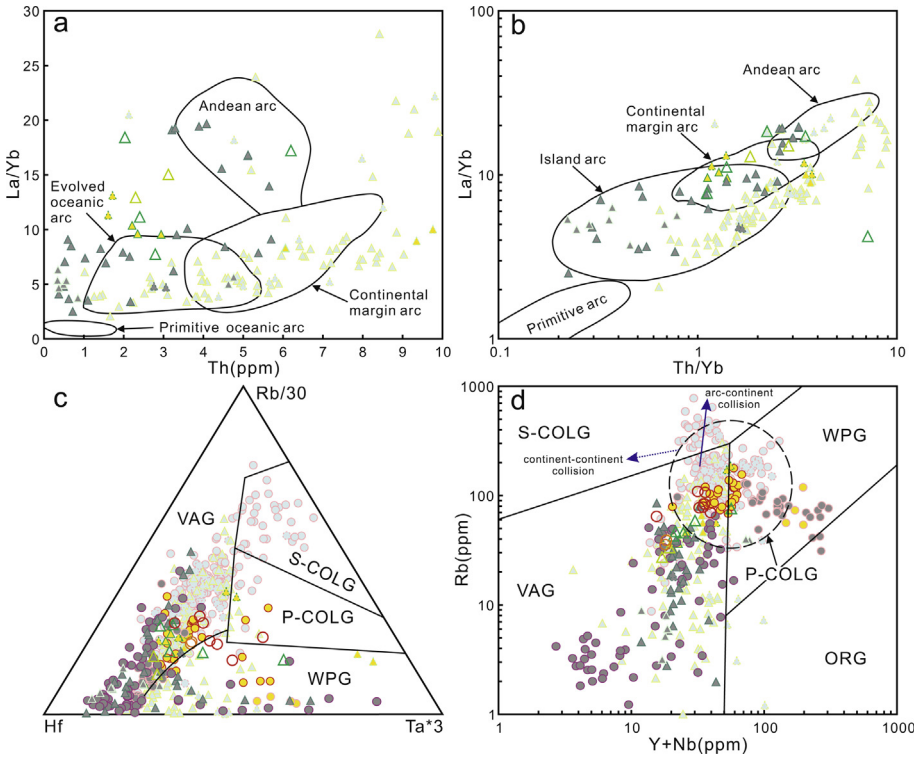

Fig. 8. (a) La/Yb vs. Th diagram (after Bailey, 1981); (b) La/Yb vs. Th/Yb diagram (after Condie, 1989); (c) Rb/30-Hf-Ta*3 discrimination diagram (after Harris et al., 1986); (d) Rb vs. (Y + Nb) discrimination diagram (after Pearce, 1996). Symbols and data sources are the same as in Fig. 4.

exhibits LREE enrichment with a weak Eu anomaly, and shows variable depletion in high field strength elements (HFSE), like Nb, Ta, Zr and Hf indicating an arc signature (Fig. 6a$_{II–III}$). In both Hf/3-Th-Ta and Y/15-La/10-Nb/8 diagrams, the majority of these mafic rocks fall into the fields of island arc tholeiites and N-type MORB (Fig. 7a–b). However, their generally low Ta/Yb and higher Th/Yb at a given Ta/Yb are consistent with being island arc basalts although some are like MORB (Fig. 7c–d). Such "bimodal" features are typical for back-arc basin basalts (BABB) (e.g., Lawton and McMillan, 1999; Taylor and Martinez, 2003; Pearce and Stern, 2006), where the early stage basalts exhibit arc-like signature due to more crustal contributions during mantle melting, whereas the later stage basalts exhibit MORB-like patterns due to subdued crustal influence. Therefore, the back-arc basin is a probable tectonic setting for the stage II magmatism. However, some of these mafic rocks show high Nb/La and TiO_2, fall into the Nb-enriched basalt field (Figs. 5c, 10b).

The intermediate rocks in stage II are rare and closely associated with mafic rocks. In Rb/30-Hf-Ta*3 and Y + Nb vs. Rb diagrams, all these intermediate rocks plot in the volcanic arc field (Fig. 8c–d). Their REE and incompatible element patterns resemble those of island arc andesites or continental arc andesites with enrichment of LREE and negative Nb-Ta and Ti anomalies (Fig. 6b$_{II–III}$). But their low Th, La/Yb and Th/Yb characteristics resemble those of island arc andesites (Fig. 8a–b).

Those N-type MORB rocks were previously suggested to represent remnants of Neoproterozoic oceanic crust (Yao et al., 2014c). Nevertheless, their high Ba/Th and U/Th indicate that they are likely derived from subduction-zone metasomatized mantle wedge (Fig. 11e–f). Their high Nb/La and TiO_2 resembling Nb-enriched basalts suggest contributions of mantle wedge metasomatized by slab melt (Figs. 5c, 10b), while their high $\varepsilon_{Hf}(t)$ and $\varepsilon_{Nd}(t)$ is consistent with mantle wedge melting with the source dominated by the depleted mantle (Figs. 3a, b, d, 12; Table 1). Thus, the stage II magmatism was largely formed as a result of regional asthenospheric upwelling and decompression melting of the former subduction-zone metasomatized mantle wedge in a back-arc basin setting. Their low Th/Yb and Nb/Yb ruled out extensive crustal assimilation during the formation of mafic rocks in the stage II magmatism (Fig. 11b).

3.3. Stage IV (ca. 805–750 Ma) continental rift development

The literature data show the ~800–790 Ma bimodal volcanic rocks from the Shangshu Formation (basalt and rhyolite; Li et al., 2003b, 2008b; Wang et al., 2012a) and the ~790–780 Ma Daolinshan riebeckite and arfvedsonite bearing peralkaline granites which intruded the Shuangxiwu Group (Fig. 2b; Li et al., 2008b; Wang et al., 2010a). There are distinct "Daly gap" between mafic rocks (SiO_2 ranging from 46.98 to 56.16 wt.%) and felsic rocks (SiO_2 ranging from 68.09 to 76.83 wt.%) (Li et al., 2008b; Wang et al., 2010a, 2012a; Yao et al., 2014c). The mafic rocks include basaltic to basaltic andesitic rocks dominated by tholeiite (Figs. 4b–c, 5a) with steep REE patterns enriched in LREEs and weakly depleted in Nb-Ta and Ti in spidergrams, indicating more likely an arc signature (Fig. 6a$_{IV}$). In both Figs. 7 and 8, most of these mafic rocks fall into the field of island arc magmatism. However, they also exhibit some MORB affinity of relatively low Th/Zr, Th/Yb and Nb/Yb, implying the possible inheritance of stage II back-arc basin magmatic source region (Fig. 11b, d). Their $\varepsilon_{Hf}(t)$ and $\varepsilon_{Nd}(t)$ characteristics are also consistent with the stage I subduction-related magmatic rocks (Figs. 3a, b, d, 12; Table 1). Therefore, partial melting of former subduction metasomatized mantle wedge in a continental rift setting may have formed these mafic rocks.

The felsic rocks are calc-alkaline to high-K calc-alkaline (Fig. 5a) and metaluminous to weakly peraluminous and show high FeO^T/(FeO^T + MgO), belonging to ferron granitoids or rhyolites (Frost

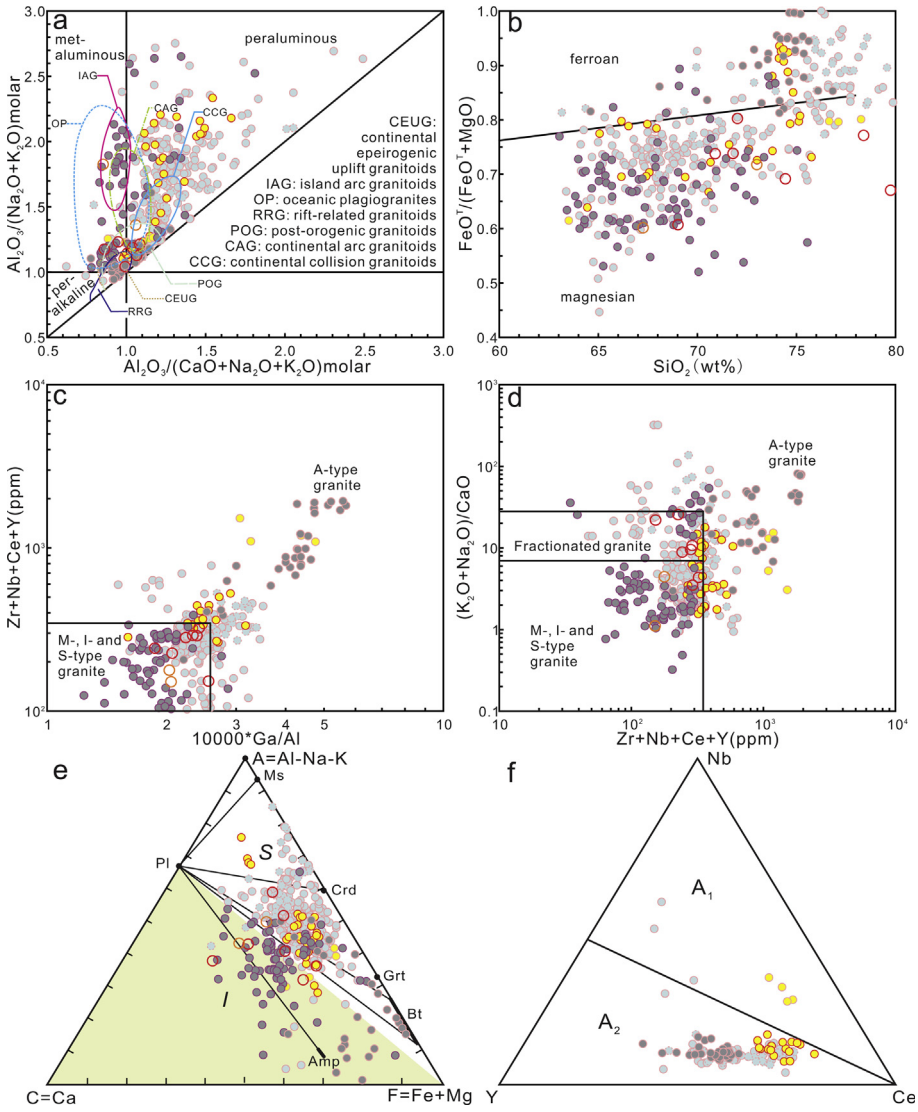

Fig. 9. (a) Chemical compositions of the Neoproterozoic igneous rocks in South China in terms of alumina saturation, where fields of granitoids from different tectonic environments are after Maniar and Piccoli (1989); (b) $FeO^T/(FeO^T + MgO)$ vs. SiO_2 diagram (after Frost et al., 2001; Frost and Frost, 2011); (c), (d) Various chemical discrimination diagrams for the Neoproterozoic igneous rocks in South China (after Whalen et al., 1987). (e) ACF diagram for the Neoproterozoic granitoids (after White and Chappell, 1977); (f) Subtype classification of A-type granitoids (after Eby, 1992). Symbols and data sources are the same as in Fig. 4.

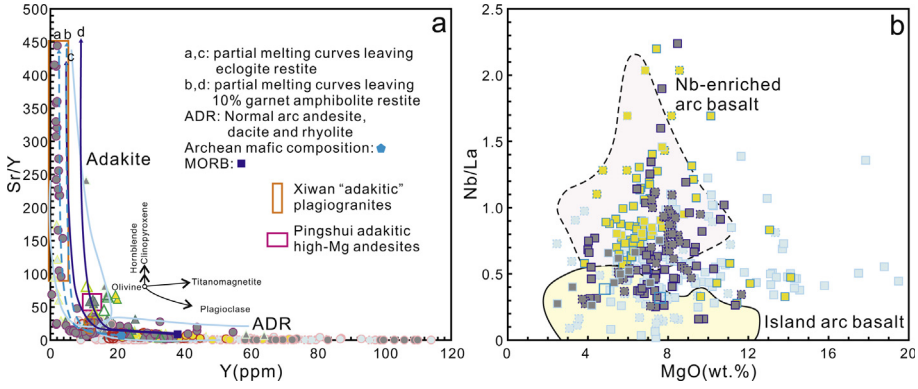

Fig. 10. (a) Sr/Y vs. Y diagram to distinguish adakite from normal arc andesite, dacite and rhyolite (ADR) lavas (after Castillo, 2012). (b) Nb/La vs. MgO diagram. The fields of the island arc basalts and Nb-enrich basalts are from Kepezhinskas et al. (1996). Symbols and data sources are the same as in Fig. 4.

et al., 2001; Fig. 9a–b). Also, their high Ga/Al and HFSE (Zr, Nb) and high Zr saturation temperature (831–1031 °C, >830 °C; Watson and Harrison, 1983) are characteristic of A-type granitoids or rhyolites (Fig. 9c–d). High Rb, Rb/Nb and Y/Nb of these granitoids and rhyolites further suggest that they belong to subgroup A_2 granites or rhyolites (Eby, 1992, Fig. 9f). They mostly plot in the volcanic arc

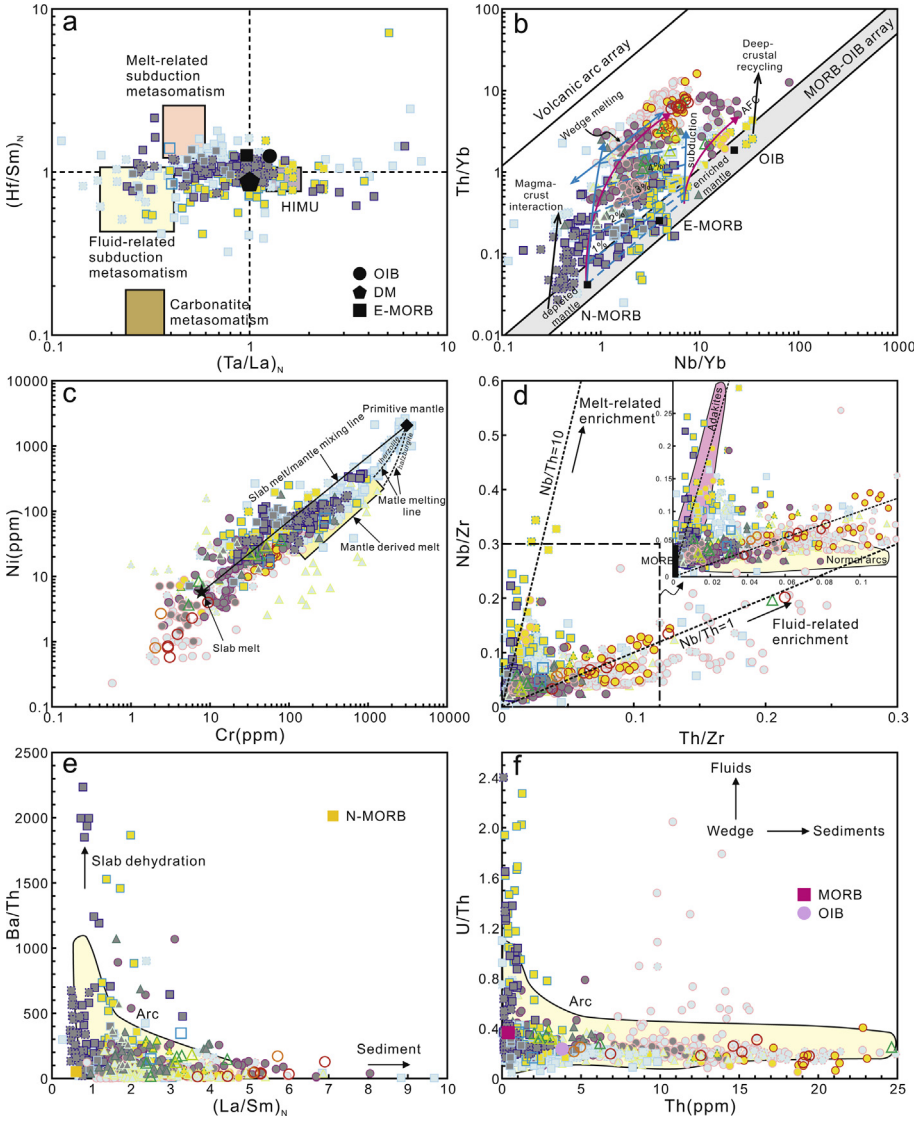

Fig. 11. (a) $(Hf/Sm)_N$ vs. $(Ta/La)_N$ diagram (after La Flèche et al., 1998); (b) Th/Yb vs. Nb/Yb diagram (after Pearce, 2008); (c) Ni vs. Cr diagram (after Tsuchiya et al., 2005); (d) Nb/Zr vs. Th/Zr diagram (after Kepezhinskas et al., 1997); (e) Ba/Th vs. $(La/Sm)_N$ diagram (after Tatsumi, 2006); (f) U/Th vs. Th diagram (after Hawkesworth et al., 1997). Chondrite values for normalization are from Sun and McDonough (1989). Symbols and data sources are the same as in Fig. 4.

filed of the Rb/30-Hf-Ta*3 diagram (Fig. 8c) and show spidergram patterns similar to island arc or continental arc with weak negative Nb-Ta and pronounced negative Sr, P and Ti anomalies (Fig. 6c_{IV}). In this scenario, a tonalitic to granodioritic meta-igneous source (Anderson, 1983; Whalen et al., 1987; Creaser et al., 1991) or previously dehydrated metasedimentary source rocks (Anderson and Thomas, 1985; Whalen et al., 1987) may be the more appropriate source for these A-type granitoids and rhyolites of the stage IV magmatism. Their arc-related geochemical features may be inherited from their source rocks. Considering their high $\varepsilon_{Hf}(t)$ and $\varepsilon_{Nd}(t)$ (Figs. 3a, b, d, 12; Table 1), they might have formed by partial melting of juvenile island arc crust. Regularly, the "Daly gap" between mafic and felsic rocks (Fig. 4a) is considered due to inadequate mixing of mantle derived basaltic magma and crust derived felsic magma (Chayes, 1963; Cann, 1968; Clague, 1978; Bonnefoi et al., 1995). However, Niu et al. (2013) pointed out that evolution of basaltic magma could also produce the "Daly gap", because Ti-Fe oxides crystallization leads to rapid increase of SiO_2 in the residual melt. Thus, these A-type granitoids with high $\varepsilon_{Hf}(t)$ and $\varepsilon_{Nd}(t)$ also might resulting from protracted fractional crystallization of synchronous mafic magmas.

4. Active continental margin and inland of Cathaysia

4.1. Stage I (ca. 1000–860 Ma) Cathaysia continental arc development

The magmatic evidence comes firstly from mafic-ultramafic bodies, which occur mainly as lenses, pods and fragments within the country rocks of quartz schist, gneiss and migmatite distributed mainly along the Wuyi-Yunkai belt, in the area of Longquan, Qingyuan, Zhenghe, Suichang, Jian'ou, Jianyang and Xinyi (Wang et al., 2014b; Figs. 1b, 2c). Except for a few ultramafic rocks (e.g., serpentinite, serpentinized peridotite) which exhibit typical cumulate textures with high MgO and low Fe_2O_3, K_2O, Na_2O and REEs (Figs. 4a–c, 6a_I; Peng et al., 2006; Wang et al., 2013b), the stage I mafic rocks include: gabbro, diabase, basalt, andesite, and also serpentinite and pyroxenite (Table 1). As mentioned above, Wang et al. (2013b) and Zhang et al. (2012a) proposed that the meta-mafic rocks from the Cathaysia Block side are mainly calc-alkaline and have geochemical affinities to MORB, Nb-enriched basalt and continent-arc basalt, implying a continental arc-back-arc system developed at ~984–969 Ma (also see Table 1). Zhang et al. (1998) also proposed that the 972 Ma rhyolitic rocks in the

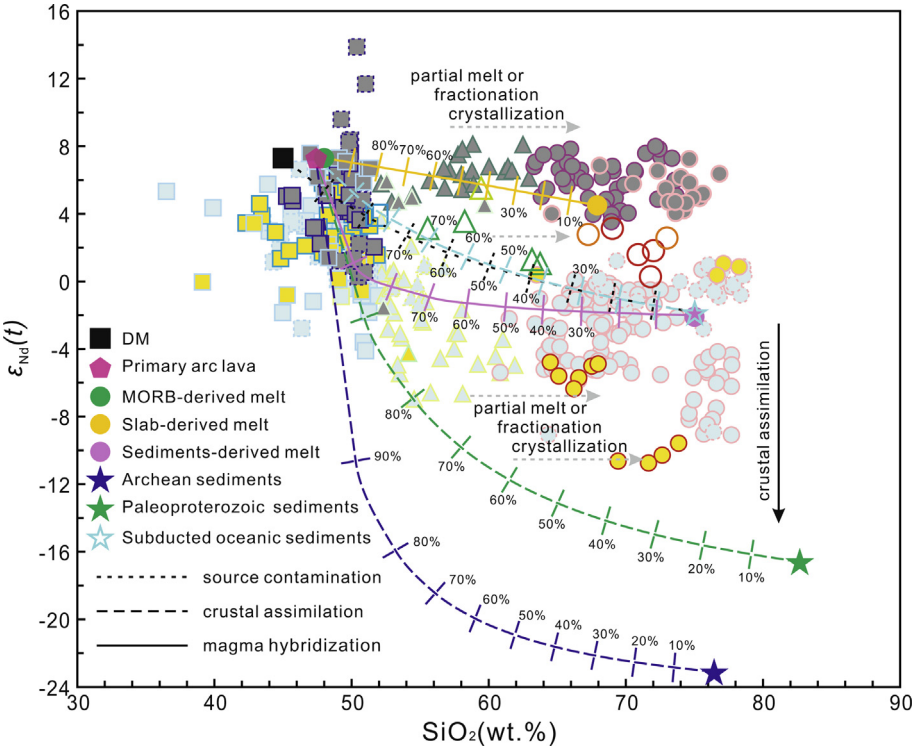

Fig. 12. $\varepsilon_{Nd}(t)$ vs. SiO_2 diagrams at 830 Ma. The parameters of end-members are selected based on the literature (e.g., Castillo, 2012; Chauvel et al., 2008. Chen et al., 2013; Class et al., 2000; Drummond et al., 1996; Kelemen et al., 2003; Niu and O'Hara, 2003; Plank and Langmuir, 1998; Wang et al., 2013b; Workman and Hart, 2005; Xia et al., 2012, 2014; Yu et al., 2012 and reference therein). The depleted mantle (DM) is represented by SiO_2 = 45 wt.%, Nd = 11.3 ppm, and $\varepsilon_{Nd}(t)$ = +7.3; MORB-derived melt by SiO_2 = 48 wt.%, Nd = 20 ppm and $\varepsilon_{Nd}(t)$ = +7.3; primary arc lava by SiO_2 = 47.4 wt.%, Nd = 10.1 ppm and $\varepsilon_{Nd}(t)$ = +7.3; slab-derived melt by SiO_2 = 67.9 wt.%, Nd = 18.5 ppm and $\varepsilon_{Nd}(t)$ = +4.5; sediments-derived melt by SiO_2 = 75 wt.%, Nd = 183 ppm and $\varepsilon_{Nd}(t)$ = −2.0; Subducted oceanic sediments by SiO_2 = 75 wt.%, Nd = 27 ppm and $\varepsilon_{Nd}(t)$ = −1.8; Paleoproterozoic sediments by SiO_2 = 82.7 wt.%, Nd = 59.6 ppm and $\varepsilon_{Nd}(t)$ = −16.6; Archean sediments by SiO_2 = 76.4 wt.%, Nd = 131 ppm and $\varepsilon_{Nd}(t)$ = −23.1. Symbols and data sources are the same as in Figs. 3 and 4.

Nanling domain and the synchronous dacite porphyry in the Yunkai domain formed in a volcanic arc setting. At Jingnan (NE Guangdong) and Hezi (S Jiangxi) of the Nanling domain, rhyolite and granodiorite with arc geochemical signatures gave the SHRIMP zircon U-Pb age of 972 ± 8 Ma and the Pb-Pb age of 996 ± 29 Ma, respectively (Liu et al., 2001; Shu et al., 2008a, 2011; Fig. 1b; also see Table 1). Recently, Wang et al. (2014b) published a set of SIMS and LA-ICP-MS zircon U-Pb ages of S-type granites from Masha and Shibei (North Wuyi), Dawei (Xunwu in Nanling), Longtang (Dingnan), Shuanglong (Luoding) and Huaixiang (Xinyi) in the Wuyi-Yunkai belt of the Cathaysia Block at ~982–909 Ma (also see Table 1).

The detrital zircons in the late Neoproterozoic and Paleozoic sedimentary rocks from the Jianyang, Zengcheng, Nanxiong and Xinyi areas of the Cathaysia Block commonly show an igneous origin and give U-Pb ages of ~1.0–0.9 Ga (peak age being ca. 940 Ma) along the Wuyi-Yunkai belt (e.g., Yu et al., 2007, 2010; Wan et al., 2007, 2010; Wang et al., 2007c, 2008a, 2008b, 2010b). The inherited grains with the U-Pb ages of ca. 1.0–0.9 Ga were also observed in the early Paleozoic granitoids in the Cathaysia Block (e.g., Ding et al., 2005; Wang et al., 2011b; Zhang et al., 2012d). These data indicate an earliest Neoproterozoic (begin no later than ~970 Ma) active continental margin rather than intraplate tectonic regime along the Wuyi-Yunkai belt of the Cathaysia Block, and the development of the earliest Neoproterozoic (~1.0–0.9 Ga) magmatism along the Wuyi-Yunkai domain in the interior of the Cathaysia Block (e.g., Shu et al., 2008a, 2011; Zhao, 2015).

The mafic rocks including diabase, basalt and gabbro, although some of them are metamorphosed (Table 1). They are mainly subalkaline and straddle the tholeiitic-calc-alkaline compositional boundary (Fig. 4a–c), but mostly fall into the calc-alkaline and high-K calc-alkaline fields in the K_2O vs. SiO_2 diagram with relatively high K_2O (Fig. 5a). These mafic rocks show diverse REE patterns with both enrichment and depletion in LREEs relative to HREEs, corresponding to island arc basalts or MORB (Fig. 6a$_I$). On primitive-mantle normalized incompatible element spidergrams, however, they more closely resemble island arc or continental arc basalts with enriched LILEs and negative Nb-Ta, P and Ti anomalies (Fig. 6a$_I$). Their positive K and Pb anomalies may be due to crustal assimilation (Fig. 6a$_I$). In the Hf/3-Th-Ta diagram (Fig. 7a), most of these mafic rocks fall into the field of island arc calc-alkaline basalts and E-type MORB, and their relatively high Zr/Y, Th/Yb and Ta/Yb also show the affinities of continental arc basalts and MORB (Fig. 7c–d). However, the majority of these mafic rocks plot in the region between back-arc basin basalts and continental basalts in the Y/15-La/10-Nb/8 diagram (Fig. 7b). Most of the stage I mafic rocks exhibit various $(Ta/La)_N$ and $(Hf/Sm)_N$ and define the trends related to both melt- and fluid-related metasomatism (Fig. 11a; La Flèche et al., 1998). Meanwhile, There are also some Nb-enriched arc basalts (Defant et al., 1992; Kepezhinskas et al., 1996) in both Wuyi and Yunkai areas with high Nb/La and TiO_2 (Figs. 5c, 10b). The occurrence of Nb-rich basalts implicitly used as supporting evidence for slab melting (e.g., Aguillón-Robles et al., 2001; Sajona et al., 1996). The increasing FeO^T/MgO, SiO_2, Th/Yb and Nb/Yb together with decreasing Cr and Ni from mafic to felsic rocks indicate an assimilation fractional crystallization (AFC) process of wedge-derived melt or the mixing between mantle-derived melt and slab melt (Figs. 4c, 11b–c). Our $\varepsilon_{Nd}(t)$ and SiO_2 modelling also support the scenario that the wedge-derived melt may be assimilated with continental or

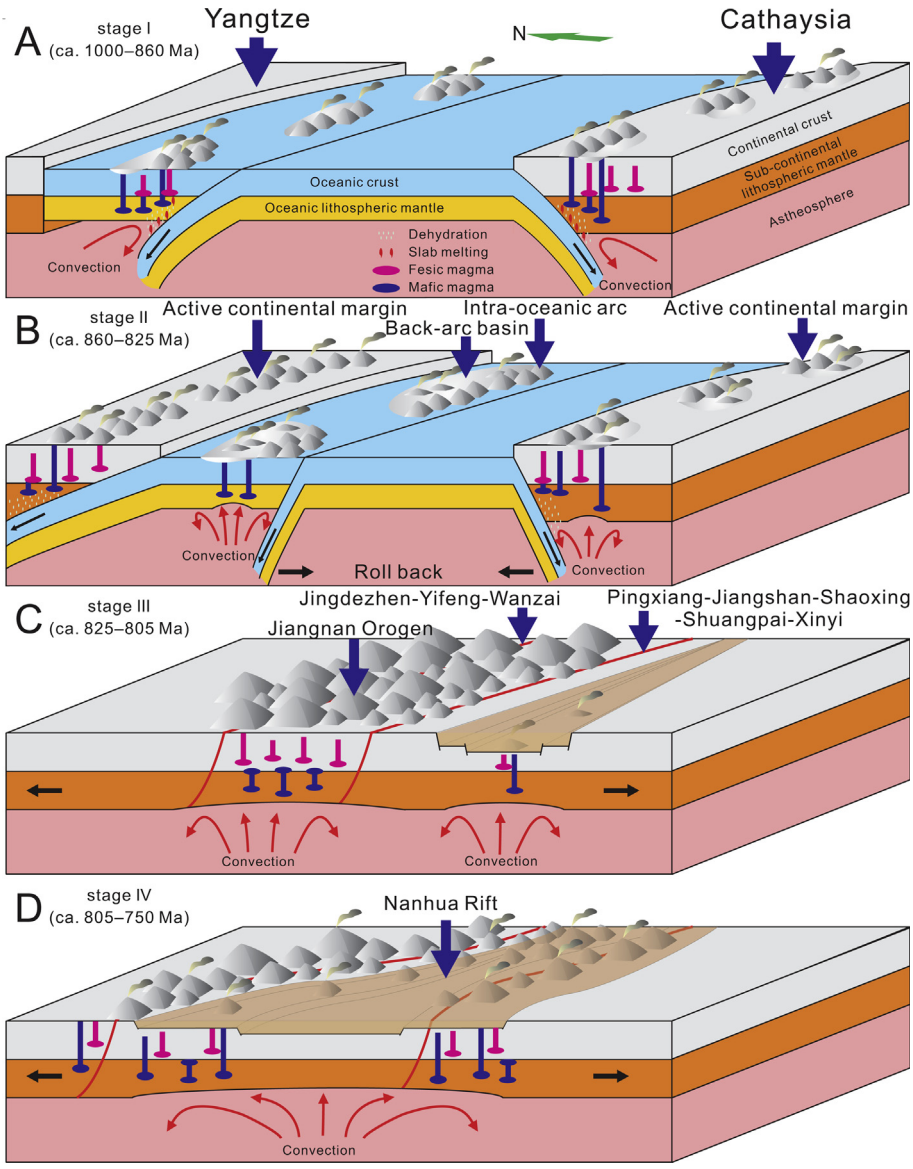

Fig. 13. Schematic cartoons showing the tectono-magmatic evolution for Neoproterozoic igneous rocks in South China.

oceanic sediments (Fig. 12). However, the high Nb/Th imply that mafic rocks have closer relationship to melt-related enrichment while intermediate and felsic rocks are closer to fluid-related enrichment (Fig. 11d).

The stage I intermediate rocks are only exposed in the Chencai area. They straddle the subalkaline-alkaline compositional boundary and plot in the calc-alkaline or high-K calc-alkaline fields (Figs. 4a–c, 5a). These intermediate rocks show steep REE patterns with enriched LREEs and markedly negative Nb-Ta, P and Ti anomalies in spidergram patterns, similar to island arc or continental arc andesites (Fig. 6b$_l$). In Rb/30-Hf-Ta*3 and Y + Nb vs. Rb diagrams, all these intermediate rocks plot in the volcanic arc field (Fig. 8c–d). Although their low Th concentrations are consistent with their being island arc andesites, the high La/Yb and Th/Yb of these intermediate rocks indicate that they belong more likely to continental arc andesites (Fig. 8a–b).

The stage I felsic rocks are mainly peraluminous (Fig. 9a), located inland and far from the Jiangshao Fault (Fig. 1b). Most of these felsic rocks fall in the S-type granite field of the AFC diagram (Fig. 9e). The Zr saturation temperatures (794–884 °C, mostly higher than 830 °C; Watson and Harrison, 1983; data from Shu et al., 2008a, 2011; Wang et al., 2014b) indicate that these felsic rocks have high initial temperatures, corresponding to the estimated temperatures using the P_2O_5 and TiO_2 saturation thermometry (Harrison and Watson, 1984; Green and Pearson, 1986) (Fig. 5b–c). However, some of these felsic rocks with high $FeO^T/(FeO^T + MgO)$ plot in the ferron granitoid field (Fig. 9b), and their high Ga/Al and HFSE (Zr, Nb, Ce, Y) indicate an A-type affinity (Fig. 9c–d). In the Nb-Y-Ce diagram (Fig. 9f), these rocks may be A_2 subgroup granite (Eby, 1992). They exhibit island arc- or continental arc-like REE and incompatible element patterns enriched in LEEEs and LILEs relative to HREEs and HFSEs with pronounced negative Eu, Nb-Ta, Sr, P and Ti anomalies (Fig. 6c$_l$). The S- and A-type association of felsic rocks with relatively high A/CNK (Fig. 9a), LREEs/MREEs, Th and low Ba/Th and U/Th (Fig. 11e–f) imply a sediment source, as supported by the low $\varepsilon_{Hf}(t)$ and $\varepsilon_{Nd}(t)$ (Figs. 3a–d, 12; Table 1). Their high CaO/Na_2O and low Al_2O_3/TiO_2, Rb/Ba, Rb/Sr and $Al_2O_3/(MgO + FeO^T)$ indicate that they are probably

derived from metagreywacke sources with the involvement of a meta-igneous component (Shu et al., 2008a, 2011; Wang et al., 2014b).

4.2. Stage II (ca. 860–825 Ma) continental arc and back-arc development

Recently, we found associated gabbro, diorite and I-type granodiorite (Fig. 2d) which are bound by the Jiangshan-Shaoxing Fault with zircon U-Pb ages of ~830 Ma to show a geochemical affinity of active continental margin magmatism with positive $\varepsilon_{Hf}(t)$ and $\varepsilon_{Nd}(t)$ (see below and Table 1). In addition, previous studies showed a series of mafic rocks (basalt, gabbro and plagioclase amphibolite) with geochemical characteristics of OIB-type basalts and zircon SHRIMP U-Pb ages of 857–836 Ma in the Zhuji, Chencai and Mamiamshan areas near the Jiang-Shao Fault. These mafic rocks are deformed in accord with the regional metamorphic foliation of Chencai and Mayuan Groups country rocks and in contact with migmatitic gneisses of the Mamianshan Group by a ductile shearing fault (Shu et al., 2011; also see Table 1). These age data are in agreement with some previous data (Table 1): the SHRIMP zircon U-Pb age of 858 ± 11 Ma for the Huaquan gabbro block included in the ophiolitic mélange (Shu et al., 2006; Fig. 1b), the zircon SHRIMP U-Pb age of 841 ± 6 Ma on the Lipu diorite, which is in fault contact with the Chencai Group (Li et al., 2010a, 2010b), the SHRIMP U-Pb zircon ages of 857 ± 0.2 Ma and 853 ± 4 Ma on Jian'ou metabasalt and tuff from Mayuan and Mamianshan Groups (Shu et al., 2008b), implying the existence of a Cathaysia Block arc and back-arc system that may last until ~830 Ma.

The Miaohou gabbros show low Ti/Zr and Zr/Y and high Th/Yb and Ta/Yb, and fall into the calc-alkaline fields in Hf/3-Th-Ta and Y/15-La/10-Nb/8 diagrams (Fig. 7a–d), indicating a continental arc. However, other mafic rocks are mainly tholeiitic basalts with low FeO^T/MgO (Fig. 4b–c) and mostly plot in the fields of alkaline within-plate basalts in Fig. 7a, b, d, which is also consistent with their OIB-like REE and spidergram patterns without significant Nb-Ta anomalies (Fig. 6a$_{II-III}$). These basalts also show high Nb/La and TiO_2 (Figs. 5c, 10b), resembling Nb-rich arc basalts (Defant et al., 1992; Kepezhinskas et al., 1996).

All the intermediate rocks, including the Miaohou and Shanhou diorites, are mainly calc-alkaline (Figs. 4b–c, 5a). Their REE and spidergram patterns are characterized by enriched LREEs and LILEs with a significant positive Pb anomaly, a weak positive Zr-Hf anomaly and negative Nb-Ta, P, Ti and Eu anomalies (Fig. 6b$_{II-III}$), resembling island arc or continental arc andesites. Their high La/Yb and Th/Yb indicate that these rocks are more consistent with being continental arc andesites (Fig. 8b). In Rb/30-Hf-Ta*3 and Y + Nb vs. Rb diagrams, the majority of these intermediate rocks plot in the volcanic arc field (Fig. 8c–d).

The stage II felsic rocks, represented by the Miaohou and Shanhou granites, are metaluminous to weakly peraluminous and fall into both I- and S-type granite categories. Their negative P_2O_5-SiO_2 and TiO_2-SiO_2 correlations might reflect apatite and titanomagnetite fractionation, and the negative P_2O_5-SiO_2 correlation is often interpreted to be characteristic of I-type granites (Fig. 5b). The P_2O_5 and TiO_2 saturation thermometers indicates that these two granites have relatively high initial temperatures (Fig. 5b, c; Harrison and Watson, 1984; Green and Pearson, 1986), which is in accordance with their Zr saturation temperatures (725–812 °C, Watson and Harrison, 1983) and Ti-in-zircon temperatures (average of 745–805 °C). They all show REE and spidergram patterns similar to those of island arc or continental arc granitoids with pronounced negative Nb-Ta, Sr, P and Ti anomalies (Fig. 6c$_{II-III}$).

The Miaohou and Shanhou complexes together with other intermediate rocks show a continental arc-like REE and spidergram patterns (Fig. 6a–c$_{II-III}$), and yield an AFC trend or magma mixing trend according to the increasing Th/Yb and Nb/Yb and the decreasing Cr and Ni and $\varepsilon_{Hf}(t)$ and $\varepsilon_{Nd}(t)$ with a negative $\varepsilon_{Nd}(t)$-SiO_2 relationship from mafic to felsic rocks (Figs. 3a–d, 12; Table 1). In Fig. 4c, they also yield a fractional crystallization trend of mantle-derived melt. Their high U/Th and Ba/Th and low Nb/Th also resemble those of normal arc rocks (Fig. 11d–f), indicating that fluids from dehydration of subducted slab played a major role in slab-wedge element transport and the presence of sediments or sediment-derived melts in slab-wedge element transport is also important (Hawkesworth et al., 1997; Woodhead et al., 2001). But their relatively high $\varepsilon_{Nd}(t)$ values preclude the ancient basement assimilation and imply they may be assimilated by subducted oceanic sediments from accretionary prism or fore-arc basin due to their closer position to the Jiangshao Fault (Figs. 1b, 12; Table 1). Nevertheless, there are some other mafic rocks a little far from the Jiangshao Fault with their OIB-like signature REE and spidergram patterns with high Nb/La (Fig. 6a$_{II-III}$, 10b, 11d), suggesting that they formed by regional asthenospheric upwelling and partial melting of former subduction metasomatized wedge.

4.3. Stage stage III (ca. 825–805 Ma) continental rift development/ Stage IV (ca. 805–750 Ma) within-plate magmatism development

A younger age limit on the closure of the Cathaysia Block arc and back-arc system is constrained by the metavolcanic rocks, diabase and Mamianshan bimodal volcanic rocks in the Wuyi domain dated at ~820–790 Ma, which are better interpreted to have formed in a continental rift or within-plate setting (e.g., Li et al., 2005, 2010b; Shu et al., 2008b, 2011; Wang et al., 2012b; also see Table 1). These data, especially the formation age of 818 ± 9 Ma (SHIMP zircon U-Pb age) for Mamianshan bimodal volcanic rocks (dominantly transitional to mildly alkaline basalts and subordinate alkaline rhyolite; Li et al., 2005), indicate that the arc and back-arc system might have ended at ca. 820 Ma. Both stage III and IV magmatism in this area shares similar rock association, geochemical composition and isotopic features, thus we put stage III and IV magmatism together for further discussing.

The stage III and IV magmatisms are represented by Mamianshan bimodal volcanic rocks (Li et al., 2005) and mafic to intermediate rocks sporadically exposed in Fujian (Table 1). The Mamianshan mafic rocks, including ultramafic to intermediate rocks, are mainly alkaline with variably high K_2O (Figs. 4a, 5a), mostly have relatively high Nb/Y ratios of >0.5, transitional between subalkaline and alkaline basalts (Li et al., 2005), and have uniform LREE-enriched REE patterns and an insignificant Eu anomaly (Fig. 6a–b$_{II-III}$). In the spidergrams (Fig. 6a–b$_{II-III}$), all mafic rocks display OIB-like patterns without significant Nb-Ta depletion, which is characteristic of intra-plate alkaline basaltic rocks (Sun and McDonough, 1989). Their position in geochemical discrimination diagrams is also consistent with the within-plate setting (Fig. 7a, b, d). These mafic rocks display OIB-like patterns (Fig. 6a$_{II-III}$) and show the MORB-OIB array in Fig. 11b, similar to alkali basalts derived from OIB-like mantle sources in continental rifts. Their various $\varepsilon_{Nd}(t)$ and high K_2O and Nb/Th indicate that the AFC process of basaltic magma derived from OIB-like mantle source can account for their genesis (Figs. 3c–d, 5a, 11d; Table 1). However, other intermediate rocks are characterized by enrichment of LREEs and LILEs with significant positive Pb, Zr-Hf and negative Nb-Ta, P and Ti Eu anomalies (Fig. 6a$_{IV}$), consistent with their being island arc or continental arc andesites. In addition, the high La/Yb and Th/Yb and low Rb, Y and Nb indicate that these intermediate rocks are likely continental arc andesites (Fig. 8b, d) despite the within-plate signature in the Rb/30-Hf-Ta*3 diagram (Fig. 8c).

The felsic volcanic rocks are mainly calc-alkaline and high-K calc-alkaline variety (Fig. 5a) highly enriched in LREEs with remarkable negative Eu anomalies (Fig. 6c$_{II-III}$). However, their highly silicic nature and high Nb/Y ratios of >1.7, these felsic volcanic rocks resemble peralkaline rhyolites (Li et al., 2005; Shao et al., 2015). They are also strongly enriched in Th, Ta, Nb, Zr, Hf and Y, and display similarly enriched spidergram patterns apart from strong depletion in Sr, P, Eu and Ti due to extended fractional crystallization (Fig. 6c$_{II-III}$). These felsic rocks are characterized by weak depletion or enrichment in Nb and Ta (Fig. 6c$_{II-III}$). The Zr saturation temperatures (925–970 °C; Watson and Harrison, 1983) indicate that these felsic rocks have high initial temperatures. Although they are magnesian granitoids following Frost et al. (2001) due to relatively low $FeO^T/(FeO^T + MgO)$ (Fig. 9b), their high Ga/Al and HFSEs (e.g., Zr, Nb) qualify them as equivalent to A-type granites (Fig. 9c–d). They can be further classified as A_1-type rhyolites (Fig. 9f) following Eby (1992). There are no continuously evolving trends in abundances and ratios of incompatible trace elements for the associated felsic and basaltic rocks (Li et al., 2005), ruling out that the felsic rocks are products of extended differentiation of mafic magmas. Their relatively high $\varepsilon_{Nd}(t)$ (Figs. 3c–d, 12; Table 1) imply a mixture source of juvenile arc material and ancient basement.

5. Active continental margin of the Yangtze Block

5.1. Stage II (ca. 860–825 Ma) Yangtze continental arc development/ Stage III (ca. 825–805 Ma) collision between Yangtze and Cathaysia blocks and Jiangnan Orogen development

The active continental margin of the Yangtze Block spans much of the spatial coverage of the Jiangnan Orogen located northwest of the Jingdezhen-Yifeng-Wanzai Fault, which comprises mainly Proterozoic metasedimentary and igneous rocks. The folded basement metasedimentary sequences may have deposited in an arc foreland basin setting following arc-continent collision between the Yangtze and Cathaysia blocks (Wang et al., 2007b) and subsequently experienced deformation at low-green schist facies conditions. The U-Pb zircon ages in detrital grains from the metasedimentary units and in magmatic grains from the interlayered volcanic units indicate that the metamorphism occurred at 860–820 Ma (Wang et al., 2007b, 2013a, 2014a; Yao et al., 2013; Zhou et al., 2009). During the later stage of the amalgamation between the Yangtze and Cathaysia blocks, voluminous granitoids intruded the folded sequences. Therefore, the unconformity between the folded basement sequences and overlying cover sequences has been considered to mark the Neoproterozoic orogenic event that jointed the Yangtze and Cathaysia blocks. Considering the geological correlations and abundant newly published dating results for detrital zircons from the folded basement sequences and the magmatic zircons from the interlayered volcanic rocks and the intrusive granitoids, the folded metasedimentary basement sequences in the Jiangnan Orogen might have deposited within the time span of 860–825 Ma and the maximum depositional ages of the underlying sequences constrain the timing of the final amalgamation to later than ~825 Ma (e.g., Wang et al., 2007b, 2014a; Yao et al., 2013), although Li et al. (2009) and Wang et al. (2012d) suggested that post-orogenic extension (rifting?) took place as early as 850 Ma.

The south Anhui ophiolites (e.g., Fuchuan ophiolite) occur as elongated bodies and are tectonically intercalated within the folded Neoproterozoic Xikou Group. The pillow lavas and the altered tholeiites of south Anhui ophiolites show typical calc-alkalic continental arc-signatures with enrichment in LREEs and LILEs, and depletion in HFSEs. The chromium-spinels from the serpentinized harzburgite show varying $Cr^{\#}$ of 40–67 and $Mg^{\#}$ of 33–60 and straddle the boundary between abyssal and forearc peridotites (Niu et al., 2003), but mostly comparable with the composition of spinels from "supra-subduction zone" (SSZ) ophiolites (Zhang et al., 2013a). The wide range of $\varepsilon_{Nd}(t)$ from these mafic rocks also implies the effect of crustal assimilation (Table 1). The Neoproterozoic granitoids that intruded the folded sequences are the dominant igneous rock type in the Jiangnan Orogen (Fig. 1b), and they are mainly distributed in southern Anhui Province (i.e., the Xiuning, Xucun and Shexian plutons; Fig. 2f) and northwestern Jiangxi Province (i.e., the Jiuling and Guanyinqiao plutons) in the eastern segment of the Jiangnan Orogen and northern Guangxi Province (i.e., the Sanfang, Yuanbaoshan, Bendong, Dongma, Longyou, Dazhai, Zhaigun, Pingying and Mengdong plutons, etc.) in the western segment of the Jiangnan Orogen (Fig. 1b and Table 1). Recently published *in situ* SHRIMP and LA-ICP-MS zircon U-Pb ages suggested that these granitoids were emplaced at ~850–805 Ma (Li et al., 2003a; Ma et al., 2009; Wu et al., 2006; Wang et al., 2004, 2006a, 2013a, 2014a; Xue et al., 2010; Yao et al., 2014a; Zhang et al., 2011a; also see Table 1), with the exception of the Shi'ershan pluton (~ 780 Ma; Li et al., 2003b), which intruded the cover sequences and probably represents post-orogenic magmatism (Wang et al., 2012a). According to the compilation of published geochemical data (e.g., Li et al., 2003a; Wu et al., 2006; Wang et al., 2004, 2006a, 2013a, 2014a; Yao et al., 2014a), these 850–805 Ma granitoids are all strongly peraluminous S-type granites with an age peak of ~820 Ma (Charvet, 2013; Li et al., 2003a; Wang et al., 2006a). We thus do not tend to further distinguish stage II and III magmatism in the active continental margin of the Yangtze Block.

The high-Mg basalts from northern Hunan (e.g., Yiyang komatiitic basalt; also see Table 1), previously interpreted as evidence of plume-related high temperature magmatism (Wang et al., 2007a; Zhou et al., 2004), are later considered to be generated in a subduction zone setting (Zhao and Zhou, 2009; Zheng et al., 2008; Zhou et al., 2009). In fact, there are no report of reliable plume-derived continental flood basalt (CFB) and ocean island basalt (OIB) in this region in the Neoproterozoic. The ~830 Ma SSZ-type ophiolites in south Anhui (Ding et al., 2008; Zhang et al., 2012b, 2013a; also see Fig. 2f and Table 1), the ~850–825 Ma arc-like geochemical features of the mafic-ultramafic rocks in N Jiangxi, NE Hunan and N Guangxi (Li et al., 2004, Li et al., 2010a, 2013; Yao et al., 2014a; Zhou et al., 2004, 2009; also see Table 1) and the recognition of the 830 Ma high-Mg diorites that intruded the Sibao Group (Chen et al., 2014), as well as the high-Mg andesites and basalts (Komatiitic basalt) of the Lengjiaxi Group in the Yiyang area of northern Hunan Province (Wang et al., 2004; Zhang et al., 2012c), altogether provide solid evidence for the existence of a Neoproterozoic active continental margin of the Yangtze Block, indicating that these 850–805 Ma igneous rocks are most consistent with subduction-related and post-collisional magmatism (Wang et al., 2006a, 2006b, 2013a, 2014a; Zhou et al., 2004, 2009) rather than products of initiation of the ascending (super-) plume that may have finally led to the breakup of supercontinent Rodinia (Li et al., 1999, 2003a, 2003b; Wang et al., 2007a).

The Stage II ultramafic rocks including harzburgite, wehrlite, pyroxenite and gabbro from the Fuchuan ophiolite suite (also see Table 1). Except for the harzburgite, all these rocks show cumulate textures; compositionally (Fig. 4a–c, 11c) enriched in MgO, Cr and Ni and depleted in CaO, Al_2O_3 and REEs. Some (Zhang et al., 2012b; Ding et al., 2008) suggest that the harzburgite represents melting residues after large extent of basaltic melt extraction in the mantle and resembles the Archean subcontinental lithospheric mantle (SCLM) following Griffin et al. (1999). Such highly depleted residual harzburgite is rare in the normal oceanic lithospheric mantle

but common in the SSZ type ophiolite (Dilek and Furnes, 2011; Niu et al., 2003).

The Stage II mafic rocks (e.g., gabbro, basalt and some diabase; also see Table 1) are mainly sub-alkaline in composition (Fig. 4a), mostly shift away from the mantle array in the Ta/Yb vs. Th/Yb diagram and plot in the field of continental arc basalts (Fig. 7c–d). In both Y/15-La/10-Nb/8 and Hf/3-Th-Ta diagrams (Fig. 7a), most of these mafic rocks fall into the fields of continental arc and within-plate basalts (Fig. 7a–b). In AFM and FeO^T/MgO vs.SiO_2 diagrams, they straddle the boundary between tholeiite and calc-alkaline (Fig. 4b–c), but their relatively high K_2O is more consistent with these rocks being high-K calc-alkaline rocks (Fig. 5a). They have different incompatible trace element patterns. While most of them exhibit arc-like patterns with significant LREE/HREE fractionation and both negative and positive Eu anomalies, the others show N-type MORB patterns (Fig. 6a_{II-III}). Generally, these mafic rocks are characterized by pronounced HFSE depletion and negative Nb-Ta anomalies, consistent with being slab-dehydration induced mantle wedge melting (Fig. 6a_{II-III}). Their enrichment in Zr and Hf implies that the mantle source may have been metasomatised by subducted seafloor sediment (Fig. 6a_{II-III}). There are some high-Mg basalts classified as komatiitic series (e.g., Yiyang komatiitic basalt; also see Table 1) in this area (Wang et al., 2004, 2007a), probably associated with a mantle plume (Wang et al., 2007a). We note, however, that these rocks are of prominent arc magma characteristics without any geochemical signature of plume-derived magmas such as continental flood basalts (CFB) and ocean island basalts (OIB).

The andesite, diorite and tonalite constitute the assembly of intermediate rocks of the stage II–III magmatism. Although these rocks straddle the boundary between volcanic arc and within-plate fields in the Rb/30-Hf-Ta*3 diagram, they all plot in the volcanic arc field in the Y + Nb vs. Rb diagram (Fig. 8c–d). These intermediate rocks show steep REE patterns with enriched LREEs and a negative Eu anomaly together with markedly negative Nb-Ta, P and Ti anomalies in the spidergram, resembling island or continental arc andesites (Fig. 6b_{II-III}). Their relatively high Th, La/Yb and Th/Yb indicate they are more likely continental arc andesites (Fig. 8a–b). Recently recognized high-Mg diorites (Chen et al., 2014; Zhang et al., 2012c) with strong enrichment in Pb and depletion in Nb and Ti (Fig. 6b_{II-III}) are geochemically similar to the Setouchi high-Mg andesites (HMA), but different from adakites and Bonin HMA. In addition, the high-Mg diorites show low Sr/Y, which are significantly different from typical adakites and boninites but similar to the more common volcanic arc rocks (Fig. 10a). In the FeO^T/MgO vs. SiO_2 diagram (Fig. 4c), all stage II–III magmatic rocks yield the fractional crystallization trend of mantle-derived melt. The relatively high Cr and Ni and low Nb/Th imply that they represent partial melt from mantle wedge metasomatized by dehydration of subducted oceanic slab (Fig. 11c–d), and the increasing Th/Yb and Nb/Yb from mafic to felsic rocks indicates an assimilation fractional crystallization (AFC) process of wedge-derived melt (Fig. 11b). The low Ba/Th and U/Th together with high LREE/MREE and Th imply more sediments contribution in stage II–III magmatism (Fig. 11e–f). In addition, according to our $\varepsilon_{Nd}(t)$ and SiO_2 modelling (Fig. 12), stage II–III magmatism is consistent with the assimilation fractionation crystallization (AFC) of primary arc magma with input of ancient basement sediments.

The stage II–III felsic rocks are strongly peraluminous (Fig. 9a). Biotite is the major mafic mineral phase in all the granitoids without hornblende observed. Granitoids in the eastern and western segments of the active continental margin of the Yangtze Block show different mineralogical and geochemical characteristics (Li et al., 2003a; Wang et al., 2006a, 2006b, 2013a; Wu et al., 2006; Yao et al., 2014a). Garnet and cordierite are common in the granitoids from the eastern segment, whereas tourmaline and garnet are the common aluminum-rich minerals in the western segment. Most of these felsic rocks fall into the S-type granite field in the ACF diagram without negative correlation between P_2O_5 and SiO_2, indicating an S-type affinity (Figs. 5b, 9e). However, the P_2O_5 and TiO_2 saturation thermometry calculations indicate a wide range of initial temperatures (Fig. 5b, c; Harrison and Watson, 1984; Green and Pearson, 1986), which is in accord with their Zr saturation temperatures (651–944 °C, with an average of 778 °C; Watson and Harrison, 1983). They also exhibit island or continental arc-like REE and spidergram patterns with enrichment of LEEEs and LILEs relative to HREEs and HFSEs and pronounced negative Eu, Nb-Ta, Sr, P and Ti anomalies (Fig. 6c_{II-III}). Recent O, Hf and Nd isotope studies (Wang et al., 2013a, 2014a) indicate that some eastern segment granitoids show intermediate geochemical features between S-type and I-type granites. Wang et al. (2013a) argued that oxygen isotope values in zircons of granitoids vary from 8.5 to 10.5‰ ($\delta^{18}O$) in the western segment to 6.0–8.5‰ ($\delta^{18}O$) in the eastern segment. Hf and Nd isotope composition (Figs. 3a–d, 12; Table 1) indicate that a larger proportion of mature continental crust was incorporated into the magma sources of the western segment granitoids, whereas more juvenile materials (could be juvenile arc crust or mantle-derived mafic magma) were incorporated into the eastern segment magmas.

However, a few of stage II–III felsic rocks with high FeO^T/(FeO^T + MgO) plot in the ferron granitoid field (Fig. 9b), and their high Ga/Al and HFSE (Zr, Nb, Ce, Y) indicate an A-type affinity (Fig. 9c–d). The Nb-Y-Ce diagram (Fig. 9f) implies that they are A_2 subgroup of Eby (1992). They have major and trace element systematics similar to typical S-type granites in stage II-III (Fisg. 5a–c, 6c_{II-III}, 9a, e). Most of these A-type granitoids possess relatively high $\varepsilon_{Hf}(t)$ and $\varepsilon_{Nd}(t)$, implying more contribution of juvenile materials as arc-related meta-igneous source (Anderson, 1983; Whalen et al., 1987; Creaser et al., 1991).

5.2. Stage IV (ca. 805–750 Ma) continental rift development

The post-orogenic stage is characterized by bimodal alkaline rock suites with distinct Daly gap (see Fig. 4a) and mafic dykes in the Jiangnan Orogen (Table 1). The extension may have taken place earlier in the eastern segment of the Jiangnan Orogen, leading to the formation of the ~805–795 Ma Xucun composite dykes and the continental volcanic rocks of the Shangshu and Hongchicun Formation (Li et al., 2003b; Wang et al., 2012a; also see Table 1). Then, there are a series of bimodal alkaline rocks at ~780–750 Ma developed along the entire Jiangnan Orogen (i.e., Jingtan Formation dacite and tuff, Qianyang and Longsheng alkaline gabbro-diabase, Guzhang alkaline diabase, Tongdao mafic rocks (e.g., Pyroxenite) and Puling bimodal volcanic rocks that include basalt, rhyolite and tuff; Ge et al., 2001a; Wang et al., 2004, 2008b, 2012a; Zheng et al., 2008; also see Table 1). The bimodal magmatism seems to have stopped at ~750 Ma (Wang and Li, 2003; Li et al., 2005; Shu et al., 2008b; Shu, 2012).

The mafic rocks (with some intermediate rocks) straddle the alkaline-subalkaline boundary (Fig. 4a), and there are still some alkaline rocks (e.g., gabbro, diabase and basalt in Qianyang, Guzhang and Longsheng area; also see Table 1) with high Nb/Y ratios of >1.0 (Wang et al., 2004). The mafic rocks exhibit steep REE patterns with enriched LREEs and weak negative Nb-Ta and Ti anomalies in the spidergrams, which is a typical arc signature (Fig. 6a_{IV}). In both Figs. 7 and 8, these mafic rocks fall into the fields of continental arc magmatism with only a few samples in the within-plate basalt field. They share similar isotopic compositions with stage II–III rocks (Fig. 3a–d; Table 1), indicating that they may have also come from subduction metasomatized mantle wedge soutrce. In Fig. 11b, they all plot above the MORB-OIB array, implying crustal assimilation. The low Ba/Th and U/Th together with high LREE/

MREE and Th also emphasize the importance of sediment contribution in their petrogenesis (Fig. 11e–f). Thus, these mafic rocks show assimilation trend of the mantle-derived melt as modeled in $\varepsilon_{Nd}(t)$ vs. SiO_2 space (Fig. 12).

The felsic rocks are metaluminous to peraluminous and mostly show relatively high $FeO^T/(FeO^T + MgO)$, indicating ferron granitoids or their eruptive equivalents (Fig. 9a–b). Their high Ga/Al and HFSE (Zr, Nb) and high Zr saturation temperatures (739–919 °C, most >830 °C; Watson and Harrison, 1983) indicate that they are mainly A-type granitoids or their eruptive equivalents (Fig. 9c–d). High Rb, Rb/Nb and Y/Nb of these granitoids further suggest that they belong to the A_2 subgroup (Fig. 9f). They mostly show spidergram patterns similar to those of island or continental arc rocks with pronounced negative Nb-Ta, Sr, P and Ti anomalies (Fig. $6c_{IV}$). However, their flat REE patterns with a significant negative Eu anomaly differ from arc granitoids (Fig. $6c_{IV}$). The high LREE/MREE and Th (Figs. 9e, 11e–f) of these felsic rocks imply a dehydrated meta-sedimentary source rocks (Anderson and Thomas, 1985; Whalen et al., 1987). Considering their relatively high $\varepsilon_{Hf}(t)$ and $\varepsilon_{Nd}(t)$ (Figs. 3a, b, d, 12), they might have resulted from partial melting of a mixed source of juvenile island arc crust and ancient basement. The synchronous underplating basaltic magma might provide the required heat for juvenile crust melting.

6. Implications for the Neoproterozoic amalgamation and complex arc-trench-basin system between Yangtze and Cathaysia blocks

Based on the available data, diverse magmatic rock associations, which are widespread in the intra-oceanic arc zone, active continental margin of the Yangtze Block and active continental margin and inland of the Cathaysia Block, share distinctive but closely relative petrogenesis, indicating multiple subduction and collision processes until the final amalgamation of the two blocks followed by subsequent within-plate tectonic evolution (Fig. 13a–d).

6.1. Stage I (ca. 1000–860 Ma) oceanic arc and Cathaysia continental arc development

Integration of previous studies have demonstrated that the ~1.0–0.9 Ga intra-oceanic arc magmatic rock association with depleted mantle (DM)-like $\varepsilon_{Hf}(t)$ and $\varepsilon_{Nd}(t)$ isotopic signatures in the Shuangxiwu area of NE Zhejiang, the Zhangshudun area of NE Jiangxi and the NW of Xinyi-Luoding in the Yunkai domain (Fig. 3a–d; Table 1), manifests an earliest Neoproterozoic ocean-ocean subduction. The Tianli schist, which strongly deformed and metamorphosed to high greenschist facies, indicates that the beginning of the subduction was no later than ~1.0 Ga (Li et al., 2007b). There are also some N-type MORB-like mafic rocks found in this region (Figs. 6aI, 7a–d). All the above suggest the presence of oceanic arc-back-arc system, which led to the formation of several intra-oceanic arc terranes such as in the Shuangxiwu area, in the Zhangshudun area and the NW of Xinyi-Luoding in the Yunkai domain. The ~860 Ma glaucophane-bearing schist and the ~880 Ma Xiwan obduction-type leucogranites (Li et al., 2008a; Shu et al., 1994; Charvet et al., 1996) recorded the collision between the Shuangxiwu and Zhangshudun arc terranes and anatexis of sedimentary rocks in back-arc basins beneath ophiolite thrust sheets during the obduction of the ophiolite onto the arc crust (Pearce, 1989; Cox et al., 1999).

Meanwhile, in the Cathaysia Block, the calc-alkaline and tholeiitic mafic rocks along the Wuyi-Yunkai belt with relatively low $\varepsilon_{Hf}(t)$ and $\varepsilon_{Nd}(t)$ (Fig. 3a–d; Table 1), E-type MORB-like mafic rocks (Figs. 6aI, 7a–d) and the S- and A-type association of granitoids from the inner Cathaysia Block with relatively high A/CNK (Fig. 9a) and low $\varepsilon_{Hf}(t)$ and $\varepsilon_{Nd}(t)$ (Fig. 3a–d; Table 1) indicate an active continental margin developed in the Cathaysia Block. Thus, we infer the presence of a back-arc extension regime where mantle melting must have occurred and the underplating of such mantle-derived melts may have triggered crustal melting (e.g., meta-sedimentary basement rocks and meta-igneous component of E-type MORB chemistry), producing the S- and A-type granitoid association.

The most relevant question concerns the subduction polarity. Considering that the subduction-related rocks in the intra-oceanic arc zone and luojiamen conglomerates deposited in a foreland-basin are closer to the Jiangshao Fault (Fig. 1b; Wang et al., 2013c) while back-arc basin basalts (BABB) are closer to the Yifeng-Wanzai Fault (Fig. 1b; Li et al., 2008b; Yao et al., 2014c; Zhang et al., 2013b), the subduction polarity is expected to be northwestward. The association of adakitic rocks and Nb-enriched arc basalts in the intra-oceanic arc zone (Chen et al., 2009a; Gao et al., 2009; Li and Li, 2003; Wang et al., 2013b; Zhang et al., 2012a; also see Table 1) together with Nb-enriched arc basalts in the Cathaysia Block (Wang et al., 2013b; Zhang et al., 2012a) points to a young (≤25 Ma) oceanic crust subducting and melting beneath the intra-oceanic arc and Cathaysia Block. Niu (2014) emphasized that subduction initiation within the normal oceanic lithosphere is physically unlikely for lacking significant compositional buoyancy contrast, thus proposed that the intra-oceanic island arcs must have split off continental margins or off edges of oceanic plateaus. Without any outcrops of pre-Neoproterozoic basement rocks in intra-oceanic arc zone or other evidence that the basement of intra-oceanic arc show continental affinity, we favor that the subduction initiated at the edge of oceanic plateau.

Thus, we can draw a conclusion that the earliest stage magmatisms were associated with an intra-oceanic arc setting and active continental margin setting on the edge of the Cathaysia Block respectively (Fig. 13a). At ~1000–860 Ma, the young seafloor subducted northwestward beneath a potential oceanic plateau with subduction dehydration and mantle wedge melting. The mantle wedge may have been metasomatized by prior subduction processes (e.g., slab dehydration and melting). The island arc-like magamatic rocks formed in the intra-oceanic arc zone as a result of mantle wedge melting and varying degree of differentiation or mixing of mantle-wedge and slab melt. Meanwhile, the southeastward subduction to the Cathaysia Block also caused dehydration and melting of the subducted oceanic lithosphere. The continental arc-like mafic rocks in the Cathaysia Block must have formed this way through partial melting of mantle wedge metasomatized by subduction-related fluids and slab melt with varying degrees of assimilation with continental basement or oceanic sediments from accretionary prism or fore-arc basin. The underplating of the mantle-derived magmas provided the heat source to cause crustal melting for the felsic magmatism. The slab rollback and trench retreating (Niu, 2014) triggered the stretch of both back-arc basins in the intra-oceanic arc zone and in the Cathaysia Block. The collision between the Shuangxiwu and the Zhangshudun arc terranes at ~860 Ma led to the obduction of the Shuangxiwu arc assemblage over the Zhangshudun arc and the exhumation of the Xiwan glaucophane-bearing schist and obduction-type leucogranites.

6.2. Stage II (ca. 860–825 Ma) bidirectional subduction and continental arc development

In the intra-oceanic arc zone, the ~860–840 Ma mafic rocks show both arc and N-type MORB affinities, indicating a mature back-arc basin (Fig. 13b). This is because basalts produced in an early stage of back-arc spreading are compositionally similar to volcanic arc rocks but become indistinguishable from N-type MORB with continued opening and growth of the bach-arc basin

(Gribble et al., 1998). Yao et al. (2013) obtained an age of ~860 Ma for the flysch from the Shuangxiwu Group and proposed a fore-arc setting for the flysch. However, our synthesis and analysis show that the flysch formation is more consistent with a back-arc regime. The 860–840 Ma mafic rocks are mainly back-arc basin basalts (BABB), implying that slab rollback and trench retreating were ultimate driving force of Stage II magmatism in the intra-oceanic arc zone (Fig. 13b). Convecting and upwelling of asthenosphere heated and induced the melting of former metasomatized mantle wedge to form magmas parental to those mafic rocks. According to the Nd and Hf isotopes, both the enriched mantle wedge and the asthenospheric mantle have contributed to the generation of mantle-derived magma in this stage (Fig. 3a–d).

In the Cathaysia Block, the Miaohou and Shanhou complexes are closer to the Jiangshao Fault than the stage I magmatic rocks, implying the rollback of subducting slab under gravity (Niu, 2014; Fig. 13b). Melting experiments on basaltic eclogites have revealed that U/Th ratios become enhanced significantly at ~6 GP, corresponding to depths of ca. 150–180 km in the subducted slab front underneath the arc (Kessel et al., 2005). The lack of high U/Th ratios in the Miaohou and Shanhou complexes implies that the stage II arc magmas in the Cathaysia Block may have derived from shallower mantle domains (Fig. 11f). The other OIB-like mafic rocks located a little far from the Jiangshao Fault indicate that they may have formed by regional asthenospheric upwelling and the decompression melting of prior metasomatized mantle wedge (Fig. 13b). After that, this region may have become a typical within-plate regime. The south Anhui SSZ-type ophiolites also suggest a regional extensional setting in arc and back-arc regime such as forearc basins (Dilek and Furnes, 2011). The high-Mg basalts from northern Hunan (e.g., Yiyang komatiitic basalt; also see Table 1) and some high-Mg diorites with similar geochemical characteristics to the Setouchi high-Mg andesites (HMA) are also considered to be generated in the subduction zone. All the above reveals an active continental margin in the Yangtze Block (Fig. 13b), and the dehydration of subducting slab induced the mantle wedge metasomatism and melting to form those rocks. The wide active continental margin in the Yangtze Block also indicates the relatively shallow northwestward subduction (Fig. 13b).

Different from the intra-oceanic arc zone and the active continental margin of the Cathaysia Block, the active continental margin in the Yangtze Block is characterized by massive peraluminous granitic magmatism (Fig. 1b). Peraluminous S-type granitoids generally occur in orogenic belts as a result of juvenile crust reworking and/or experience partial melting of meta-sedimentary rocks in the lower to middle crust (Kamei, 2002). Peraluminous S-type granites can also form in an arc or back-arc regime, such as those S-type granites along the Phanerozoic circum-Pacific accretionary orogenic belts (e.g., Clemens, 2003; Collins and Richards, 2008; Kemp et al., 2009; Cawood et al., 2009, 2011). The stage II granitoids are always biotite rich, cordierite (or tourmaline and garnet)-bearing granitoids (Wang et al., 2013a), characteristic of CPGs (cordierite-bearing granitoids) subgroup, and can be linked to lower water fugacity and higher magmatic temperatures as a result of mantle upwelling or basaltic underplating (Barbarin, 1996, 1999). The increasing Rb of these granitoids also indicates an arc-continent collision (Fig. 8c–d; Pearce, 2008). The uplift and exhumation of the arc-continent collisional belt provided a significant sedimentary source for the *syn*-collisonal S-type granitoids. The amount of juvenile detritus from the exhumed arc-continental belt decreases to the western segment, which led to the decreasing $\varepsilon_{Hf}(t)$ and $\varepsilon_{Nd}(t)$ from eastern to western segments (Figs. 3a–d, 12; Wang et al., 2014a). Thus, the stage II syncollisonal granitoids (Charvet, 2013; Wang et al., 2014a) in active continental margin of the Yangtze Block formed in a compressional setting due to the collision between intra-oceanic arc and the Yangtze Block (Fig. 13b), and the underplating of synchronous subduction-related mantle-derived melt provided the heat.

6.3. Stage III (ca. 825–805 Ma) collision between Yangtze and Cathaysia blocks and Jiangnan Orogen development

The arc-like magmatic rocks in the active continental margin of the Yangtze Block cluster in ~850–825 Ma and the peak age of the formation of peraluminous granitic magmatism is ~825 Ma (Charvet, 2013; Wang et al., 2014a and this study; also see Table 1). There are abundant age data in the recent literature on the folded meta-sedimentary basement sequences in the Jiangnan Orogen, which place constraints on the timing of the final amalgamation of the intra-oceanic arc zone and the Yangtze Block at ~825 Ma along the Jingdezhen-Yifeng-Wanzai Fault (Wang et al., 2007b, 2014a; Yao et al., 2013; this work). The arc-continent collision led to the crustal shortening and thickening, i.e., the Jiangnan orogenesis and the orogen. Generally, the processed following further shortening of the thickened crust are exhumation, retrograde metamorphism and orogenic collapse etc. as result from mantle-crust isostatic re-equilibration (e.g., Kay and Kay, 1993; Leech, 2001). Post-collisional orogenic collapse led to widespread extension in the prior active continental margin of the Yangtze Block and intra-oceanic arc zone. Meanwhile, the sedimentary sequences (e.g., Luojiamen, Baizhu and Hetong Formations, the bottom of the cover sequences) are typically conglomeratic, indicating rapid uplift, erosion, short transport and deposition in response to the orogenic collapse and resulting extension (Wang and Li, 2003). There are also some peraluminous granitoids showing an A-type granite affinity, characteristic of A_2 subgroup, which are often regarded as formation in post-collisional tectonic settings (Figs. 8c–d; 9b–d, f; Bonin et al., 1998; Eby, 1992). The absence of the arc-like mafic rocks in this stage indeed implies the ending of the oceanic plate-continent subduction (Table 1). The final closure of arc-trench-basin system due to the amalgamation of the intra-oceanic arc and the Yangtze Block led to the folding of the meta-sedimentary basement sequences. Although there is no stage III magmatism developed in the intra-oceanic arc zone, a fair amount of post-collisional granitoids intruded the folded sedimentary sequences in the Yangtze Block at ~825–805 Ma due to decompression melting of the basement sediments with varying amounts of juvenile arc-related detritus (Fig. 13c).

In the Cathaysia Block, rocks of stage III magmatism only expose sporadically in the Mamianshan area (Fig. 1b; Table 1). Lacking of available ages, it is hard to constrain precisely the sequence of the arc-continent collision between the intra-oceanic arc and the Yangtze Block and between the intra-oceanic arc and the Cathaysia Block. In addition, the Neoproterozoic folded meta-sedimentary basement sequences are only exposed in the Jiangnan Orogen (Fig. 1a) but hardly found in the Cathaysia Block, implying a soft collision between the intra-oceanic arc and the Cathaysia Block. However, the presence of the ~830 Ma continental arc magmatism represented by the Miaohou and Shanhou complexes and the ~820 Ma Mamianshan bimodal volcanic rocks (Fig. 1b; Table 1) indicate that the final collision of the intra-oceanic arc and the Cathaysia Block along the Jiangshan-Shaoxing-Pingxiang-Shuangpai-Xinyi might be almost synchronous with the collision of the intra-oceanic arc and the Yangtze Block. The two arc-continent collision event welded together the Yangtze and Cathaysia blocks and the intra-oceanic arc became the binder between the two blocks (Fig. 13c). The Mamianshan peralkaline bimodal volcanic rocks consist of OIB-like mafic rocks and A_1-type felsic rocks (Fig. 6, 9b–d, f). Whalen et al. (1987) and Bonin (2007) argued that A-type granite could be produced in various tectonic environments, so long as such environments can produce favorable conditions (high temperature and low-water) for A-type granite

formation, including ocean islands, continental rifts, attenuated crust, intra-continental ring complexes, post-orogenic environments involving arc-arc or arc-continent collisions, transcurrent fault, or even subduction environments (Eby, 1992; Whalen et al., 1987; Bonin, 2007). However, the peralkaline A_1-type felsic rocks in the Cathaysia Block preclude the post-collisional setting as in active continental margin of the Yangtze Block and indicate an anorogenic environment (Fig. 8c–d). Furthermore, the mafic rocks display geochemical and Nd isotopic features strikingly similar to those of typical within-plate alkaline basalts developed in continental rifts (Figs. 7a–b, d, 12). Thus, the continental rift and upwelling of asthenosphere due to lithosphere extension following the orogenic collapse may have induced decompression melting of prior metasomatized mantle wedge to form those mafic rocks and the melting of juvenile crust and basement rocks to form those related felsic rocks in time and space (Fig. 13c).

6.4. Stage IV (ca. 805–750 Ma) continental rift development

The South China Block also preserves record of continental rifting, with sedimentary sequences deposited in two different basins: the N-E trending Nanhua rift basin and the N-S trending Kangdian rift basin (Li et al., 2002; Wang and Li, 2003; Zhao and Cawood, 2012; Fig. 1a). In Kangdian rift basin, the late Mesoproterozoic Kunyang and Huili Groups were unconformably overly by Neoproterozoic Liubatang and Yanbian Groups (Zhao and Cawood, 2012). The bimodal volcanic rocks and plutonic rocks indicated the age rang of ~805–750 Ma for the Kangdian rifting (Li et al., 2002; Wang and Li, 2003). The Nanhua rift basin pulled open along the pre-existing fault zones, especially along the Jiangshao Fault (Shu, 2012), filled with a thick Nanhuan-Sinian-Lower Paleozoic sequence and bimodal dyke swarms and involved the whole intra-oceanic arc zone, active continental margin and inland of the Cathaysia Block and active continental margin of the Yangtze Block (Wang and Li, 2003; Yao et al., 2014c, 2014d). Some previous research suggested the initial opening of the Nanhua rift at ~850 Ma (e.g., Li et al., 2008b; Wang and Li, 2003). However, recent studies of bimodal magmatism argued for the transition from orogenesis to within-plate setting at ~805 Ma (Wang et al., 2012a; Yao et al., 2014c; also see Table 1).

Our study also reveals that after ~805 Ma, the intra-oceanic arc zone and the active continental margin of the Yangtze Block turned to within-plate regime while active continental margin and inland of the Cathaysia Block had already undergone intra-plate process since ~825 Ma. Felsic rocks of the widespread bimodal volcanism show an A-type affinity and A_2 subgroup characteristics, which are derived from a mixed source of juvenile oceanic arc crust and ancient basement. Although A_2 subgroup granitoids are thought to represent post-collisional setting, the sedimentary facies associations in the Nanhua rife basin evolved from continental volcanic facies (e.g., Hongchicun, Shangshu and Jingtan Formations), through submarine volcanic facies association (e.g., Sanmenjie Formation), to littoral to shallow-marine facies associations (e.g., Dongmen and Xiuning Formations) during the time period of ~805–750 Ma, corresponding to the marine transgression in open folds with rifting-facies depositional features in South China (Wang and Li, 2003). The bimodal volcanic rocks from the Puling, Jingtan and Shangshu Formations are mainly subalkaline, but there are still some alkaline rocks exposed (e.g., alkaline gabbro-diabase from Qianyang, Guzhang and Longsheng; Daolinshan riebeckite and arfvedsonite bearing peralkaline granites; also see Table 1). Furthermore, these alkaline mafic rocks seem to form by the interaction of metasomatized mantle-derived melt and crustal materials, indicating an extensional intra-plate setting (Fig. 8c–d). Thus, at ~805 Ma, the continental rift and upwelling of asthenosphere induced the melting of the lithosphere and interaction of such melt with crust produced the bimodal magmas (Fig. 13d). The bimodal magmatism seems to have stopped at ~750 Ma (Wang and Li, 2003; Li et al., 2005; Shu et al., 2008b; Shu, 2012 and this study).

During the Nanhua rift basin development, the east segment experienced a small-scale breakup, whereas the west segment experienced an intensive breakup that split the intra-oceanic arc zone and active continental margin of the Yangtze Block along the previous suture zone into the two segments (Shu, 2012; Wang and Li, 2003; Yao et al., 2014d). The Nanhua basin was filled with detritus from both arc and continent due to exhumation and strong erosion. For instance, the sandstones of the Cambrian strata near Shaoguan was derived from dissected arc while the sandstones of the Cambrian strata near Yangjiang was derived from continental block (Yao et al., 2014d). The intensive activity of the Nanhua rift eroded Neoproterozoic magmatic rocks in both intra-oceanic arc zone and active continental margin of the Cathaysia Block, and subsequent deposition buried the evidence of Neoproterozoic subduction and collision and make it difficult to identify the boundary and amalgamation process between Yangtze and Cathaysia blocks.

7. Tracing the South China Block within Rodinia supercontinent

The location of the South China Block within the Rodinia supercontinent has been debated (e.g. Cawood et al., 2013; Charvet, 2013; Greentree et al., 2006; Li et al., 1995, 1999, 2002, 2007b, 2008c; Ling et al., 2003; Wang et al., 2003, Wang et al., 2007a, 2010a, 2013b, 2014b; Xiang and Shu, 2010; Yao et al., 2014c; Yang et al., 2004; Yu et al., 2010; Zhao and Cawood, 2012). Some researchers proposed that the Jiangnan Orogeny in South China occurred prior to ~850 Ma (ca. 1.2–0.9 Ga), which was coincident with the Grenvillian-aged Orogeny (ca. 1.0–1.3 Ga) in association with a global orogenic event, probably related to the assembly of the supercontinent Rodinia. In this context, the 850–750 Ma igneous rocks in the Yangtze Block have been interpreted as products of anorogenic magmatism in intra-continental rift basins related to mantle plume activity during the breakup of Rodinia (Li et al., 1999, 2002, 2003a, 2003b, 2008b, 2008c, 2008d; Wang and Li, 2003; Wang et al., 2010a). These authors further suggested an internal position for the South China within the Rodinia supercontinent in the latest Mesoproterozoic to earliest Neoproterozoic with Australia on the western side (Li et al., 2009) and Siberia on the eastern side (e.g. Li, 1999; Li et al., 2008c).

However, our study reveals a complex arc-trench-basin system during the amalgamation of the Yangtze and Cathaysia blocks with the final collision at ~825 Ma, significantly younger than the global Grenvillian-aged Orogenic event (ca. 1.0–1.3 Ga) along Laurentia, Australia and east Antarctica (e.g., Boger et al., 2000; Jayananda et al., 2000) when the central Rodinia supercontinent have already amalgamated without any continent-continent collision event developed within the central Rodinia supercontinent (Li et al., 2008c). Synchronous subduction-related magmatism also developed along the western and northern margins of the Yangtze Block, along the Panxi-Hannan fold belt that was active from 1000 to 750 Ma (Dong et al., 2012), although Li et al. (2002, 2008c) proposed that the 850–750 Ma magmatism along these margins resulted from a mantle plume that led to the breakup of Rodinia. Moreover, stratigraphic studies yield a similar result that the Neoproterozoic strata in South China had no connection with the Grenvillian-aged orogeny (Zhao et al., 2011). In fact, this study has substantiated that the Neoproterozoic magmatic activities took place in a complex arc-trench-basin system of destructive plate margins and the syncollsional to post-collisional settings as the result of the amalgamation of South China Block. In this context, it is worth to note that while mantle plumes may contribute to

supercontinent breakup, complete continental breakup requires subduction zones that drive seafloor spreading and continental drift (Niu, 2014). That is, without seafloor spreading and continental drift, continental breakup cannot be accomplished without broken continental masses drifting apart. This is a physically straightforward concept to be considered in building global tectonic models.

Yu et al. (2008, 2010) argued that the Cathaysia Block had a close relationship with the eastern India-East Antarctic domain of eastern Gondwana at the time of the supercontinent Rodinia and advocate a position of the South China Block between India to the west and Australia to the east. Some others indicated that the early Neoproterozoic amalgamation event might be part of a northwestward exterior accretionary orogen between Western Australia and East Antarctica around the periphery of Rodinia (e.g., Cawood et al., 2013; Wang et al., 2010a, 2013b, 2014b). The paleomagnetic records in the Neoproterozoic to early Paleozoic strata from the South China Block also suggest a location adjacent to the west coast of Australia (Macouin et al., 2004; Yang et al., 2004). All these relations suggested that the South China Block was most likely located on the margin of Rodinia until the closure of the arc systems at ~805 Ma, after which the continental rift developed in response to the breakup of Rodinia (Johnson et al., 2005; Li et al., 1999, 2008c). However, more reliable data are needed to further constrain the precise location of the South China Block within the Rodinia supercontinent. Again, we must emphasize that without subduction, without seafloor spreading and continental drift, supercontinent breakup is essentially not possible.

8. Conclusions

Integration of new and recently available geochronological, geochemical and isotopic data of Neoproterozoic igneous rocks in the South China Block provides an insight into the amalgamation and tectono-magmatic evolution between the Yangtze and Cathaysia blocks. The main conclusions are as follows:

(1) According to the temporal-spatial distribution of Neoproterozoic igneous rocks and related rocks in South China, it is reliable to divide the amalgamation domain between the Yangtze Block and Cathaysia Block into three zones: intra-oceanic arc zone, active continental margin and inland of Cathaysia and active continental margin of Yangtze. We can also detail the giant tectonomagmatic event into four stages: stage I (~1000–860 Ma) of oceanic arc and Cathaysia continental arc development; stage II (~860–825 Ma) of bidirectional subduction and continental arc development; stage III (~825–805 Ma) of collision between the Yangtze Block and Cathaysia Block that led to the Jiangnan Orogenisis; stage IV (~805–750 Ma) of continental rift development between the Yangtze Block and Cathaysia Block.

(2) In stage I, the young seafloor subducted both northwestward and southeastward beneath a potential oceanic plateau and the Cathaysia Block respectively with slab dehydration and melting formed the intra-oceanic arc and the active continental margin in Cathaysia Block. In stage II, slab rollback and trench retreat caused back-arc basin development in the intra-oceanic arc zone and the formation of arc and back-arc magmatism in the Cathaysia Block. A northwestward subduction of oceanic plate beneath the Yangtze Block form the active continental margin in the Yangtze Block. In stage III, the continent-arc-continent collision and final amalgamation between the Yangtze and Cathaysia blocks led to the Jiangnan Orogenisis. The Yangtze Block was dominated by a post-collisional extensional environment while the Cathaysia Block turned to within-plate regime. In stage IV, the Nanhua rift opened and split the west part of intra-oceanic arc zone and active continental margin of the Yangtze into two segments, which eroded and camouflaged the evidence of the boundary between the Yangtze and Cathaysia blocks.

(3) Our results do not support the argument for the role of Grenvillian-aged Orogenesis in South China in association with the assembly of the Rodinian supercontinent and mantle plume activities during the breakup of Rodinia. Considering all the evidence and arguments, we suggest that the South China Block was most likely located on the margin of Rodinia rather than in an interior position within the Rodinia supercontinent. More reliable data are needed to further constrain the precise location of South China Block within the Rodinia supercontinent. We emphasize, however, that supercontinent breakup cannot be accomplished without subduction, which drives seafloor spreading and continental drift, but mantle plumes, if existed, do not.

Acknowledgments

This work was supported by National Natural Science Foundation of China (Grant 41430208), National Basic Research Program of China (2012CB416701) and National Natural Science Foundation of China (Grant 41602046).

References

Aguillón-Robles, A., Caimus, T., Bellon, H., Maury, R.C., Cotton, J., Bourgois, J., Michaud, F., 2001. Late Miocene adakite and Nb-enriched basalts from Vizcaino Peninsula, Mexico: indicators of East Pacific Rise subduction below southern Baja California. Geology 29, 531–534.
Alabaster, T., Pearce, J.A., Malpas, J., 1982. The Volcanic Stratigraphy and Petrogenesis of the Oman Ophiolite Complex. Contrib. Miner. Petrol. 81, 168–183.
Albarède, F., Simonetti, A., Vervoort, J.D., Blichert-Toft, J., Abouchami, W.A., 1998. A Hf-Nd isotopic correlation in ferromanganese nodules. Geophys. Res. Lett. 25, 3895–3898.
Anderson, J.L., 1983. Proterozoic anorogenic granite plutonism of North America. Geol. Soc. Am. Mem. 161, 133–154.
Anderson, J.L., Thomas, W.M., 1985. Proterozoic anorogenic two-mica granites: Silver Plume and St Vrain batholiths of Colorado. Geology 13, 177–180.
Bailey, J.C., 1981. Geochemical criteria for a refined tectonic discrimination of orogenic ande-sites. Chem. Geol. 32, 139–154.
Barbarin, B., 1996. Genesis of the two main types of peraluminous granitoids. Geology 24, 295–298.
Barbarin, B., 1999. A review of the relationships between granitoid types, their origins and their geodynamic environments. Lithos 46, 605–626.
Beard, J.S., 1986. Characteristic mineralogy of arc-related cumulate gabbros: implications for the tectonic setting of gabbroic plutons and for andesite genesis. Geology 14 (10), 848–851.
Blichert-Toft, J., Albarède, F., 1997. The Lu-Hf geochemistry of chondrites and the evolution of the mantle-crust system. Earth Planet. Sci. Lett. 148, 243–258.
Boger, S.D., Carson, C.J., Wilson, C.J.L., Fanning, C.M., 2000. Neoproterozoic deformation in the Radok Lake region of the northern Prince Charles Mountains, East Antarctica: evidence for a single protracted orogenic event. Precambr. Res. 104, 1–24.
Bonin, B., 2007. A-type granites and related rocks: evolution of a concept, problems and prospects. Lithos 97, 1–29.
Bonin, B., Azzouni-Sekkal, A., Bussy, F., Ferrag, S., 1998. Alkali-calcic and alkaline post-orogenic (PO) granite magmatism: petrologic constraints and geodynamic settings. Lithos 45, 45–70.
Bonnefoi, C.C., Provost, A., Alberade, F., 1995. The 'Daly gap' as a magmatic catastrophe. Nature 378, 270–272.
Cabanis, B., Lecolle, M., 1989. Le diagramme La/10-Y/15-Nb/8: un outil pour la discrimination des séries volcaniques et la mise en évidence des processus de mélange et/ou de contamination crustale. C. R. Acad. Sci. Ser. II 309, 2023–2029.
Calanchi, N., Peccerillo, A., Tranne, C.A., Lucchini, F., Rossi, P.L., Kempton, P., Barbieri, M., Wu, T.W., 2002. Petrology and geochemistry of volcanic rocks from the island of Panarea: implications for mantle evolution beneath the Aeolian island arc (southern Tyrrhenian sea). J. Volcanol. Geoth. Res. 115, 367–395.
Cann, J.R., 1968. Bimodal distribution of rocks from volcanic islands. Earth Planet. Sci. Lett. 4, 479–480.
Castillo, P.R., 2012. Adakite petrogenesis. Lithos 134–135, 304–316.

Cawood, P.A., Kröner, A., Collins, W.J., Kusky, T.M., Mooney, W.D., Windley, B.F., 2009. Accretionary orogens through Earth history. In: Cawood, P.A., Kröner, A. (Eds.), Earth Accretionary Systems in Space and Time, vol. 318. Geological Society of London Special Publication, pp. 1–36.
Cawood, P.A., Leitch, E.C., Merle, R.E., Nemchin, A.A., 2011. Orogenesis without collision: stabilizing the Terra Australis accretionary orogen, eastern Australia. Geol. Soc. Am. Bull. 123 (11–12), 2240–2255.
Cawood, P.A., Wang, Y.J., Xu, Y.J., Zhao, G.C., 2013. Locating south China in Rodinia and Gondwana: a fragment of greater India lithosphere? Geology 41 (8), 903–906.
Chappell, B.W., 1999. Aluminium saturation in I- and S-type granites and the characterization of fractionated haplogranites. Lithos 46, 535–551.
Charvet, J., 2013. The Neoproterozoic-Early Paleozoic tectonic evolution of the South China Block: An overview. J. Asian Earth Sci. 74, 198–209.
Charvet, J., Shu, L.S., Shi, Y.S., Guo, L.Z., Faure, M., 1996. The building of south China: collision of Yangtze and Cathaysia blocks, problems and tentative answers. J. Asian Earth Sci. 13 (3–5), 223–235.
Charvet, J., Shu, L.S., Faure, M., Choulet, F., Wang, B., Lu, H.F., Breton, N.L., 2010. Structural development of the Lower Paleozoic belt of South China: genesis of an intracontinental orogen. J. Asian Earth Sci. 39, 309–330.
Chauvel, C., Lewin, E., Carpentier, M., Arndt, N.T., Marini, J.C., 2008. Role of recycled oceanic basalt and sediment in generating the Hf-Nd mantle array. Nat. Geosci. 1 (1), 64–67.
Chayes, F., 1963. Relative abundance of intermediate members of the oceanic basalt-trachyte association. J. Geophys. Res. 68, 1519–1534.
Chen, J.F., Jahn, B.M., 1998. Crustal evolution of southeastern China: Nd and Sr isotopic evidence. Tectonophysics 284 (1–2), 101–133.
Chen, J., Foland, K.A., Xing, F., Xu, X., Zhou, T., 1991. Magmatism along the southeast margin of the Yangtze block: Precambrian collision of the Yangtze and Cathaysia block of China. Geology 19, 815–818.
Chen, Z.H., Guo, K., Dong, Y., Chen, R., Li, L., Liang, Y., Li, C., Yu, X., Zhao, L., Xing, G., 2009a. Possible early Neoproterozoic magmatism associated with slab window in the Pingshui segment of the Jiangshan-Shaoxing suture zone: evidence from zircon LA-ICP-MS U-Pb geochronology and geochemistry. Sci. China, Ser. D Earth Sci. 52, 925–939.
Chen, Z.H., Xing, G.F., Guo, K.Y., Dong, Y.G., Chen, R., Zeng, Y., Li, L.M., He, Z.Y., Zhao, L., 2009b. Petrogenesis keratophyres in the Pingshui Group, Zhejiang: constraints from zircon U-Pb ages and Hf isotopes. Chin. Sci. Bull. 54, 1570–1578.
Chen, K., Gao, S., Wu, Y.B., Guo, J.L., Hu, Z.C., Liu, Y.S., Zong, K.Q., Liang, Z.W., Geng, X. L., 2013. 2.6–2.7 Ga crustal growth in Yangtze Craton, South China. Precambrian Research 224, 472–490.
Chen, X., Wang, D., Wang, X.L., Gao, J.F., Shu, X.J., Zhou, J.C., Qi, L., 2014. Neoproterozoic chromite-bearing high-Mg diorites in the western part of the Jiangnan orogen, southern China: geochemistry, petrogenesis and tectonic implications. Lithos 200–201, 35–48.
Clague, D.A., 1978. The oceanic basalt–trachyte association: an explanation of the Daly Gap. J. Geol. 86, 739–743.
Class, C., Miller, D.M., Goldstein, S.L., Langmuir, C.H., 2000. Distinguishing melt and fluid subduction components in Umnak Volcanics, Aleutian Arc. Geochem. Geophys. Geosyst. 1, 1004. http://dx.doi.org/10.1029/1999GC000010.
Clemens, J.D., 2003. S-type granitic magmas—petrogenetic issues, models and evidence. Earth Sci. Rev. 61 (1–2), 1–18.
Collins, W.J., Richards, S.W., 2008. Geodynamic significance of S-type granites incircum-Pacific orogens. Geology 36, 559–562.
Condie, K.C., 1989. Geochemical changes in basalts and andesites across the Archean-Proterozoic boundary: Identification and significance. Lithos 23, 1–18.
Cox, J., Searle, M., Pedersen, R., 1999. The petrogenesis of leucogranitic dykes intruding the northern Semail ophiolite, United Arab Emirates: field relationships, geochemistry and Sr/Nd isotope systematics. Contrib. Miner. Petrol. 137, 267–287.
Creaser, R.A., Price, R.C., Wormald, R.J., 1991. A-type granites revisited: assessment of a residual-source model. Geology 19, 163–166.
Defant, M.J., Drummond, M.S., 1990. Derivation of some modern arc magmas by melting of young subducted lithosphere. Nature 347, 662–665.
Defant, M.J., Kepezhinskas, P., 2001. Evidence suggests slab melting in arc magmas. EOS Trans. Am. Geophys. Union 82, 62–70.
Defant, M.J., Jackson, T.E., Drummond, M.S., de Boer, J.Z., Bellon, H., Feigenson, M.D., Maury, R.C., Stewart, R.H., 1992. The geochemistry of young volcanism throughout western Panama and southern Costa Rica, an overview. Geol. Soc. London J. 149, 569–579.
Dilek, Y., Furnes, H., 2011. Ophiolite genesis and global tectonics: geochemical and tectonic fingerprinting of ancient oceanic lithosphere. Geol. Soc. Am. Bull. 123, 387–411.
Ding, X., Zhou, X.M., Sun, T., 2005. The episodic growth of the continental crustalbasement in South China: single zircon LA-ICPMS U-Pb dating of Guzhai granodiorite in Guangdong. Geol. Rev. 51 (4), 383–392 (in Chinese with English abstract).
Ding, B.H., Shi, R.D., Zhi, X.C., Zheng, L., Chen, L., 2008. Neoproterozoic (~850 Ma) subduction in the Jiangnan orogen: evidence from the SHRIMP U-Pb dating of the SSZ-type ophiolite in southern Anhui Province. Acta Petrol. Mineral. 27 (5), 375–388 (in Chinese with English abstract).
Dong, Y., Liu, X., Santosh, M., Chen, Q., Zhang, X., Li, W., He, D., Zhang, G., 2012. Neoproterozoic accretionary tectonics along the northwestern margin of the Yangtze Block, China: Constraints from zircon U-Pb geochronology and geochemistry. Precambr. Res. 196–197, 247–274.
Drummond, M.S., Defant, M.J., Kepezhinskas, P.K., 1996. Petrogenesis of slab derived trondhjemite-tonalite-dacite-adakite magmas. Trans. R. Soc. Edinb. Earth Sci. 87, 205–215.
Eby, G.N., 1992. Chemical subdivision of the A-type granitoids: petrogenetic and tectonic implications. Geology 20, 641–644.
Ellam, R.M., Cox, K.G., 1991. An interpretation of Karoo picrite basalts in terms of interaction between asthenospheric magmas and the mantle lithosphere. Earth Planet. Sci. Lett. 105, 330–342.
Fan, J.L., Luo, J.H., Cao, Y.Z., Han, W., Zhang, J.Y., 2010. Feature of geochemistry, isotopie chronology and geological significance of Neoproterozoic granitic rocks in southeastern Guizhou, China. J. Northwest Univ. (Nat. Sci. Ed.) 40 (4), 672–678 (in Chinese with English abstract).
Frost, C.D., Frost, B.R., 2011. On ferroan (A-type) granitoids: their compositional variability and modes of origin. J. Petrol. 52, 39–54.
Frost, B.R., Barnes, C.G., Collins, W.J., Arculus, R.J., Ellis, D.J., Frost, C.D., 2001. A geochemical classification for granitic rocks. J. Petrol. 42, 2033–2048.
Fujian BGMR (Bureau of Geology and Mineral Resources of Fujian Province), 1985. Regional Geology of the Fujian Province. Geological Publishing House, Beijing, pp. 1–610 (in Chinese with English abstract).
Gao, S., Ling, W.L., Qiu, Y., Zhou, L., Hartmann, G., Simon, K., 1999. Contrasting geochemical and Sm-Nd isotopic compositions of Archean metasediments from the Kongling high-grade terrain of the Yangtze craton: evidence for cratonic evolution and redistribution of REE during crustal anatexis. Geochim. Cosmochim. Acta 63, 2071–2088.
Gao, J., Klemd, R., Long, L.L., Xiong, X.M., Qian, Q., 2009. Adakitic signature formed by fractional crystallization: an interpretation for the Neo-Proterozoic meta-plagiogranites of the NE Jiangxi ophiolitic mélange belt, South China. Lithos 110, 277–293.
Gao, S., Yang, J., Zhou, L., Li, M., Hu, Z.C., Guo, J.L., Yuan, H.L., Gong, H.J., Xiao, G.Q., Wei, J.Q., 2011. Age and growth of the Archean Kongling terrain. South China, with emphasis on 3.3 Ga granitoid gneisses. Am. J. Sci. 311, 153–182.
Gao, L.Z., Ding, X.Z., Liu, Y.X., Zhang, C.H., Zhang, H., Huang, Z.Z., Xu, X.M., Zhou, Z.Y., 2014. SHRIMP zircon U-Pb dating of Neoproterozoic Chencai Complex in Jiangshan- Shaoxing fault zone and its implications. Geol. Bull. China 33 (5), 641–648 (in Chinese with English abstract).
Ge, W.C., Li, X.H., Li, Z.X., Zhou, H.W., Wang, J., Lee, C.Y., 2000a. "Longsheng ophiolite" in north Guangxi revisited. Acta Petrol. Sin. 16 (1), 111–118 (in Chinese with English abstract).
Ge, W.C., Li, X.H., Li, Z.X., Zhou, H.W., Wang, J., Lee, C.Y., 2000b. Geological and geochemical evidence for the genesis of tremolitized mafic rocks from Baotan in northern Guangxi. Geochimica 29 (3), 253–257 (in Chinese with English abstract).
Ge, W.C., Li, X.H., Li, Z.X., Zhou, H.W., 2001a. Mafic intrusions in Longsheng area: age and its geological implications. Chin. J. Geol. 36, 112–118 (in Chinese with English abstract).
Ge, W.C., Li, X.H., Li, Z.X., Zhou, H.W., Lee, C.Y., 2001b. Geochemical studies on two types of Neoproterozoic peraluminous granitoids in northern Guangxi. Geochimica 30 (1), 24–34 (in Chinese with English abstract).
Ge, W.C., Li, X.H., Liang, X.R., Wang, R.C., Li, Z.X., Zhou, H.W., 2001c. Geochemical and geological implications of maficultramafic rocks with age of ~825 Ma in Yuanbaoshan-Baotan area of northern Guangxi. Geochimica 30 (2), 123–130 (in Chinese with English abstract).
Green, T.H., Pearson, N.J., 1986. Ti-rich accessory phase saturation in hydrous mafic-felsic compositions at high P, T. Chem. Geol. 54, 185–201.
Greentree, M.R., Li, Z.X., Li, X.H., Wu, H., 2006. Late Mesoproterozoic to earliest Neoproterozoic basin record of the Sibao orogenesis in western South China and relationship to the assembly of Rodinia. Precambr. Res. 151, 79–100.
Gribble, R.F., Stern, R.J., Newman, S., Bloomer, S.H., O'Hearn, T., 1998. Chemical and isotopic composition of lavas from the Northern Mariana Trough: implications for magma genesis in back-arc-arc basins. J. Petrol. 39, 125–154.
Griffin, W.L., O'Reilly, S.Y., Ryan, C.G., 1999. The composition and origin of subcontinental lithospheric mantle. In: Fei, Y., Bertka, C.M., Mysen, B.O. (Eds.), Mantle Petrology: Field Observations and High-Pressure Experimentation: A Tribute to Francis R. (Joe) Boyd. The Geochemical Society, Houston, pp. 13–45. Geochemical Society Special Publication No. 6.
Grove, T.L., Till, C.B., Krawczynski, M.J., 2012. The role of H_2O in subduction zone magmatism. Annu. Rev. Earth Planet. Sci. 40, 413–439.
Guo, L.Z., Shi, Y.S., Ma, R.S., 1980. The geotectonic framework and crustal evolution of South China. In: Scientific Paper on Geology for International Exchange. J. Geological Publishing House, Beijing, pp. 109–116 (in Chinese with English abstract).
Guo, L.Z., Shi, Y.S., Ma, R.S., Lu, H.F., Ye, S.F., 1985. Plate movement and crustal evolution of the Jiangnan Proterozoic mobile belt, Southeast China. Earth Sci. (Chikyu Kagaku) 39 (2), 156–166.
Harris, N.B.W., Pearce, J.A., Tindle, A.G., 1986. Geochemical characteristics of collision zone magmatism. In: Coward, M.P., Reis, A.C. (Eds.), Collision Tectonics, vol. 19. Geological Society of London Special Publication, pp. 67–81.
Harrison, T.M., Watson, E.B., 1984. The behavior of apatite during crustal anatexis: equilibrium and kinetic considerations. Geochim. Cosmochim. Acta 48, 1467–1477.
Hawkesworth, C.J., Lightfoot, P.C., Fedorenko, V.A., Blake, S., Naldrett, A.J., Doherty, W., Gorbachev, N.S., 1995. Magma differentiation and mineralisation in the Siberian continental flood basalts. Lithos 34, 61–88.
Hawkesworth, C.J., Turner, S.P., Mcdermott, F., Peate, D.W., van Calsteren, P., 1997. U-Th isotopes in arc magmas: implications for element transfer from subducted crust. Science 276, 555–561.

Irvine, T.N., Baragar, W.R.A., 1971. A guide to the chemical classification of the common volcanic rocks. Can. J. Earth Sci. 8, 523–548.
Jayananda, M., Moyen, J.F., Martin, H., Peucat, J.J., Auvray, B., Mahabaleswar, B., 2000. Late Archaean (2550–2520 Ma) juvenile magmatism in the Eastern Dharwar craton, southern India: constraints from geochronology, Nd-Sr isotopes and whole rock geochemistry. Precambr. Res. 99, 225–254.
Jiao, W.F., Wu, Y.B., Yang, S.H., Peng, M., Wang, J., 2009. The oldest basement rock in the Yangtze Craton revealed by zircon U-Pb age and Hf isotope composition. Sci. China Ser., D 52, 1393–1399.
Johnson, S.P., Rivers, T., De Waele, B., 2005. A review of the Mesoproterozoic to early Palaeozoic magmatic and tectonothermal history of south-central Africa: implications for Rodinia and Gondwana. J. Geol. Soc. 162, 433–450.
Kamei, A., 2002. Petrogenesis of Cretaceous Peraluminous granite suites with low initial Sr isotopic ratios, Kyushu Island, Southwest Japan Arc. Gondwana Res. 5, 813–822.
Kay, R.W., Kay, S.M., 1993. Delamination and delamination magmatism. Tectonophysics 219, 177–189.
Kelemen, P.B., Hanghøj, K., Greene, A.R., 2003. One view of the geochemistry of subduction-related magamatic arcs, with emphasis on primitive andesite and lower crust. In: Rudnick, R.L. (Ed.), The Crust. In: Holland, H.D., Turekian, K.K. (Eds.), Treatise on Geochemistry. Elsevier-Pergamon, Oxford, pp. 593–659.
Kemp, A.I.S., Hawkesworth, C.J., Collins, W.J., Gray, C.M., Blevin, P.L., 2009. Isotopic evidence for rapid continental growth in an extensional accretionary orogen: the Tasmanides, eastern Australia. Earth Planet. Sci. Lett. 284, 455–466.
Kepezhinskas, P.K., Defant, M.J., Drummond, M.S., 1996. Progressive enrichment of island-arc mantle by melt-peridotite interaction from Kamchatka adakites. Geochim. Cosmochim. Acta 60, 1217–1229.
Kepezhinskas, P., McDermott, F., Defant, M.J., Hochstaedter, A., Drummond, M.S., 1997. Trace element and Sr-Nd-Pb isotopic constraints on a three-component model of Kamchatka Arc petrogenesis. Geochim. Cosmochim. Acta 61 (3), 577–600.
Kessel, R., Schmidt, M.W., Ulmer, P., Pettke, T., 2005. Trace element signature of subduction-zone fluids, melts and supercritical liquids at 120–180 km depth. Nature 437, 724–727.
Kuno, H., 1968. Differentiation of basalt magmas. In: Hess, H.H., Poldervaart, A. (Eds.), Basalts: The Poldervaart Treatise on Rocks of Basaltic Composition, Interscience, Vol. 2. New York, N.Y., pp. 623–688.
La Flèche, M.R., Camire, G., Jenner, G.A., 1998. Geochemistry of post-Acadian, Carboniferous continental intraplate basalts from the Maritimes Basin, Magdalen islands, Quebec, Canada. Chem. Geol. 148, 115–136.
Lao, Q.Y., Hu, S.L., 1997. The $^{40}Ar/^{39}Ar$ age date of silicalite of Yunkai Group and their Geological significance. Acta Geosci. Sin. 18, 98–101 (in Chinese with English abstract).
Lawton, T.F., McMillan, N.J., 1999. Arc abandonment as a cause for passive continental rifting: comparison of the Jurassic Mexican Borderland rift and the Cenozoic Rio Grande rift. Geology 27, 779–782.
Leat, P.T., Larter, R.D., Millar, I.L., 2007. Silicic magmas of Protector Shoal, South Sandwich arc: indicators of generation of primitive continental crust in an island arc. Geol. Mag. 144, 179–190.
Leech, M.L., 2001. Arrested orogenic development: eclogitization, delamination, and tectonic collapse. Earth Planet. Sci. Lett. 185, 149–159.
Li, J.L., 1993. Texture of Lithosphere and Geological Evolution of Southeastern China. Metallurgic Industry Press, Beijing, pp. 1–217 (in Chinese with English abstract).
Li, X.H., 1999. U-Pb zircon ages of granites from the southern margin of the Yangtze margin: timing of Neoproterozoic Jinning: Orogen in SE China and implication for Rodinia assembly. Precambr. Res. 97, 43–57.
Li, W.X., Li, X.H., 2003. Adakitic granites within the NE Jiangxi ophiolites, South China: geochemical and Nd isotopic evidence. Precambr. Res. 122, 29–44.
Li, X.H., Zhou, G.Q., Zhao, J.X., Fanning, C.M., Compston, W., 1994. SHRIMP ion microprobe zircon U-Pb age and Sm-Nd isotopic characteristics of the NE Jiangxi ophiolite and its tectonic implications. Geochimica 13, 317–325.
Li, Z.X., Zhang, L., Powell, C.M., 1995. South China in Rodinia: part of the missing link between Australia-East Antarctica and Laurentia? Geology 23, 407–410.
Li, X.H., Zhao, J.X., McCulloch, M.T., Zhou, G.Q., Xing, F.M., 1997. Geochemical and Sm-Nd isotopic study of Neoproterozoic ophiolites from southeastern China: petrogenesis and tectonic implications. Precambr. Res. 81, 129–144.
Li, Z.X., Li, X.H., Kinny, P.D., Wang, J., 1999. The breakup of Rodinia: did it start with a mantle plume beneath South China? Earth Planet. Sci. Lett. 173, 171–181.
Li, Z.X., Li, X.H., Zhou, H., Kinny, P.D., 2002. Grenvillian continental collision in South China: new SHRIMP U-Pb zircon results and implications for the configuration of Rodinia. Geology 30, 163–166.
Li, X.H., Li, Z.X., Ge, W., Zhou, H.W., Li, W.X., Wingate, M.T.D., 2003a. Neoproterozoic granitoids in South China: crystal melting above a mantle plume at ca. 825Ma? Precambr. Res. 122, 45–83.
Li, Z.X., Li, X.H., Kinny, P.D., Wang, J., Zhang, S., Zhou, H.W., 2003b. Geochronology of Neoproterozoic syn-rift magmatism in the Yangtze Craton, South China and correlations with other continents: evidence for amantle superplume that broke up Rodinia. Precambr. Res. 122, 85–109.
Li, W.X., Li, X.H., Li, Z.X., 2005. Neoproterozoic bimodal magmatism in the Cathaysia Block of South China and its tectonic significance. Precambr. Res. 136, 51–66.
Li, P.C., Chen, G.H., Xu, D.R., He, Z.L., Fu, G.G., 2007a. Petrological ang geochemical characteristics and petrogenesis of Neoproterozoic peraluminous granites in northeastern Hunan province. Geotect. Metal. 31 (1), 126–136 (in Chinese with English abstract).
Li, Z.X., Wartho, J.A., Occhipinti, S., Zhang, C.L., Li, X.H., Wang, J., Bao, C.M., 2007b. Early history of the eastern Sibao Orogen (South China) during the assembly of Rodinia: new mica $^{40}Ar/^{39}Ar$ dating and SHRIMP U-Pb detrital zircon provenance constraints. Precambr. Res. 159, 79–94.
Li, W.X., Li, X.H., Li, Z.X., Lou, F.S., 2008a. Obduction-type granites within the NE Jiangxi Ophiolite: implications for the final amalgamation between the Yangtze and Cathaysia blocks. Gondwana Res. 13, 288–301.
Li, X.H., Li, W.X., Li, Z.X., Liu, Y., 2008b. 850–790 Ma bimodal volcanic and intrusive rocks in northern Zhejiang, South China: a major episode of continental rift magmatism during the breakup of Rodinia. Lithos 102, 341–357.
Li, Z.X., Bogdanova, S.V., Collins, A.S., Davidson, A., De Waele, B., Ernst, R.E., Fitzsimons, I.C.W., Fuck, R.A., Gladkochub, D.P., Jacobs, J., Karlstrom, K.E., Lu, S., Natapov, L.M., Pease, V., Pisarevsky, S.A., Thrane, K., Vernikovsky, V., 2008c. Assembly, configuration, and break-up history of Rodinia: a synthesis. Precambr. Res. 160, 179–210.
Li, Z.X., Li, X.H., Li, W.X., Ding, S.J., 2008d. Was Cathaysia part of Proterozoic Laurentia? New data from Hainan Island, south China. Terra Nova 20, 154–164.
Li, X.H., Li, W.X., Li, Z.X., Lo, C.H., Wang, J., Ye, M.F., Yang, Y.H., 2009. Amalgamation between the Yangtze and Cathaysia blocks in South China: constraints from SHRIMP U-Pb zircon ages, geochemistry and Nd-Hf isotopes of the Shuangxiwu volcanic rocks. Precambr. Res. 174, 117–128.
Li, W.X., Li, X.H., Li, Z.X., 2010a. Ca. 850 Ma bimodal volcanic rocks in northeastern Jiangxi South China: initial extension during the breakup of Rodinia. Am. J. Sci. 310, 951–980.
Li, Z.X., Li, X.H., Wartho, J.A., Clark, C., Li, W.X., Zhang, C.L., Bao, C., 2010b. Magmatic and metamorphic events during the Early Paleozoic Wuyi-Yunkai Orogeny, south-eastern South China: new age constraints and pressure–temperature conditions. Geol. Soc. Am. Bull. 122, 772–793.
Li, L.M., Lin, S.F., Xing, G.F., Davis, D.W., Davis, W.J., Xiao, W.J., Yin, C.Q., 2013. Geochronology and geochemistry of volcanic rocks from the Shaojiwa Formation and Xingzi Group, Lushan area, SE China: implications for Neoproterozoic back-arc basin in the Yangtze Block. Precambr. Res. 238, 1–17.
Ling, W., Gao, S., Zhang, B., Li, H., Liu, Y., Cheng, J., 2003. Neoproterozoic tectonic evolution of the northwestern Yangtze craton South China: implications for amalgamation and break-up of the Rodinia supercontinent. Precambr. Res. 122, 111–140.
Liu, B.X., Liu, C.G., Qiu, Y.Q., 2001. The Pb-Pb isotopic ages and geologic significance of gneissic granite in Hezi, Jiangxi. Volcanol. Min. Resour. 22 (4), 264–268 (in Chinese with English abstract).
Ma, T.Q., Chen, L.X., Bai, D.Y., Zhou, K.J., Li, G., Wang, X.H., 2009. Zircon SHRIMP dating and geochemical characteristics of Neoproterozoic granites in southeastern Hunan. Geol. China 36 (1), 65–73 (in Chinese with English abstract).
Macouin, M., Besse, J., Ader, M., Gilder, S., Yang, Z., Sun, Z., Agrinier, P., 2004. Combined paleomagnetic and isotopic data from the Doushantuo carbonates, South China: Implications for the "snowball Earth" hypothesis. Earth Planet. Sci. Lett. 224, 387–398.
Maniar, P.D., Piccoli, P.M., 1989. Tectonic discrimination of granitoids. Geol. Soc. Am. Bull. 101, 635–643.
Mao, J.W., Pirajno, F., Cook, N., 2011. Mesozoic metallogeny in East China and corresponding geodynamic settings-an introduction to the special issue. Ore Geol. Rev. 43, 1–7.
Mao, J.W., Cheng, Y.B., Chen, M.H., Pirajno, F., 2013. Major types and time-space distribution of Mesozoic ore deposits in South China and their geodynamic settings. Miner. Deposita 48, 267–294.
Middlemost, E.A.K., 1994. Naming materials in the magma/igneous rock system. Earth Sci. Rev. 37, 215–224.
Miyashiro, A., 1974. Volcanic rock series in island arcs and active continental margins. Am. J. Sci. 274, 321–355.
Moyen, J.F., 2009. High Sr/Y and La/Yb ratios: the meaning of the "adakitic signature". Lithos 112, 556–574.
Nan, Y., 1994. Division and geologica age of Yunkai Group in western Guangdong. Guangdong Geol. 9 (4), 1–11.
Niu, Y.L., 2014. Geological understanding of plate tectonics: Basic concepts, illustrations, examples and new perspectives. Glob. Tecton. Metal. 10, 1–24.
Niu, Y.L., O'Hara, M.J., 2003. Origin of ocean island basalts: a new perspective from petrology, geochemistry, and mineral physics considerations. J. Geophys. Res. 108, 2209–2228.
Niu, Y.L., O'Hara, M.J., Pearce, J.A., 2003. Initiation of subduction zones as a consequence of lateral compositional buoyancy contrast within the lithosphere: a petrologic perspective. J. Petrol. 44, 851–866.
Niu, Y.L., Zhao, Z.D., Zhu, D.C., Mo, X.X., 2013. Continental collision zones are primary sites for net continental crust growth–A testable hypothesis. Earth-Sci. Rev. 127, 96–110.
Pan, G.T., Xiao, Q.H., Lu, S.N., Deng, J.F., Feng, Y.M., Zhang, K.X., Zhang, Z.Y., Wang, F. G., Xing, G.F., Hao, G.J., Feng, Y.F., 2009. Subdivision of tectonic units in China. Geol. China 36, 1–28 (in Chinese with English abstract).
Pearce, J.A., 1989. High T/P metamorphism and granite genesis beneath ophiolite thrust sheets. Ofioliti 14, 195–211.
Pearce, J.A., 1996. Sources and settings of granitic rocks. Episodes 19, 120–125.
Pearce, J.A., 2008. Geochemical fingerprinting of oceanic basalts with applications to ophiolites classification and the search for Archean oceanic crust. Lithos 100, 14–48.
Pearce, J.A., Stern, R.J., 2006. The origin of back-arc basin magmas: trace element and isotope perspectives. In: Christie, D.M., Fisher, C.R., Lee, S.-M., Givens, S. (Eds.), Back-Arc Spreading Systems: Geological, Biological, Chemical and Physical Interactions, vol. 166. American Geophysical Union Geophysical Monograph, pp. 63–86.

Pearce, J.A., Lippard, S.J., Roberts, S., 1984. Characteristics and tectonic significance of supra-subduction zone ophiolites. In: Kokelaar, B.P., Howells, M.F. (Eds.), Marginal Basin Geology. Blackwell, Oxford, pp. 77–94. Geol. Soc. Spec. Publ. No. 16.
Peccerillo, R., Taylor, S.R., 1976. Geochemistry of Eocene calcalkaline volcanic rocks from the Kastamonu area, northern Turkey. Contrib. Miner. Petrol. 58, 63–81.
Peng, S.B., Jin, Z.M., Fu, J.M., He, L.Q., Cai, M.H., Liu, Y.H., 2006. The geochemical evidences and tectonic significance of Neoproterozoic ophiolite in Yunkai area, western Guangdong Province, China. Acta Geol. Sin. 80 (6), 814–825 (in Chinese with English abstract).
Plank, T., Langmuir, C.H., 1998. The chemical composition of subducting sediment and its consequences for the crust and mantle. Chem. Geol. 145, 325–394.
Qi, Q., Zhou, X.M., Wang, D.Z., 1986. The origin of the spilite-keratophyre series and the characteristic of the related mantle-derived granitic rocks in Xiqiu Zhejiang. Acta Petrol. Mineral. 5, 299–308 (in Chinese with English abstract).
Qin, X.F., Zhou, F.S., Hu, G.A., Li, G.N., Xie, L.F., Zhou, K.H., Huang, X.Q., Pan, Y.W., 2005. First discovery of MORB volcanic rock and its tectonic significance on the north margin of the Yunkai Block, SE Guangxi. Geol. Sci. Technol. Inf. 24 (3), 20–24 (in Chinese with English abstract).
Qin, X.F., Pan, Y.M., Li, L., Li, R.S., Zhou, F.S., Hu, G.A., Zhong, F.Y., 2006. Zircon SHRIMP U-Pb geochronology of the Yunkai metamorphic complex in southeastern Guangxi, China. Geol. Bull. China 25 (5), 553–559 (in Chinese with English abstract).
Qin, X.F., Pan, Y.M., Xia, B., Li, R.S., Zhou, F.S., Hu, G.A., Lu, G.B., 2007. Geochemical characteristics and tectonic significances of metabasic volcanic rocks in the northern margin of Yunkai Block, SE Guangxi. Geochimica 36 (3), 311–322 (in Chinese with English abstract).
Qiu, Y.M., Gao, S., McNaughton, N.J., Groves, D.I., Ling, W.L., 2000. First evidence of ~3.2 Ga continental crust in the Yangtze craton of south China and its implications for Archean crustal evolution and Phanerozoic tectonics. Geology 28, 11–14.
Sajona, F.G., Maury, R.C., Bellon, H., Cotten, J., Defant, M., 1996. High field strength element enrichment of Pliocene-leistocene island arc basalts, Zamboanga Peninsula, western Mindanao (Philippines). J. Petrol. 37, 693–726.
Shao, F.L., Niu, Y.L., Regelous, M., Zhu, D.C., 2015. Petrogenesis of peralkaline rhyolites in an intra-plate setting: Glass House Mountains, Southeast Queensland, Australia. Lithos 216–217, 196–210.
Shi, Z.G., Gao, L.Z., Li, T.D., Ding, X.Z., Wang, J., Song, Z.R., Huang, Z.Z., Zhang, H., 2014. Zircon U-Pb isotopes dating of Hanyangfeng Formation in Lushan area and its geological significance. Geol. China 41 (2), 326–334 (in Chinese with English Abstract).
Shu, L.S., 2012. An analysis of principal features of tectonic evolution in South China Block. Geol. Bull. China 31 (7), 1035–1053 (in Chinese with English Abstract).
Shu, L.S., Charvet, J., 1996. Kinematics and geochronology of the Proterozoic Dongxiang – Shexian ductile shear zone: with HP metamorphism and ophiolitic melange (Jiangnan region, South China). Tectonophysics 267, 291–302.
Shu, L.S., Zhou, G.Q., Shi, Y.S., Yin, J., 1994. Study of high pressure metamorphic blueschist and its late Proterozoic age in the eastern Jiangnan belt. Chin. Sci. Bull. 39, 1200–1204.
Shu, L.S., Faure, M., Jiang, S.Y., Yang, Q., Wang, Y.J., 2006. SHRIMP zircon U-Pb age, litho- and biostratigraphic analyses of the Huaiyu Domain in South China—evidence for a Neoproterozoic orogenic belt, not Late Paleozoic-Early Mesozoic collision. Episodes 29 (4), 244–252.
Shu, L.S., Deng, P., Yu, J.H., Wang, Y.B., Jiang, S.Y., 2008a. The age and tectonic environment of the rhyolitic rocks on the western side of Wuyi Mountain, South China. Sci. China (D) 38 (8), 950–959.
Shu, L.S., Faure, M., Wang, B., Zhou, X.M., Song, B., 2008b. Late Paleozoic-Early Mesozoic Geological Features of South China: response to the Indosinian collision event in Southeast Asia. C.R. Geosci. 340, 151–165.
Shu, L.S., Faure, M., Yu, J.H., Jahn, B.M., 2011. Geochronological and geochemical features of the Cathaysia Block (South China): new evidence for the Neoproterozoic breakup of Rodinia. Precambr. Res. 187 (3–4), 263–276.
Shui, T., 1987. Structural framework of the continental basement in southeast China. Sci. China Ser., B 4, 414–422 (in Chinese).
Shui, T., Xu, B.T., Liang, R.H., Qiu, Y.S., 1986. The old continent joint of Shaoxing-Jiangshan. Chin. Sci. Bull. 6, 444–448 (in Chinese).
Sun, S.S., McDonough, W.F., 1989. Chemical and isotopic systematics of oceanic basalts: implication for mantle composition and process. In: Sauders, A.D., Norry, M.J. (Eds.), Magmatism in the Ocean Basins, Geological Society, vol. 42. London, Special Publications, pp. 313–345.
Sun, W.D., Yang, X.Y., Fan, W.M., Wu, F.Y., 2012. Mesozoic large scale magmatism and mineralization in South China: preface. Lithos 150, 1–5.
Tamura, Y., Tasumi, Y., 2002. Remelting of an andesitic crust as a possible origin for rhyolitic magma in oceanic arcs: an example from the Izu-Bonin arc. J. Petrol. 43, 1029–1047.
Tatsumi, Y., 2006. High-Mg andesites in the Setouchi volcanic belt, southwestern Japan: analogy to Archean magmatism and continental crust formation? Annu. Rev. Earth Planet. Sci. 34, 467–499.
Taylor, B., Martinez, F., 2003. Back-arc basin basalt systematics. Earth Planet. Sci. Lett. 210, 481–497.
Tsuchiya, T., Suzuki, S., Kimura, J.I., Kagami, H., 2005. Evidence for slab melt/mantle reaction: petrogenesis of early Cretaceous and Eocene high-Mg andesites from the Kitakami Mountains, Japan. Lithos 79, 179–206.
Vervoort, J.D., Blichert-Toft, J., 1999. Evolution of the depleted mantle: Hf isotope evidence from juvenile rocks through time. Geochim. Cosmochim. Acta 63, 533–556.
Wan, Y.S., Liu, D.Y., Xu, M., Zhuang, J., Song, B., Shi, Y., Du, Y.L., 2007. SHRIMP U-Pb zircon geochronology and geochemistry of metavolcanic and metasedimentary rocks in Northwestern Fujian, Cathaysia block, China: tectonic implicationsand the need to redefine lithostratigraphic units. Gondwana Res. 12 (1–2), 166–183.
Wan, Y.S., Liu, D.Y., Wilde, S.A., Cao, J.J., Chen, B., Dong, C.Y., Song, B., Du, L.L., 2010. Evolution of the Yunkai Terrane, South China: evidence from SHRIMP zircon U-Pb dating, geochemistry and Nd isotope. J. Asian Earth Sci. 37, 140–153.
Wang, J., Li, Z.X., 2003. History of Neoproterozoic rift basins in South China: implications for Rodinia break-up. Precambr. Res. 122, 141–158.
Wang, M., Shu, L.S., 2007. Rock geochemical characteristics of the Neoproterozoic Wuyishan Ophiolite mélange. Geol. China 34 (4), 572–583 (in Chinese with English abstract).
Wang, X.L., Zhou, J.C., Qiu, J.S., Gao, J.F., 2004. Geochemistry of the Meso- to Neoproterozoic basic-acid rocks from Hunan Province, South China: implications for the evolution of the western Jiangnan orogen. Precambr. Res. 135, 79–103.
Wang, X.L., Zhou, J.C., Qiu, J.S., Zhang, W.L., Liu, X.M., Zhang, G.L., 2006a. LA-ICP-MS U-Pb zircon geochronology of the Neoproterozoic igneous rocks from Northern Guangxi, South China: implications for petrogenesis and tectonic evolution. Precambr. Res. 145, 111–130.
Wang, X.L., Zhou, J.C., Qiu, J.S., Zhang, W.L., Liu, X.M., Zhang, G.L., 2006b. Petrogenesis of the Neoproterozoic strongly peraluminous granitoids from Northern Guangxi: constraints from zircon geochronology and Hf isotopes. Acta Petrol. Sin. 22 (2), 326–342 (in Chinese with English abstract).
Wang, X.C., Li, X.H., Li, W.X., Li, Z.X., 2007a. Ca. 825 Ma komatiitic basalts in South China: First evidence for >1500 °C mantle melts by a Rodinian mantle plume. Geology 35 (12), 1103–1106.
Wang, X.L., Zhou, J.C., Griffin, W.L., Wang, R.C., Qiu, J.S., O'Reilly, S.Y., Xu, X.S., Liu, X. M., Zhang, G.L., 2007b. Detrital zircon geochronology of Precambrian basement sequences in the Jiangnan orogen: dating the assembly of the Yangtze Cathaysia blocks. Precambr. Res. 159, 117–131.
Wang, Y.J., Fan, W.M., Zhao, G.C., Ji, S.C., Peng, T.P., 2007c. Zircon U-Pb geochronology of gneisses in Yunkai Mountains and its implications on the Caledonian event in South China. Gondwana Res. 12 (4), 404–416.
Wang, X.L., Zhao, G.C., Zhou, J.C., Liu, Y.S., Hu, J., 2008a. Geochronology and Hf isotopes of zircon from volcanic rocks of the Shuangqiaoshan Group, South China: implications for the Neoproterozoic tectonic evolution of the eastern Jiangnan orogen. Gondwana Res. 18 (14), 355–367.
Wang, X.L., Zhou, J.C., Qiu, J.S., Jiang, S.Y., Shi, Y.R., 2008b. Geochronology and geochemistry of Neoproterozoic mafic rocks from western Hunan, South China: implications for petrogenesis and post-orogenic extension. Geol. Mag. 145 (2), 215–233.
Wang, Y.J., Fan, W.M., Cawood, P.A., Li, S.Z., 2008c. Sr-Nd-Pb isotopic constraints on multiple mantle domains for Mesozoic mafic rocks beneath the South China Block hinterland. Lithos 106 (3–4), 297–308.
Wang, Q., Wyman, D.A., Li, Z.-X., Bao, Z.-W., Zhao, Z.-H., Wang, Y.-X., Jian, P., Yang, Y.-H., Chen, L.-L., 2010a. Petrology, geochronology and geochemistry of ca. 780 Ma A-type granites in South China: petrogenesis and implications for crustal growth during the breakup of the supercontinent Rodinia. Precambr. Res. 178, 185–208.
Wang, Y.J., Zhang, F.F., Fan, W.M., Zhang, G.W., Chen, S.Y., Cawood, P.A., Zhang, A.M., 2010b. Tectonic setting of the South China Block in the early Paleozoic: resolving intracontinental and ocean closure models from detrital zircon U-Pb geochronology. Tectonics 29. http://dx.doi.org/10.1029/2010TC002750.
Wang, M., Dai, C.G., Wang, X.H., Chen, J.S., Ma, H.Z., 2011a. In-situ zircon geochronology and Hf isotope of muscovite-bearing leucogranites from Fanjingshan, Guizhou Province, and constraints on continental growth of the Southern China block. Earth Sci. Front. 18 (5), 213–223 (in Chinese with English Abstract).
Wang, Y.J., Zhang, A.M., Fan, W.M., Zhao, G.C., Zhang, G.W., Zhang, F.F., Zhang, Y.Z., Li, S.Z., 2011b. Kwangsian crustal anatexis within the eastern South China Block: geochemical, zircon U-Pb geochronological and Hf isotopic fingerprints from the gneissoid granites of Wugong and Wuyi-Yunkai Domains. Lithos 127, 239–260.
Wang, X.L., Shu, L.S., Xing, G.F., Zhou, J.C., Tang, M., Shu, X.J., Qi, L., Hu, Y.H., 2012a. Post-orogenic extension in the eastern part of the Jiangnan Orogen: evidence from ca 800–760 Ma volcanic rocks. Precambr. Res. 222–223, 404–423.
Wang, X.L., Shu, X.J., Xing, G.F., Xie, S.W., Zhang, C.H., Xia, H., 2012b. LA-ICP-MS zircon U-Pb ages of the Shijiao-Huangshan instrusive rocks in Zhuji area, Zhejiang Province: implications for the ultramafic orbicular rocks. Geol. Bull. China 31 (1), 75–81.
Wang, W., Zhou, M.F., Yan, D.P., Li, J.W., 2012c. Depositional age, provenance, and tectonic setting of the Neoproterozoic Sibao Group, southeastern Yangtze Block, South China. Precambr. Res. 192–195, 107–124.
Wang, X.C., Li, X.H., Li, Z.X., Li, Q.L., Tang, G.Q., Gao, Y.Y., Zhang, Q.R., Liu, Y., 2012d. Episodic Precambrian crust growth: evidence from U-Pb ages and Hf-O isotopes of zircon in the Nanhua Basin, central South China. Precambr. Res. 222–223, 386–403.
Wang, Y.J., Wu, C.M., Zhang, A.M., Fan, W.M., Zhang, Y.H., Zhang, Y.Z., Peng, T.P., Yin, C.Q., 2012e. Kwangsian and Indosinian reworking of the eastern South China Block: constraints on zircon U-Pb geochronology and metamorphism of amphibolite and granulite. Lithos 150, 227–242.
Wang, X.L., Zhou, J.C., Wan, Y.S., Kitajima, K., Wang, D., Bonamici, C., Qiu, J.S., Sun, T., 2013a. Magmatic evolution and crustal recycling for Neoproterozoic strongly peraluminous granitoids from southern China: Hf and O isotopes in zircon. Earth Planet. Sci. Lett. 366, 71–82.

Wang, Y.J., Zhang, A.M., Cawood, P.A., Fan, W.M., Xu, J.F., Zhang, G.W., Zhang, Y.Z., 2013b. Geochronological, geochemical and Nd-Hf-Os isotopic fingerprinting of an early Neoproterozoic arc-back-arc system in South China and its accretionary assembly along the margin of Rodinia. Precambr. Res. 231, 343–371.
Wang, D., Wang, X.L., Zhou, J.C., Shu, X.J., 2013c. Unraveling the Precambrian crustal evolution by Neoproterozoic conglomerates, Jiangnan orogen: U-Pb and Hf isotopes of detrital zircons. Precambr. Res. 233, 223–236.
Wang, X.L., Zhou, J.C., Griffin, W.L., Zhao, G.C., Yu, J.H., Oiu, J.S., Zhang, Y.J., Xing, G.F., 2014a. Geochemical zonation across a Neoproterozoic orogenic belt: isotopic evidence from granitoids and metasedimentary rocks of the Jiangnan orogen, China. Precambr. Res. 242, 154–171.
Wang, Y.J., Zhang, Y.Z., Fan, W.M., Geng, H.Y., Zou, H.P., Bi, X.W., 2014b. Early Neoproterozoic accretionary assemblage in the Cathaysia Block: geochronological, Lu-Hf isotopic and geochemical evidence from granitoid gneisses. Precambr. Res. 249, 144–161.
Watson, E.B., Harrison, T.M., 1983. Zircon saturation revisited: temperature and composition effects in a variety of crustal magma types. Earth Planet. Sci. Lett. 64, 295–304.
Whalen, J.B., Currie, K.L., Chappell, B.W., 1987. A-type granites: geochemical characteristics, discrimination and petrogenesis. Contrib. Miner. Petrol. 95, 407–419.
White, A.J.R., Chappell, B.W., 1977. Ultrametamorphism and granitoid genesis. Tectonophysics 43, 7–22.
Wood, D.A., 1980. The application of a Th-Hf-Ta diagram to problems of tectonomagmatic classification and to establishing the nature of crustal contamination of basaltic lavas of the British Tertiary volcanic province. Earth Planet. Sci. Lett. 50, 11–30.
Woodhead, J.D., Hergt, J.M., Davidson, J.P., Eggins, S.M., 2001. Hafnium isotope evidence for 'conservative' element mobility during subduction zone processes. Earth Planet. Sci. Lett. 192, 331–346.
Workman, R.K., Hart, S.R., 2005. Major and trace element composition of the depleted MORB mantle (DMM). Earth Planet. Sci. Lett. 231, 53–72.
Wu, G.Y., Chen, H.M., Jia, B.H., He, J.N., 2001. Genetic mechanism of the Changsanbei granitic intrusion in northern Hunan. Geol. Min. Resour. South China 1, 23–35 (in Chinese, with English Abstract).
Wu, R.X., Zheng, Y.F., Wu, Y.B., Zhao, Z.F., Zhang, S.B., Liu, X.M., Wu, F.Y., 2006. Reworking of juvenile crust: element and isotope evidence from Neoproterozoic granodiorite in South China. Precambr. Res. 146, 179–212.
Xia, Y., Xu, X.S., Zhu, K.Y., 2012. Paleoproterozoic S- and A-type granites in southwestern Zhejiang: magmatism, metamorphism and implications for the crustal evolution of the Cathaysia basement. Precambr. Res. 216–219, 177–207.
Xia, Y., Xu, X.S., Zou, H.B., Liu, L., 2014. Early Paleozoic crust-mantle interaction and lithosphere delamination in South China Block: evidence from geochronology, geochemistry, and Sr-Nd-Hf isotopes of granites. Lithos 184–187, 416–435.
Xia, Y., Xu, X.S., Zhao, G.C., Liu, L., 2015. Neoproterozoic active continental margin of the Cathaysia block: evidence from geochronology, geochemistry, and Nd–Hf isotopes of igneous complexes. Precambr. Res. 269, 195–216.
Xiang, L., Shu, L.S., 2010. Pre-Devonian tectonic evolution of the eastern South China block: geochronological evidence from detrital zircons. Sci. China Earth Sci. 53 (10), 1427–1444.
Xing, F.M., Xu, X., Ren, S.M., Li, Y.Y., 1988. The petrochemistry and formational age and conditions of the Shexian instrusion in southern Anhui province. Geol. Rev. 34 (5), 400–413 (in Chinese with English abstract).
Xu, B., Qiao, G.S., 1989. Sm-Nd isotopic age of the Late Proterozoic ophiolite suite in northeastern Jiangxi Province and its primary tectonic environment. J. Nanjing Univ. (Earth Sci.) 1 (3), I108–I114 (in Chinese with English abstract).
Xu, X.S., O'Reilly, S.Y., Griffin, W.L., Wang, X.L., Pearson, N.J., He, Z.Y., 2007. The crust of Cathaysia: age, assembly and reworking of two terranes. Precambr. Res. 158, 51–78.
Xue, H.M., Ma, F., Song, Y.Q., Xie, Y.P., 2010. Geochronology and geochemistry of the Neoproterozoic granitoid association from eastern segment of the Jiangnan orogen, China: constraints on the timing and process of amalgamation between the Yangtze and Cathaysia blocks. Acta Petrol. Sin. 26 (11), 3215–3244 (in Chinese with English abstract).
Yang, Z., Sun, Z., Yang, T., Pei, J., 2004. A long connection (750–380 Ma) between South China and Australia: paleomagnetic constraints. Earth Planet. Sci. Lett. 220, 423–434.
Yang, M.G., Huang, S.B., Lu, F.S., Tang, W.X., Mao, S.B., 2009. Major types and time-space distribution of Mesozoic ore deposits in South China: implications for geodynamic settings. Geol. China 36, 528–543 (in Chinese with English abstract).
Yao, J.L., Shu, L.S., Santosh, M., Li, J.Y., 2013. Geochronology and Hf isotope of detrital zircons from Precambrian sequences in the eastern Jiangnan Orogen: constraining the assembly of Yangtze and Cathaysia Blocks in South China. J. Asian Earth Sci. 74, 225–243.
Yao, J.L., Shu, L.S., Santosh, M., Zhao, G.C., 2014a. Neoproterozoic arc-related mafic–ultramafic rocks and syn-collision granite from the western segment of the Jiangnan Orogen, South China: constraints on the Neoproterozoic assembly of the Yangtze and Cathaysia Blocks. Precambr. Res. 243, 39–62.
Yao, J.L., Shu, L.S., Santosh, M., Xu, Z.Q., 2014b. Palaeozoic metamorphism of the Neoproterozoic basement in NE Cathaysia: zircon U-Pb ages, Hf isotope and whole-rock geochemistry from the Chencai Group. J. Geol. Soc., London 171, 281–297.
Yao, J.L., Shu, L.S., Santosh, M., 2014c. Neoproterozoic arc-trench system and breakup of the South China Craton: constraints from N-MORB type and arc-related mafic rocks, and anorogenic granite in the Jiangnan orogenic belt. Precambr. Res. 247, 187–207.
Yao, W.H., Li, Z.X., Li, W.X., Li, X.H., Yang, J.H., 2014d. From Rodinia to Gondwanaland: a tale of detrital zircon provenance analyses from the southern Nanhua Basin, South China. Am. J. Sci. 314, 278–313.
Ye, M.F., Li, X.H., Li, W.X., Liu, Y., Li, Z.X., 2007. SHRIMP zircon U-Pb geochronological and whole-rock geochemical evidence for an early Neoproterozoic Sibaoan magmatic arc along the southeastern margin of the Yangtze Block. Gondwana Res. 12, 144–156.
Yu, J.H., O'Reilly, Y.S., Wang, L.J., Griffin, W.L., Jiang, S.Y., Wang, R.C., Xu, X.S., 2007. Finding of ancient materials in Cathaysia and implication for the formation of Precambrian crust. Chin. Sci. Bull. 52, 13–22.
Yu, J.H., O'Reilly, S.Y., Wang, L.J., Griffin, W.L., Zhang, M., Wang, R.C., Jiang, S.Y., Shu, L.S., 2008. Where was South China in the Rodinia supercontinent? Evidence from U-Pb geochronology and Hf isotopes of detrital zircons. Precambr. Res. 164, 1–15.
Yu, J.H., Wang, L.J., O'Reilly, Y.S., Griffin, W.L., Zhang, M., Li, C.Z., Shu, L.S., 2009. A Paleoproterozoic orogeny recorded in a long-lived cratonic remnant (Wuyishan terrane), eastern Cathaysia Block, China. Precambr. Res. 174, 347–363.
Yu, J.H., O'Reilly, Y.S., Wang, L.J., Griffin, W.L., Zhou, M.F., Zhang, M., Shu, L.S., 2010. Components and episodic growth of Precambrian crust in the Cathaysia Block, South China: evidence from U-Pb ages and Hf isotopes of zircons in Neoproterozoic sediments. Precambr. Res. 181, 97–114.
Yu, J.H., O'Reilly, S.Y., Zhou, M.F., Griffin, W.L., Wang, L.J., 2012. U-Pb geochronology and Hf-Nd isotopic geochemistry of the Badu Complex, South-Eastern China: implications for the Precambrian crustal evolution and paleogeography of the Cathaysia Block. Precambr. Res. 222–223, 424–449.
Zeng, W., Zhang, L., Zhou, H.W., Zhong, Z.Q., Xiang, H., Liu, R., Jin, S., Lu, X.Q., Li, C.Z., 2008. Caledonian reworking of Paleoproterozoic basement in the Cathaysia Block: constraints from zircon U-Pb dating, Hf isotopes and trace elements. Chin. Sci. Bull. 53 (6), 895–904.
Zhang, S.B., Zheng, Y.F., 2013. Formation and evolution of Precambrian continental lithosphere in South China. Gondwana Res. 23, 1241–1260.
Zhang, B.T., Ling, H.F., Shen, W.Z., Liu, J.S., Yang, J.D., Tao, X.C., 1990. Sm-Nd isochronic age of spilite-keratophyre of Shuangxiwu Group in Xiqiu, Shaoxing, Zhejiang Province. J. Nanjing Univ. (Earth Sci.) 2, 9–14 (in Chinese with English Abstract).
Zhang, Z.L., Yuan, H.H., Nan, Y., 1998. Whole grain zircon evaporation for age of Luoyu formation, Yunkai Group. Mineral. Petrol. 18, 85–90 (in Chinese with English abstract).
Zhang, F.F., Wang, Y.J., Fan, W.M., Zhang, A.M., Zhang, Y.Z., 2011a. Zircon U-Pb geochronology and Hf isotopes of the Neoproterozoic granites in the central of Jiangnan uplift. Geotect. Metal. 35 (1), 73–84 (in Chinese with English abstract).
Zhang, Y.J., Zhou, X.H., Liao, S.B., Zhang, X.D., Yu, M.G., Ren, J., Yang, J., 2011b. Geological and geochemical characteristics and petrogenesis of the Mafic Rocks from Zhangyuan, Northern Jiangnan Orogen. Geol. J. China Univ. 17 (3), 393–405.
Zhang, A.M., Wang, Y.J., Fan, W.M., Zhang, Y.Z., Yang, J., 2012a. Earliest Neoproterozoic (ca. 1.0 Ga) arc-back-arc-basin nature along the northern Yunkai Domain of the Cathaysia Block: geochronological and geochemical evidence from the metabasite. Precambr. Res. 220–221, 217–233.
Zhang, S.B., Wu, R.X., Zheng, Y.F., 2012b. Neoproterozoic continental accretion in South China: geochemical evidence from the Fuchuan ophiolite in the Jiangnan orogen. Precambr. Res. 220–221, 45–64.
Zhang, Y.Z., Wang, Y.J., Fan, W.M., Zhang, A.M., Ma, L.Y., 2012c. Geochronological and geochemical constraints on the metasomatised source for the Neoproterozoic (~825 Ma) high-mg volcanic rocks from the Cangshuipu area (Hunan Province) along the Jiangnan domain and their tectonic implications. Precambr. Res. 220–221, 139–157.
Zhang, F.F., Wang, Y.J., Zhang, A.M., Fan, W.M., Zhang, Y.Z., Zi, J.W., 2012d. Geochronological and geochemical constraints on the petrogenesis of middle Paleozoic (Kwangsian) massive granites in the eastern South China Block. Lithos 150, 188–208.
Zhang, C.L., Santosh, M., Zou, H.B., Li, H.K., Huang, W.C., 2013a. The Fuchuan ophiolite in Jiangnan Orogen: geochemistry, zircon U-Pb geochronology, Hf isotope and implications for the Neoproterozoic assembly of South China. Lithos 179, 263–274.
Zhang, Y.Z., Wang, Y.J., Geng, H.Y., Zhang, Y.H., Fan, W.M., Zhong, H., 2013b. Early Neoproterozoic (~850 Ma) back-arc basin in the Central Jiangnan Orogen (Eastern South China): geochronological and petrogenetic constraints from meta-basalts. Precambr. Res. 231, 325–342.
Zhao, G.C., 2015. Jiangnan Orogen in South China: developing from divergent double subduction. Gondwana Res. 27 (3), 1173–1180.
Zhao, G.C., Cawood, P.A., 1999. Tectonothermal evolution of the Mayuan assemblage in the Cathaysia Block: implications for Neoproterozoic collision-related assembly of the South China craton. Am. J. Sci. 299, 309–339.
Zhao, G.C., Cawood, P.A., 2012. Precambrian geology of China. Precambr. Res. 222–223, 13–54.
Zhao, J.H., Zhou, M.F., 2009. Neoproterozoic high-Mg basalts formed by melting of ambient mantlein South China. Precambr. Res. 233, 193–205.
Zhao, J.H., Zhou, M.F., Yan, D.P., Zheng, J.P., Li, J.W., 2011. Reappraisal of the ages of Neoproterozoic strata in South China: no connection with the Grenvillian orogeny. Geology 39, 299–302.
Zhao, K.D., Jiang, S.Y., Sun, T., Chen, W.F., Ling, H.F., Chen, P.R., 2013. Zircon U-Pb dating, trace element and Sr-Nd-Hf isotope geochemistry of Paleozoic granites

in the Miao' ershan-Yuechengling batholith, South China: implication for petrogenesis and tectonic-magmatic evolution. J. Asian Earth Sci. 74, 244–264.

Zhejiang BGMR (Bureau of Geology and Mineral Resources of Zhejiang Province), 1989. Regional Geology of the Zhejiang Province. Geological Publishing House, Beijing, pp. 1–688 (in Chinese with English abstract).

Zheng, J.P., Griffin, W.L., O'Reilly, S.Y., Lu, F.X., Wang, C.Y., Zhang, M., Wang, F.Z., Li, H.M., 2004. 3.6 Ga lower crust in central China: new evidence on the assembly of the North China Craton. Geology 32, 229–232.

Zheng, J.P., Griffin, W.L., OReilly, S.Y., Zhang, M., Pearson, N., Pan, Y.M., 2006. Widespread Archean basement beneath the Yangtze craton. Geology 34, 417–420.

Zheng, Y.F., Zhang, S.B., Zhao, Z.-F., Wu, Y.B., Li, X.H., Li, Z.X., Wu, F.-Y., 2007. Contrasting zircon Hf and O isotopes in the two episodes of Neoproterozoic granitoids in South China: implications for growth and reworking of continental crust. Lithos 96, 127–150.

Zheng, Y.F., Wu, R.X., Wu, Y.B., Zhang, S.B., Yuan, H.L., Wu, F.Y., 2008. Rift melting of juvenile arc-derived crust: geochemical evidence from Neoproterozoic volcanic and granitic rocks in the Jiangnan Orogen, South China. Precambr. Res. 163, 351–383.

Zheng, J.P., Griffin, W.L., Li, L.S., O'Reilly, S.Y., Pearson, N.J., Tang, H.Y., Liu, G.L., Zhao, J.H., Yu, C.M., Su, Y.P., 2011. Highly evolved Archean basement beneath the western Cathaysia Block, South China. Geochim. Cosmochim. Acta 75, 242–255.

Zheng, Y.F., Xiao, W.J., Zhao, G.C., 2013. Introduction to tectonics of China. Gondwana Res. 23, 1189–1206.

Zhou, G.Q., 1989. The discovery and significance of the northeastern Jiangxi Province ophiolite (NEJXO), its metamorphic peridotite and associated high temperature-high pressure metamorphic rocks. J. SE Asian Earth Sci. 3, 237–247.

Zhou, X., Zhu, Y., 1993. Late Proterozoic collisional orogen and geosuture in southeastern China: petrological evidence. Chin. J. Geochem. 12, 239–251 (in Chinese with English Abstract).

Zhou, M.F., Yan, D.P., Kennedy, A.K., Li, Y.Q., Ding, J., 2002. SHRIMP U-Pb zircon geochronological and geochemical evidence for Neoproterozoic arc-magmatism along the western margin of the Yangtze Block, South China. Earth Planet Sci. Lett. 196, 51–67.

Zhou, J.C., Wang, X.L., Qiu, J.S., Gao, J.F., 2003. The discovery of Nanqiao highly depleted N-MORB and geological significance. Acta Petrol. Mineral. 22, 211–216 (in Chinese with English abstract).

Zhou, J.C., Wang, X.L., Qiu, J.S., Gao, J.F., 2004. Geochemistry of Meso- and Neoproterozoic mafic-ultramafic rocks from northern Guangxi, China: arc or plume magmatism? Geochem. J. 38, 139–152.

Zhou, X.M., Sun, T., Shen, W.Z., Shu, L.S., Niu, Y.L., 2006. Petrogenesis of Mesozoic granitioids and volcanic rocks in South China: a response to tectonic evolution. Episodes 29, 26–33.

Zhou, J.C., Wang, X.L., Qiu, J.S., 2009. Geochronology of Neoproterozoic mafic rocks and sandstones from northeastern Guizhou, South China: coeval arc magmatism and sedimentation. Precambr. Res. 170, 27–42.

Zhou, X.H., Zhang, Y.J., Liao, S.B., Yu, M.G., Chen, Z.H., Zhao, X.L., Jiang, Y., Jiang, R., 2012. LA-ICP-MS Zircon U-Pb geochronology of volcanic rocks in the Shuangqiaoshan group at Anhui-Jiangxi boundary region and its geological implication. Geol. J. China Univ. 18 (4), 609–622 (in Chinese with English Abstract).

Zou, H.B., Zhou, G.Q., Zhou, X.M., 1993. A study of two ophiolite suites within the Late Proterozoic collision-type orogenic belt in south China. In: Li, J.L. (Ed.), The Structure and Geological Evolution of the Continental Lithosphere in Southeast China. Metallurgic Industry Press, Beijing, pp. 130–140 (in Chinese with English Abstract).